Layer-by-layer nanoparticles for glaucoma therapy

Dissertation to obtain the Degree of Doctor of Natural Sciences

(Dr. rer. nat.)

from the Faculty of Chemistry and Pharmacy

University of Regensburg

Presented by

Michaela Guter

from Kirchberg/Iller

February 2018

This work was carried out from January 2014 until December 2017 at the Department of Pharmaceutical Technology of the University of Regensburg.

The thesis was prepared under supervision of PD Dr. Miriam Breunig.

To my family

Table of Contents

Chapter 1

Hyaluronan as a promising excipient for ocular drug delivery

Abstract
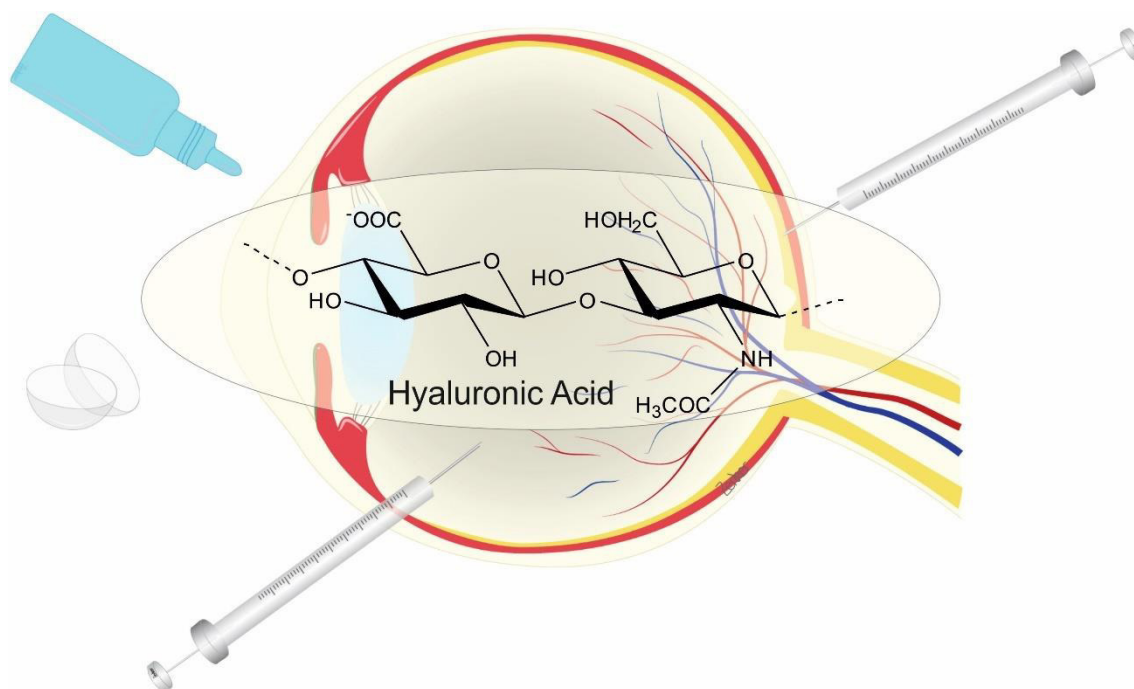
Hyaluronan (HA) is a naturally occurring polysaccharide and well known for its exceptional properties such as high biocompatibility and biodegradability, along with a low immunogenicity. Besides its use for various biomedical applications it recently came into focus as a favorable excipient for the formulation of various ocular therapeutics. This review article summarizes the ocular distribution of HA and its most heavily investigated binding protein "cluster of differentiation 44" (CD44) which is the rationale for the clinical use of HA, primarily as an additive in ocular applications ranging from eye drops to contact lenses. Moreover, examples will be given for using HA in various pre-clinical approaches to generate entirely new therapeutics, most notably in the field of nanotechnology.

1   Introduction

Ocular diseases are numerous and diverse. Some present few symptoms or a mild progression, while others may be associated with pain, double vision, inflammation, and ultimately vision loss. In the past decade, significant progress has been achieved toward a better understanding of the pathogenesis and genetics of many ocular diseases such as glaucoma or ocular neovascularization (e.g., age-related macular degeneration (AMD) or diabetic retinopathy (DR) [1]). Over the same time period, the field has seen a substantial expansion of both therapeutic options and routes of delivery. For many years, ocular medicines have been applied predominantly as eye drops. Despite their potency, these medications have a long list of drawbacks, including poor compliance, inadequate application by patients, poor bioavailability, and systemic side effects [2]. In addition, these therapeutic options fail at treating diseases that originate in the posterior segment of the eye. The emergence of biologics has helped fill this therapeutic gap; intra-vitreal injections are now routine procedures [3]. In addition, research and development on novel drug delivery materials and strategies for therapeutics, ranging from small molecules to biologics and nucleic acids, have advanced the field tremendously (for reviews please refer to [4–8]).

More recently, the polysaccharide HA has come into focus as a favorable excipient for the formulation of various ocular drug delivery systems. HA is a naturally occurring structural component of the extracellular matrix (ECM) and can be gained by extraction from animal tissues such as the rooster comb but also via bacterial fermentation in Streptococci or Bacilli [9,10]. Its non-immunogenic, non-fouling and favorable physicochemical properties (e. g. high water binding capacity, pseudoplasticity, optical transparency) have made the use of HA in biomedical applications quite popular. For example, it has been applied as an artificial lubricant in joints [11], a substitute material for the vitreous body [12], and a scaffold material for tissue engineering [13]. Additionally, HA has contributed to the development of cancer diagnostics and therapy [14,15]; for instance, HA-based hydrogels have been used for local delivery of macromolecular drugs (e.g., for interferon-α2 [16,17], trastuzumab [18], and nucleic acids [19]). HA-drug conjugates have also shown promise when formulated to improve drug solubility and stability, in a similar fashion to PEGylation [20]. Lastly, HA has been used successfully as a targeting sequence to guide drug-loaded nanoparticles (NPs) to their final destination [15]. Despite these efforts, HA-based excipients are just beginning to garner recognition as powerful catalysts for new drug delivery applications in the field of ocular pathology.

Here, we first present a general overview of HA and its properties. Then, we describe the distribution of HA and its binding protein CD44 in the anterior and posterior segment of the eye. Finally, we provide a critical review of recent developments in the field of HA-assisted ophthalmic drug delivery and highlight HA's potential therapeutic effects.

2 HA and its interaction with the CD44 receptor

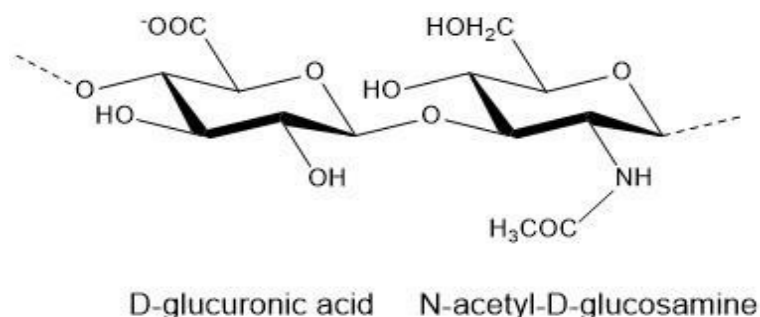D-glucuronic acid   N-acetyl-D-glucosamine

Figure 1. Chemical structure of HA. HA is a natural heteropolysaccharide composed of the repeating disaccharide unit D-glucuronic acid / N-acetyl-D-glucosamine. The monomers are linked via β-1,4- and β-1,3-glycosidic bonds until the molecular weight reaches values of up to 10^7 kDa.

HA is the main component of the ECM and can therefore be found ubiquitously in the human body. The largest amount is present in the skin, which accounts for over 50 % of total body HA [15]. However, the concentration is also high in the vitreous body, from which it was originally isolated in 1934 [21]. Its significant role in the body is underlined by its high synthesis rate and an extremely rapid turnover of 5 g per day in an adult of 70 kg [22].

HA is composed of alternating units of D-glucuronic acid and N-acetyl-glucosamine (Figure 1). The monomers are linked via β-1,4- and β-1,3-glycosidic bonds and form a long, linear polymer chain. The pK_a value of the carboxylic acid groups is between 3 and 4 [23]. Consequently, the polysaccharide is negatively charged at physiological pH. Native HA is present as high molecular weight (MW) material up to 10^7 kDa and is well known for being biocompatible, biodegradable, non-toxic, and non-immunogenic [24]. Although the chemical structure is very simple, HA exhibits exceptional properties and various biological functions [25]. Due to its hydrophilic character and long chain length, HA can bind enormous amounts of water and may thus swell up to a volume 1000-fold greater than its original solid volume [15,26]. HA solutions are viscous and characterized by shear thinning and pseudo-plastic flow behavior [27]. Consequently, the polymer is ideally suited as a lubricant in several

biological functions and was rapidly deployed as an artificial viscosupplement, which diminishes friction and abrasion in the joint gap [28].

HA promotes the structure formation and hydration of the ECM throughout various tissues in the body and enables their mechanical functionality and stability [26,29]. Interactions with several extracellular binding proteins (e.g., versican, aggrecan, and neurecan), distributed unevenly across tissues, strengthen the structure of the matrix [30]. In addition, hydration and electrostatic repulsion of anionic carboxyl groups on the polysaccharide chain contribute to the expansion of the polymer [25]. The resulting pressure caused by the swelling is strong enough to separate neighboring tissues, allowing cells to migrate within the newly emptied spaces. This HA-induced "cell migration highway" is of special importance in tissue development, wound healing, and cancer metastasis. Cellular receptors for HA such as CD44, receptor of hyaluronan mediated mobility (RHAMM) and lymphatic vessel endothelial hyaluronan receptor 1 (LYVE-1) link cells to the ECM, mediate cellular mobility, transduce signals from the extracellular environment to the intracellular space and are responsible for HA internalization and degradation. Some HA-binding proteins share a structural domain known as "link module" but other binding sites have also been identified [31].

The most heavily investigated of the HA-binding proteins is the CD44 receptor, which exists in multiple isoforms due to a significant degree of alternative splicing [32]. Glycosylation also broadens CD44 structural diversity and influences receptor activity. Given the polyanionic character of HA, it is at first glance surprising that hydrogen bonding and van der Waals forces dominate the CD44-HA interaction (at least for the murine CD44 receptor), as found by Banerji et al. via co-crystallization [33]. However, the anionic charges are unevenly distributed over the polymer, resulting in a substantial hydrophobic surface along the polyelectrolyte chain. A minimum chain length of six monosaccharides is necessary for monovalent binding of HA to the CD44-receptor [34]. Multivalent binding enhances receptor affinity and can be observed when the polysaccharide chain length exceeds 20 monomers. Mizrahi et al. implemented a model to estimate both, the binding strength between HA and its receptor CD44 and the receptor coverage by HA of different MW [35]. They immobilized a recombinant human CD44-Fc chimera on a surface plasmon resonance (SPR) sensor chip and evaluated the number of receptors occupied by free HA. Additionally, they assessed binding of HA-functionalized NPs. Strong binding of free HA was measurable at or above an HA MW of 132 kDa and coverage was found to match theoretical predictions (Table 1). In contrast, when the HA-chains were affixed to the NP surface, binding strength

was strongly reduced, most likely due to restricted polymer mobility. However, when the MW was increased to 700 kDa, free and immobilized HA exhibited similar binding characteristics. As these results were achieved using a planar and cell-free model, one should exercise caution when extrapolating results to an *in vivo* environment.

Table 1. Estimated CD44-Fc coverage by free HA at different MWs. Assuming a receptor density of 3 receptors per 1000 nm² and taking into account the radius of gyration of differently sized HA-chains, the receptor coverage was calculated. With permission taken from [35].

HA MW [kDa]	Radius of gyration [nm]	Area [nm²]	CD44 coverage (CD44 molecules available per HA)
6.4	4	49	1 (0.16)
31	10	327	1
132	24	1709	5-6
700	66	13678	44
1500	105	34365	110

After binding to the CD44 receptor, HA can be internalized via receptor-mediated endocytosis and degraded [25,36]. Subsequently, downstream signaling cascades may be activated, triggering cell survival, migration or inflammation. HA-CD44-interactions thus play a role in physiological and pathophysiological processes like embryonic development or tumorigenesis. Depending on the tissue, the degree of polymerization and the binding proteins involved, HA mediates different – and often opposing – effects as a messenger molecule. Whereas high MW HA has non-immunogenic and anti-proliferative properties, smaller degradation products seem to promote angiogenesis, inflammation and tumor growth [15]. However, very short HA fragments may in turn transduce an entirely different set of signals that effect suppression of tumor growth [26]. The complex interplay between HA, its receptors, synthases and cleaving enzymes, along with the therapeutic concepts based on these findings, are the subject of several review articles [26,37–39]. These investigations do not primarily refer to ocular cells because a deeper analysis and understanding of the CD44 receptor characteristics of primary ocular cells or ocular-derived cell lines, respectively, has to the best of our knowledge not been addressed so far.

It is important to mention that the use of HA is also associated with some drawbacks. Because HA is of natural origin, variations are possibly more important than they are for synthetic polymers [40]. Significant batch-to-batch variations may complicate further downstream processing. But the clinical use of several biopolymers – therapeutically or as an excipient (e. g. heparin, alginate, protamine or gelatin to name just a few) has demonstrated that detailed specifications of individual characteristics such as MW, grade of purification or

biological offspring, can diminish differences between batches thereby facilitating further processing. In addition, the production of HA by extraction from animal sources is a common procedure – but contamination with proteins or viruses are possible and might become a problem in certain applications. Equally, the fermentation in bacteria carries the chance of mutation of the bacterial strain and the co-production of toxins or pyrogens [41]. Especially if the usage is not limited to topical administration, the allergic potential and the risk of developing an anaphylactic reaction cannot be denied. Luckily, the microbiological production and purification methods have made tremendous progress in the past few years. Another point is the pharmacological effect of HA itself. As discussed earlier, depending on the MW and concentration, HA is involved in tumor metastasis, cell migration and proliferation on the cellular level. These effects also depend on the organ and tissue type and are not fully understood yet. Consequently, it is hard to fully estimate the overall effect of HA-based formulations.

3 Anatomy of the eye
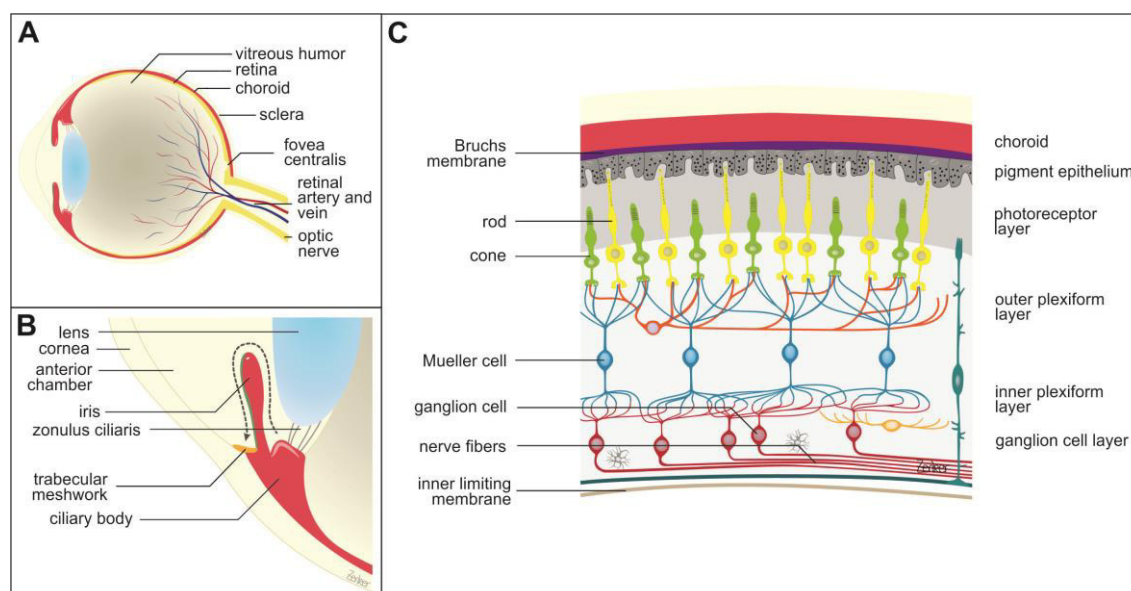
Figure 2. Anatomy of the eye. A) General structure of the eye bulb. B) Anterior chamber of the eye. Arrow shows the outflow pathway of the aqueous humor produced in the ciliary body. C) Cross-section of the back of the eye.

The structure of the eye is unique and provides many advantages for drug delivery, e.g. immune privilege – the absence of immunological reactions against diverse antigens – and accessibility for local administration [42]. In the following section, the prevalence of HA and

CD44 in the eye is described to provide support for the notion of using HA as a component in ocular drug delivery formulations.

The eye can be divided into two functional regions as illustrated in Figure 2. The anterior segment makes up approximately one third of the total volume of the eye and comprises the cornea, iris, ciliary body and lens (Figure 2B) [43]. Aqueous humor (AH), which provides nutrients to the cornea and lens, fills the spaces within the anterior segment. It is produced in the ciliary body, flows through the gap between lens and iris into the anterior chamber where it drains through the trabecular meshwork (TM) and Schlemm's canal into the episcleral vein (arrow in Figure 2B) [44]. By adjusting the AH production and drainage, the intraocular pressure (IOP) is regulated and adapted to guarantee the correct shape – and thus, optimal optical properties – of the eye bulb under changing conditions [45]. Belonging to the posterior segment, the vitreous body represents the largest part of the eye bulb. This clear, highly hydrated gel fills the space between the lens and the retina and serves structural, optical and developmental functions [46]. The back of the eye contains the retina, the choroid and the optic nerve (Figure 2C). The retina is composed of several structures: neuronal ganglia and sensory cells, separated from the vitreous by an inner limiting membrane [47]. Rods and cones, responsible for perception of light/dark and colors, respectively, are two types of photoreceptors found in the retina. Müller glia cells in the neuronal layer stabilize the retina and support the functions of the photoreceptors, for example by providing nutrients, removing metabolic products and regulating neuronal excitability [48]. The retinal pigment epithelium (RPE) is the outermost layer of the retina, and plays an important role in maintaining the viability of the photoreceptors. Among other tasks, the pigmented cells absorb scattered light, protect retinal cells against photo-oxidative stress, transport substances between photoreceptors and choroidal capillaries, and help to regenerate sensory cells [49]. Bruch's membrane divides the retina from the choroid, which is the vascular layer of the posterior segment of the eye [47]. Blood vessels provide the outer retinal areas with nutrients and oxygen.

Albeit to a varying extent, HA is present in all described structures of the eye and is often found in close proximity to CD44 receptors. To improve the comprehensibility of the following, the distribution of HA and CD44 is described from front to back of the eye.

3.1   Anterior segment of the eye

HA is an integral component of the cornea, typically collocated with its receptor CD44. In particular, immunostaining revealed high CD44 receptor density in the corneal epithelium

and endothelium, whereas lower density was observed in the hydrophilic corneal stroma (Figure 3) [50,51]. Interestingly, inflammation and other destructive processes affecting the cornea lead to a change of CD44 isotype (alternative splicing) and an increase in receptor density [52–54]. These observations are consistent with the influence of HA on epithelial cell mobility during wound healing; re-epithelialization occurs at a faster rate in the presence of HA [55,56]. In this case, interactions between epithelial CD44 receptors and HA on the ocular surface likely facilitate cell movement along this polysaccharide chains. Additionally, high MW HA seems to have a protective effect in UVB (radiation) exposed corneal epithelial cells due to its inhibitory effect on apoptotic signals and inflammatory cytokines [57]. The HA "reservoir" in tears is produced by corneal epithelial cells [58,59] and contributes significantly to the integrity of the ocular surface.
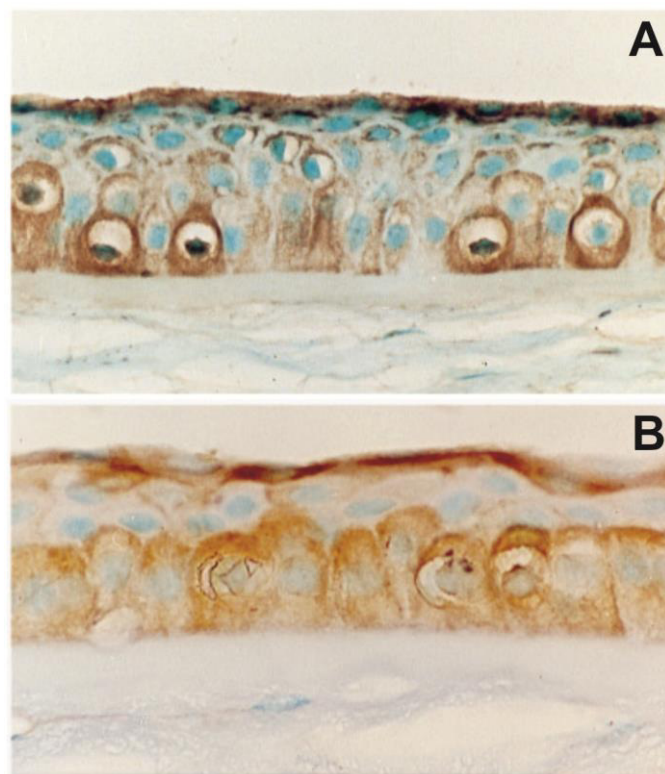

Figure 3. Central portion of the human cornea illustrating the distribution of HA and CD44 in the corneal epithelium and stroma. A) HA (brown) is localized on the basal and superficial epithelium but hardly in the stroma. Magnification: x 132. B) Intense staining for CD44 (brown) can be detected on the basal and superficial epithelium and is similar to the distribution pattern of HA. Magnification: x 150. Counterstaining with light green. With permission taken from [51].

HA has also been detected and quantified in the AH of enucleated eyes from humans, mammals and birds [60]. It might be involved in maintaining IOP, as it is capable of binding large amounts of water and therefore generating a high swelling pressure. IOP regulation is controlled primarily by varying outflow resistance to AH in the TM. In the TM, HA makes

up 20-25% of the total glycosaminoglycans of the ECM [61] and is mainly associated with the sieve-like networked epithelia of the trabecular beams [62,63] (Figure 2B). HA therefore co-determines the structure of the aqueous outflow pathway and as such is directly involved in regulating IOP. Interestingly, the aqueous HA concentration increases with age in healthy individuals, but is reduced in patients suffering from primary open angle glaucoma (POAG), a severe eye disease characterized by elevated IOP damaging the optic nerve [64,65]. Low HA concentrations are accompanied by an increased level of free CD44s, a soluble degradation product of the CD44 receptor [66], since the quantity of available HA is insufficient to inactivate CD44s. As CD44s – especially the hypophosphorylated form – is toxic to retinal ganglion cells and supporting cells in the prelaminar portion of the optic nerve, it might contribute to the degradation of neuronal cells and vision loss in POAG, provided its concentration exceeds a certain limit [67]. Consequently, Nolan et al. have proposed the use of CD44s as a protein marker for visual field loss in POAG [68].

Finally, HA has been detected in the iris and lens. Similar to observations made in the cornea, HA concentration and CD44 receptor density have been found to rise upon injury to these structures [69,70]. Apparently, HA also promotes tissue regeneration in the internal space of the anterior segment [71,72]. It has been shown via *in vitro* cell culture that migration of human lens epithelial cells on laminin or collagen coated plates is dependent on CD44 receptor interactions [73]. However, as very few HA-based therapeutics have been investigated for this site of application, scant detail is available.
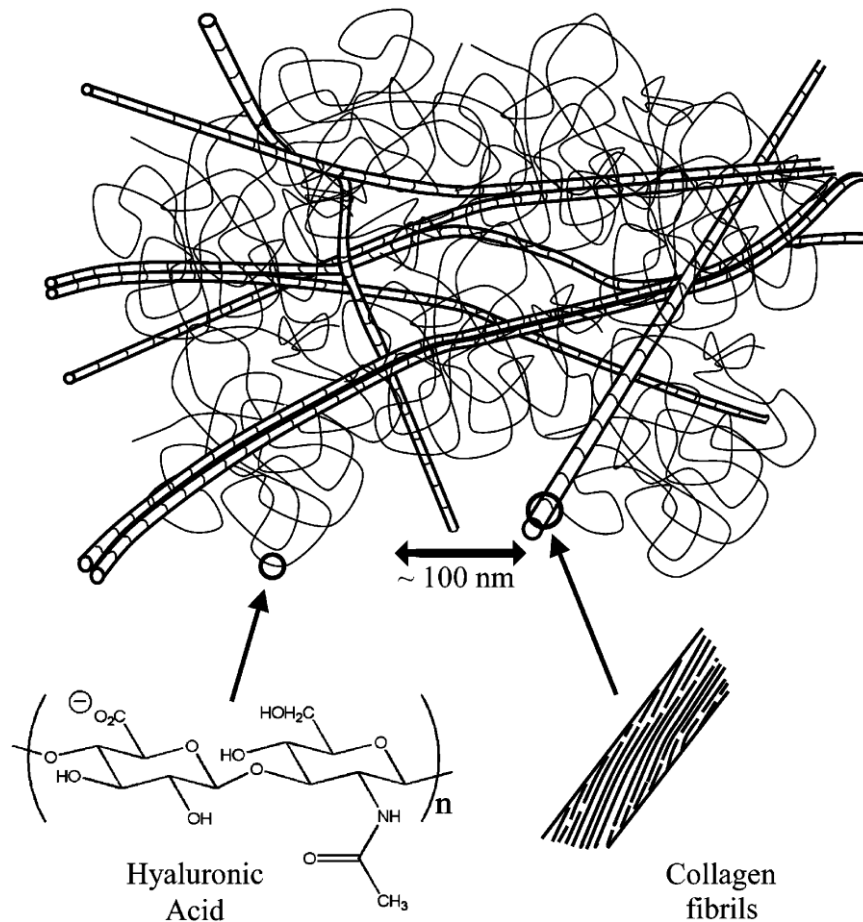
3.2   Posterior segment of the eye

Figure 4. Schematic drawing of the vitreous structure. Collagen fibrils form the hydrogel scaffold. HA immobilizes water within the spaces and leads to stretching of the collagen fibers. With permission taken from [46].

The vitreous of the eye was the first structure in which HA was detected in 1934 [21]. Today, the distribution and function of HA is well-known; HA is the principal glycosaminoglycan of the vitreous and found in concentrations varying from 65 to 400 μg/mL in humans, increasing with age [74]. A network of collagen fibers of different types forms the scaffold of the vitreous. High MW HA chains fill the spaces between the protein fibers and immobilize large amounts of water. The resulting swelling pressure leads to stretching of the collagen fibers, which mediates the internal tension of the vitreous (Figure 4) [46]. Experimental *ex vivo* treatment of vitreous with hyaluronidase reduces its water content and stiffness, but also increases contraction of its collagen fibers. These first two properties generated clinical interest (including a phase III clinical trial [75]) around use of hyaluronidase as a liquefaction agent to be applied prior to vitro-retinal surgery, which is often required to

treat retinal detachment or DR. However, intensified traction on retinal structures may increase the risk of exacerbating retinal damage, with the potential for subsequent vision loss [76]. Hyaluronidase also promotes natural HA turnover, and is partially responsible for maintaining the gel structure [77]. Depending on the species, the half-life of vitreal HA is estimated to range from 10 to 70 days. This differs significantly from other tissues, where half-life is no more than one week, and typically less than one day [78]. This extremely long half-life could be due to a combination of high vitreal HA concentration and scarce HA-secreting cells. Thus, faster replacement of the polymer would impair vitreal functionality.

In the back of the eye, Müller glia and cells of the RPE produce extracellular HA for the retina and the choroid [79,80]. *In vitro* studies have been conducted to investigate the synthesis of HA by RPE cells [81]. RPE cells secrete HA preferentially from the apical surface and are thus responsible for the significant amount of HA present in the interphotoreceptor matrix. Other cell types are involved in HA homeostasis. Gross-Jendroska et al. showed that the production of a paracrine factor by fetal RPE stimulates HA synthesis in neighboring choroidal mesenchymal fibroblasts [82]. The corresponding CD44 receptor can be found on Müller glia microvilli in the retina (Figure 5) [83]. There, the receptor can be detected during all stages of fetal development and is regarded as a surface marker for progenitor cells destined to become Müller glia [84,85]. The interactions between HA and its receptor contribute to structuration of the ECM around photoreceptors and neurons and enhance the internal strength of the tissue [86,87]. Again, CD44 expression has been shown to increase after retinal injury. This observation supports evidence of CD44 upregulation in proliferating cells *in vitro* and informs an understanding of the impact of HA on healing processes in the cornea and lens, as discussed earlier [88–90].
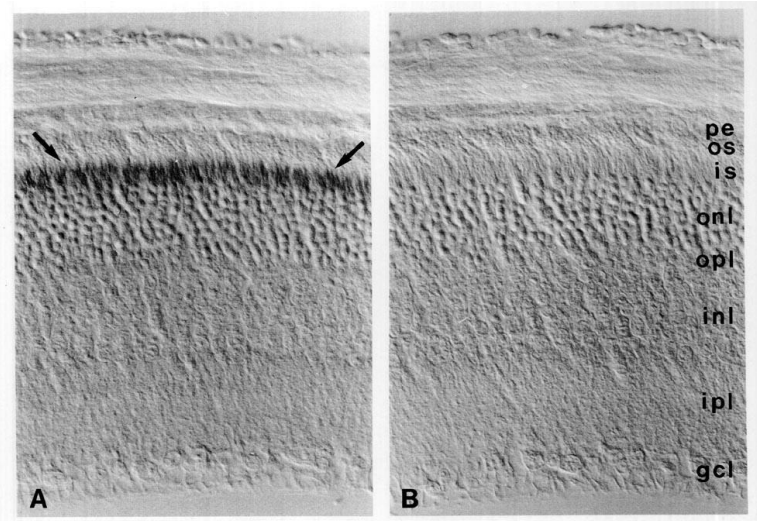
Figure 5. A) Immunoperoxidase labeling on sections of fixed adult mouse retina illustrating the presence of CD44 at the outer limiting membrane and directly adjacent tissue. These structures include the Müller glia microvilli and the lower portion of the photoreceptor inner matrix. However, discrimination between both structures was not possible. Hence it was not clear if the staining included only one or both components. B) No label was seen if an isotype control was used. pe = pigment epithelium; os = outer segments; is = inner segments; onl = outer nuclear layer; opl = outer plexiform layer; inl = inner nuclear layer; ipl = inner plexiform layer; gcl = ganglion cell layer. Magnification: A x450, B x460, C x500. With permission taken from [83].

HA and CD44 are also involved in pathological alterations of the posterior segment. In particular, the Mochimaru group has investigated the impact of HA and CD44 on the development of choroidal neovascularization (CNV) [91]. CNV is characterized by an abnormally high degree of new blood vessel formation in the choroid. These blood vessels are not restricted to the choroid but rather grow through Bruch's membrane into the retina. As vessels developed in this way are prone to bleeding and leakage, the retina can be damaged, potentially impacting a patient's vision. Treatment with a hyaluronsynthase-2 inhibitor (4-methylumbelliferone) or with an anti-CD44-antibody reduced CNV-severity by 25% (Figure 6): an impressive result, given that many other factors contribute to the development of CNV. This observation was explained in reference to the proangiogenic effect of HA and its potential to recruit macrophages; a high number of HA receptor LYVE-1-positive macrophages were found in healthy human choroids [92]. Similarly, the interaction of HA with its receptor CD44 is involved in inflammatory cell migration [93]. In experimental autoimmune uveoretinitis, a model for serious inflammatory reactions in the eye, the rolling of CD44 positive leukocytes along the HA-rich endothelium of venules and postcapillary venules in the retina enables blood cells to cross the blood-retina-barrier. In this case, too, the administration of anti-CD44-antibodies reduced the severity of inflammation and showed promise as a potential therapeutic strategy.
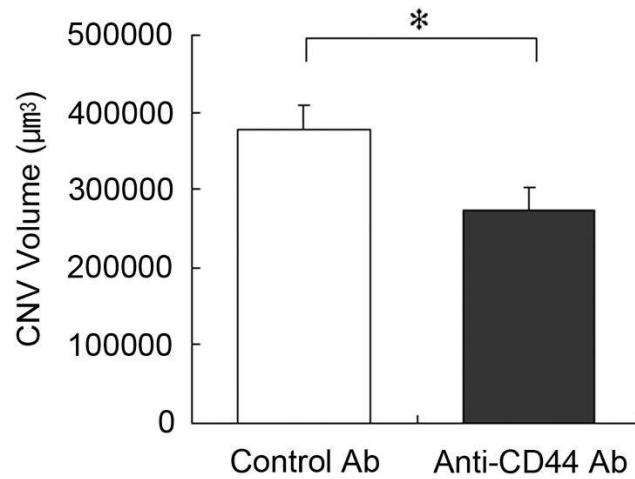
Figure 6. Reduction of CNV severity by antibody blockade of CD44. The anti-CD44 antibody was significantly more effective in reducing the CNV volume compared to a non-targeting isotype-control antibody. n = 44 for all. *p < 0.01. With permission taken from [91].

HA fulfills other functions in the choroid. During the process of developing clear and sharp vision (emmetropization), the choroidal thickness is adjusted to an individual's requirements via choroidal deposition of HA and osmotically driven water retention [94–96]. This adjusts the length of the optical path (distance between lens and retina). Even though the investigations uncovering this mechanism were performed in chickens, HA is expected to play a role in this process in humans, as well.
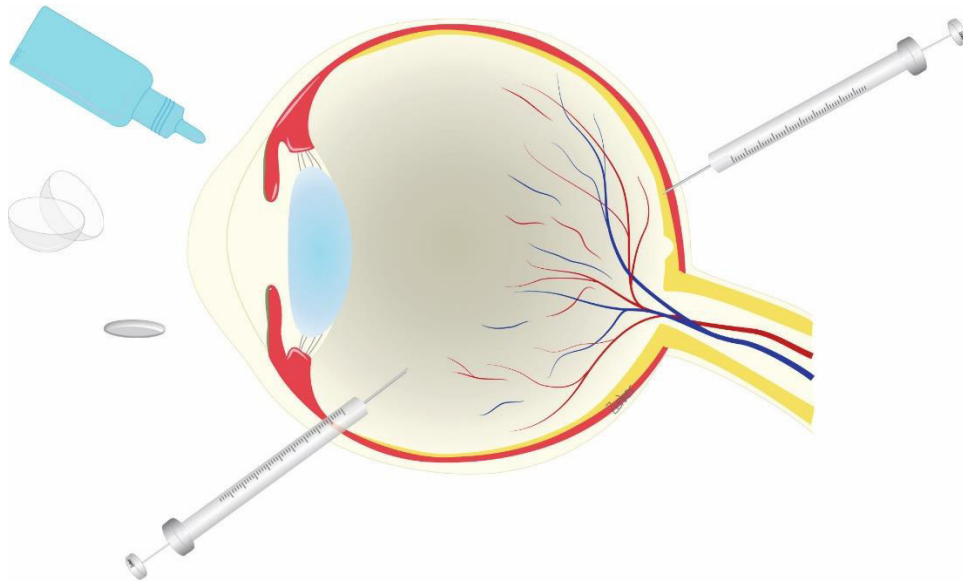
4   Applications of HA in the eye

Figure 7. Possible sites of HA application in the ocular environment. Topical administration of therapeutics by eye drops, lenses or inserts is preferred due to ease of accessibility. However, some substances must be applied by injections into the vitreous cavity or the retina.

Figure 7 summarizes typical therapeutic agent application sites in and on the eye. The topical route is the preferred mode of administration due to ease of accessibility. This works well for substances which have their effect in the anterior segment of the eye, such as lubricating eye drops or glaucoma therapeutics. However, if the drug must reach a structure in the posterior eye, like the retina, topical administration is ruled out; intravitreal injection is necessary to bring the therapeutic closer to its target. The broad distribution of HA and its binding proteins in the eye feature prominently in HA's potential as a component of new therapeutic modalities. In this section, we discuss a broad range of applications for HA: as an excipient to improve the effectiveness of ocular dosage forms, as a therapeutic itself and as an enabling compound for novel drug delivery approaches. For an overview refer to Table 2.

Table 2. Overview of HA-related applications in the eye according to the type of administration.

Formulation Type	Target	Benefits of HA formulation	Possible Challenges	References
Topical administration				
Lubricating eye drops	Ocular surface	Long-term lubrication without foreign item sensations or induced lacrimation; accelerated healing of corneal lesion	Application several times a day	[97–101]
Drug containing eye drops	Cornea, conjunctiva, anterior segment of the eye	Increased viscosity and mucoadhesivity prolongs ocular residence time of applied eye drops, increased bioavailability	Incompatibility between drug substance and HA	[102–108]
Nanoparticles	Ocular surface	"solubility enhancement" of poorly water soluble drugs, mucoadhesivenes and HA-CD44 interactions prolong precorneal residence time	Complex manufacturing, possible difficulties during approval	[109–111]
	Corneal epithelial cells	Reduced toxicity, high NP uptake (HA-CD44-interactions), bypass of lysosomal degradation	Complex manufacturing, possible difficulties during approval	[112–116]
Contact lenses	Ocular surface	Long-term delivery of HA as lubricant; improved characteristics of CLs with the possibility of an extended wearing time: enhanced wettability, reduced protein- and bacteria adsorption with lower risk of infection and inflammation	Tailoring HA release profile Immobilization of HA in CL material	[117–123]
Ocular inserts	Ocular surface, anterior chamber	High biocompatibility of system for sustained drug delivery	Challenging application because handling may be difficult especially for older patients	[124,125]
Intracameral administration				
Intraocular lenses	Lens	Reduced adhesion of lens epithelial cells and bacteria, less posterior capsule opacification and infection	No routine application	[126]

Formulation Type	Target	Benefits of HA formulation	Possible Challenges	References
Intravitreal administration				
Vitreous substitutes	Vitreous body	Biocompatibility, easy injection, biodegradability, suitable optical properties	Biodegradation too fast, batch-to-batch variation	[12,127]
Nanoparticles	Retina	Enhanced mobility in vitreous without impaired interaction with cells; possibility of specific targeting	Complex manufacturing, possible difficulties during approval	[128–130]
Retinal administration				
Retinal patches	Retina	Non-toxic, self-adhesive	Visit to doctor necessary because application not possible by patients	[131,132]
Hydrogels for protein and stem cell delivery	Retina	High biocompatibility, suitable mechanical properties	Still in experimental stadium, no clinical trial so far	[133–135]

4.1 Topical administration

Many medicines are applied topically to the eye, and for good reason. Accessibility, proximity to target structures and a reduced risk of side effects when compared with systemic dosing are all positive features of topical administration. In addition, this application route has economic benefits.

Lubricating and drug containing eye drops

Instillation of eye drops is a procedure which can easily be managed by the patient, reducing costly visits to the ophthalmologist. Unfortunately, not all topical treatments are effective. Sometimes the active ingredients drain too quickly or are unable to overcome ocular barriers, the latter of which represents a major hurdle for retinal therapeutics in particular [136]. Corneal epithelia and endothelia, corneal stroma, attached mucins or AH flow are just some of the main hurdles that must be traversed with topical application, depending of course on the physicochemical properties of the drug (e.g., partition coefficient and MW). Nevertheless, eye drops remain a valuable method for ocular drug delivery.

Lubricating eye drops (e. g. HyloVision®, ArtelacSplash®, Hyabak®) are one of the most prominent applications for HA in the ocular environment. Several artificial tear solutions

utilize HA as a viscosity-enhancing and mucoadhesive excipient for the treatment of dry eye disease (DED). The world prevalence of DED is approximately 6 to 34 %, and an age over 50 years and being female are known risk factors [137]. Patients are affected by ocular irritation, pain and transient visual impairment [138] caused by tear film instability, increased hyperosmolarity of the tear film and inflammation of the ocular surface [139]. The first-line therapeutic option is supplementation with artificial tears to lubricate the eye, replace missing tear fluid and normalize tear film osmolarity [140,141]. Viscous HA solutions or higher concentrated hydrogels are frequently applied to slow drainage of the eye-drop formulation, prolonging its therapeutic effect [142,143]. Compared to other excipients, such as polyvinyl alcohol or celluloses, the main advantage of high-viscosity HA solutions is their shear-thinning behavior [144]. Consequently, foreign item sensations and induced lacrimation, unpleasant symptoms themselves, are avoided.

To quantify the moisturizing potential of eye drops, one can measure tear film thickness. Following application of a 0.15 % HA formulation, tear film thickness was elevated for up to 40 minutes. Supplementation with 3 % trehalose increased tear film thickness by 30 % compared to the baseline value and extends the duration of the effect for up to 3 hours (Figure 8) [100,101]. These features could lead to decreased eye drop application frequency with no loss of therapeutic effect, representing a substantial benefit for the patient.
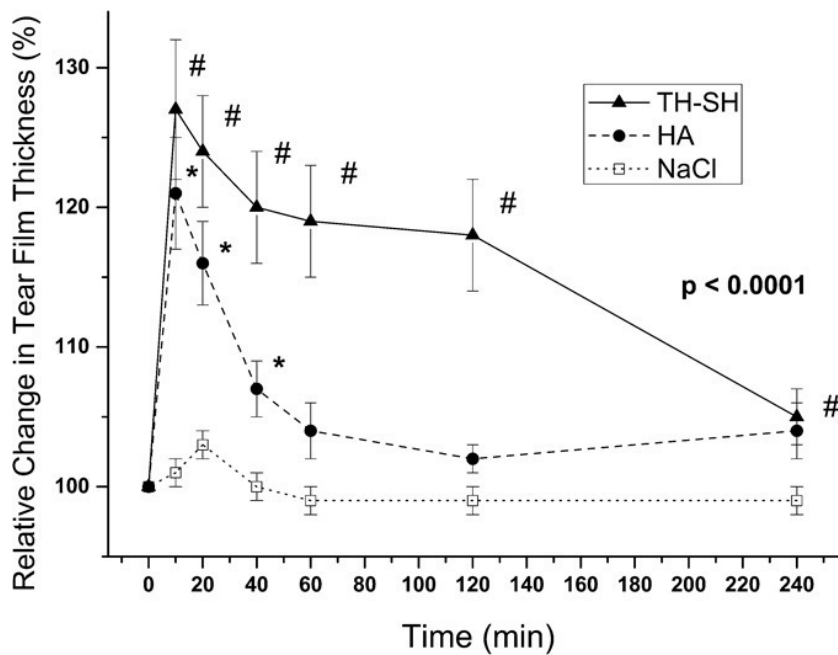

Figure 8. Relative tear film thickness as a surrogate parameter for the moisturizing potential of different types of eye drops. (TH-SH: 3 % trehalose + 0.15 % HA, HA: 0.15 % HA, NaCl: 0.9 % NaCl). HA-containing eye drops are able to stabilize the tear film for 40 minutes. With addition of trehalose, the effect can be extended for three hours. With permission taken from [101].

HA solutions have also been investigated as a treatment for pathologically elevated tear fluid osmolarity, regarded as a key factor in the pathogenesis of DED. Troiano et al. compared two unpreserved 0.4 % HA eye drops, one of them isotonic (300 mosmol/l), the other hypotonic (150 mosmol/l) [99]. After a treatment period of one week, hypotonic eye drops were more effective at reducing the symptoms of dry eye compared to isotonic drops. Rose Bengal staining also showed that hypotonic drops improved the vitality of corneal epithelial cells. Importantly, two thirds of the treated patients preferred the hypotonic formulation at the end of the study.

HA eye drops have also demonstrated additional beneficial effects in the treatment of pathological alterations in DED. In particular, an impressive correlation between the velocity of corneal lesion healing and the concentration of the instilled HA solution was reported in rabbits (Figure 9) [97]. Relative to a 0.1 % HA solution, healing was accelerated by a factor of 2 within 24 hours when 0.2 % HA was applied. It seems like improvement of epithelial cell migration and proliferation is a dose-dependent and therefore a pharmacological effect. Additionally, viscosity and lubrication of the eye drops increase with higher HA concentrations, reducing mechanical damages like friction or abrasion during blinking to the ocular surface. Investigations in diabetic rats have arrived at similar results [98].
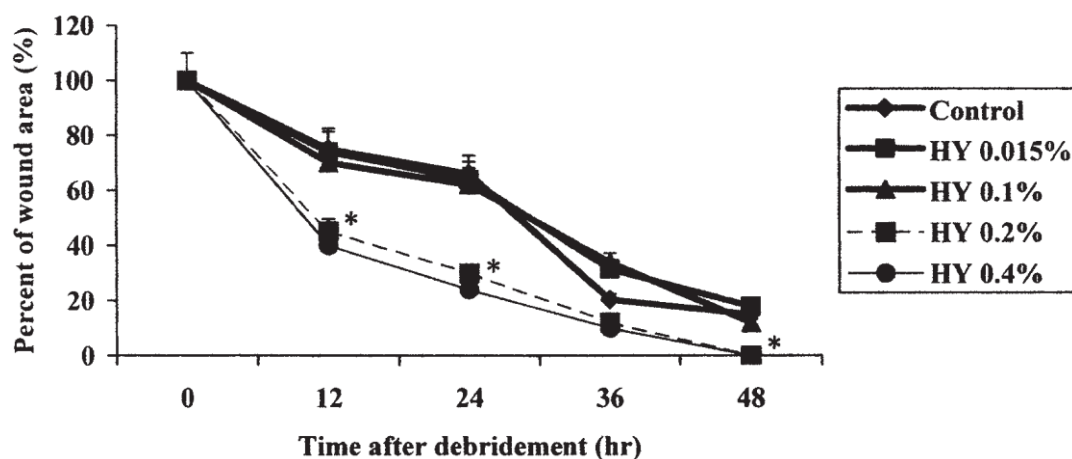

Figure 9. *In vivo* effects of HA (800 – 1400 kDa) on corneal epithelium wound healing. Eye drops were applied directly after corneal denudation of rabbits and again 2, 4, 6, 24, 28 and 30 hours later. Wound closure was measured by staining with 1 % fluorescein. n=4, p=0.05. Control: 0.9 % NaCl-solution. With permission taken from [97].

Beside its usage as a wetting and lubricating agent, HA is also used as a viscous, mucoadhesive excipient in general to prolong ocular residence time and reduce the systemic drainage of drug-containing eye drops [106,107]. For example, HA was used to increase the bioavailability of anti-glaucoma parasympathomimetic pilocarpine eye drops in rabbits [108].

Bioavailability of the drug, measured as the area under the curve (AUC) for miosis (pupil constriction) after topical instillation, was increased with increasing HA concentrations in the formulation. The prolongation of drug response, rather than an amplification of its effect, confirms similar findings found in previous studies [102]. Additionally, increasing the MW of HA applied led to lower concentrations of the excipient being required to obtain the same pupil-constricting effect, e. g. 0.75 % for 1600 kDa HA but only 0.125 % for 4600 kDa HA [108].

Bernatchez et al. have investigated the potential of HA in regards to enhancing the bioavailability of the antibiotic gentamicin in eye drops [105]. In comparison to buffered aqueous solution, the concentration of gentamicin in the tear fluid was increased by a factor of 2 for at least ten minutes upon inclusion of HA in the formulation. While these characteristics would not reduce application frequency, the increased concentration might improve the corneal penetration and bioavailability of the drug, enhancing its therapeutic efficacy. Herrero-Vanrell et al. have described the mucoadhesive properties and surface tension of corneal mucin and HA along with other excipients such as carboxymethylcellulose or polyacrylic acid; they then combined these polymers with the antimuscarinic drug tropicamide and investigated its bioavailability and mydriatic potential [103]. HA was found to increase the bioavailability by 70% relative to the excipient-free drug solution mainly due to prolongation of the mydriatic response. The effect was explained by reference to the similar properties of mucus and HA, as acidic groups of the polymers interact with the sialic parts of ocular mucins in a comparable fashion to mucus glycoproteins itself. Since tropicamide is used as a short-term mydriaticum, the benefit of using HA in formulations of this drug is limited. However, the results may be generalized and applied to other therapeutic substances with higher clinical relevance.

In general, increasing the solution viscosity is a common approach for prolonging the ocular residence time of eye drops. The usage of *in situ* gelling excipients represents a particularly elegant approach, combining the simple administration of common low-viscosity eye drops with the favorable features of a more viscous formulation. Poloxamers or polyethylene glycol-polypropylene glycol block co-polymers are a frequently used class of thermogelators that may be used for this purpose; gelation occurs upon warming to body temperature as the hydrophilicity and hydration of the polyethylene part decreases, enabling stronger hydrophobic interactions and the formation of poloxamer micelles. The volume fraction of micelles increases and the liquid becomes a gel when it exceeds a certain limit [145]. Cho et al. combined the thermogelation of poloxamer 407 with the mucoadhesivenes of HA by

grafting both polymers with EDC/NHS chemistry (a technique for linking two educts via their reactive esters with 1-ethyl-3-(3-dimethylaminopropyl)carbodiimide and N-hydroxysuccinimide) [104]. The two polymers' properties combine to extend drug release profiles, as shown below for the model substance ciprofloxacin (Figure 10). An HA amount of at least 7 % by weight must be exceeded to observe a relevant effect.
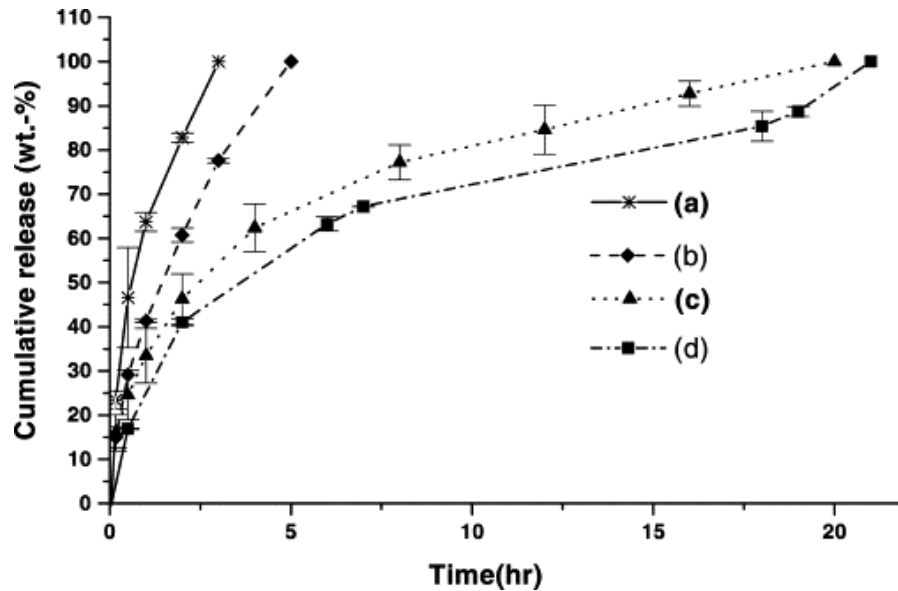

Figure 10. Release profile of ciprofloxacin from in-situ-gelling poloxamer 407-HA-hydrogels. (a) poloxamer 407 alone (b) graft copolymer (HA, 1.18 wt.%), (c) graft copolymer (HA 6.87 wt.%) and (d) graft copolymer (HA 13.99 wt.%), all with 1.75 wt.% ciprofloxacin. With permission taken from [104].

NP formulations

NP formulations represent another therapeutic opportunity to take advantage of HA's unique properties. Development of HA-modified NPs for topical ocular instillation has been motivated by two end goals. The first is – again - prolongation of ocular residence time for a drug substance. Drainage of NPs is slower than that of common eye drop formulations because they are able to interact with the corneal epithelium. Second, NPs can serve as a delivery vehicle for entry of various therapeutics into corneal cells. If the NP composition is chosen carefully, cellular specificity and the degree of cellular uptake can be enhanced, for example by leveraging NP-cell surface receptor interactions.

If a drug substance is poorly water soluble, extension of the precorneal residence time is of special importance, as it provides a straightforward and easy way to enhance bioavailability. An excellent example is cyclosporine A (CyA), an immunosuppressive drug used to increase tear production in patients with DED. Loading of CyA into NP composed of benzalkonium

chloride and poly-ε-caprolactone boosted corneal CyA concentration by a factor of 6 to 8 compared to that achieved with a castor oil formulation (Figure 11) [111]. This effect was attributed amongst others to the formulation as a NP and the presence of benzalkonium chloride. Corneal CyA concentration was even higher for HA-modified NP, possibly due to increased mucoadhesion and interactions with corneal CD44 receptors.
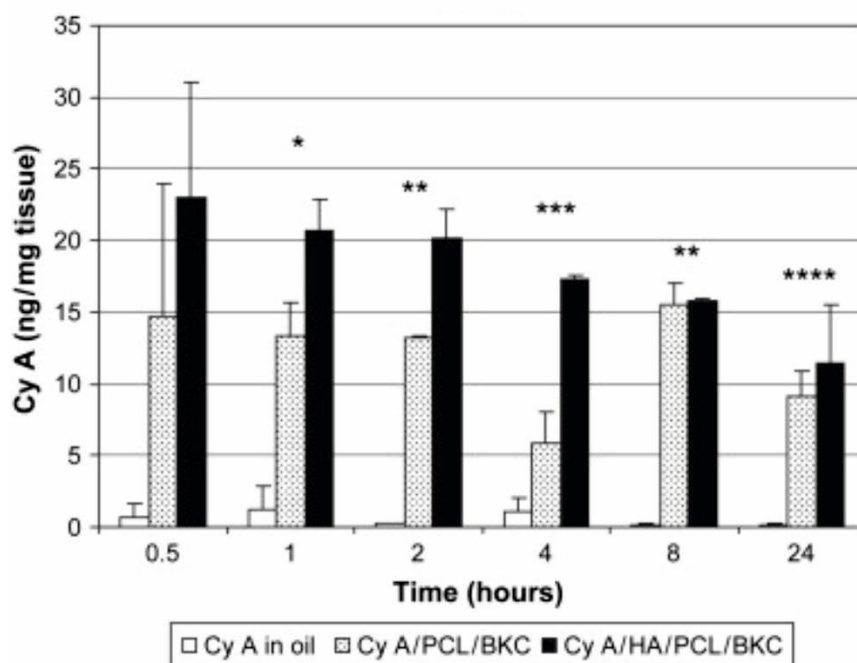

Figure 11. CyA concentration in rabbit corneas. 25 μl of CyA formulation was applied four times with a delay of ten minutes in between applications to both eyes of New Zealand rabbits. Samples were obtained following the last instillation. Corneal CyA levels were significantly higher for the NP formulation composed of poly-ε-caprolactone and benzalkonium chloride (CyA/PCL/BKC) compared to that of the castor oil formulation (CyA in oil). If the NPs were modified with HA 1000 kDa (CyA/HA/PCL/BKC), corneal CyA accumulation exhibited further increase. With permission taken from [111].

Similar results concerning corneal CyA concentrations were observed for nano-sized microgels formed *in situ* [110]. Thermoresponsive N-isopropylacrylamide was grafted to 11 kDa HA to combine the unique properties of both polymers. An increase in temperature to a value greater than the critical solution temperature of the polymer, upon application of the eye drops, led to the formation of microgels. Corneal CyA levels reached their maximum value two hours after application and were 6-fold higher than those of the castor oil formulation. Ibrahim et al. have also demonstrated use of HA's mucoadhesive properties [109]. They prepared NPs from Eudragit, a commercial available polymer for the fabrication of sustained release dosage forms, and loaded them with gatifloxacin and prednisolone.

These NPs were able to release their antibiotic and anti-inflammatory payloads over a period of up to ten hours *in vitro*, depending on their composition. In order to benefit clinically from this sustained drug release, NPs must also remain on the ocular surface for an extended period of time. Consequently, the authors coated their NPs with HA. With this HA-modified NP formulation, the corneal bioavailability of gatifoxacin was increased to 28 μg*hour/g compared to only 3.6 μg*hour/g for commercial eye drops.

Instead of using NPs to simply retard lacrimal drainage of a drug substance, they can also serve as a vehicle for delivering diverse therapeutic agents into corneal epithelial cells. In order to succeed as an intracellular drug delivery vehicle, NPs must reach their target cells without being hindered by components of the ocular surface. Additionally, they must be stable until entering the cell, at which point they must be able to release their cargo. Hornof and de la Fuente, for example, exploited HA as a targeting moiety for delivery of genetic material into cells of the cornea and conjunctiva [115]. In general, complexation of DNA with polyethyleneimine (PEI) yields acceptable transfection efficiencies due to the cationic charge of the complexes and their endosomolytic properties. However, blood proteins or ECM-components as proteoglycans or glycoproteins tend to adsorb onto the complexes and limit their ability to interact with cell membranes. By coating the complexes with low MW HA, nonspecific binding of proteins and other anionic compounds was reduced and stability of the complexes was increased. Despite the negative surface charge of the HA-coated complexes, and their concomitantly reduced affinity to cell membranes, uptake and transfection efficiency into human corneal epithelia cells was similar to the uncoated control. *In vitro*, beta-galactosidase expression was increased by a factor of 10 to 15 compared with naked DNA. This result is surprising, as positively charged particles, such as uncoated polyplexes (complexes of anionic nucleic acids and polycations), are known to be significantly more effective at transfection than neural or anionic particles. By antibody-mediated blockade of CD44 on the cellular surface, the group also showed that uptake must be a receptor-mediated process.

In addition, the therapeutic potential of DNA-loaded HA-chitosan NPs was analyzed *in vitro* [116]. Here, higher HA content increased transfection efficiency in proliferative ocular cell lines (human corneal and conjunctival epithelia). Again, a connection between NP uptake and CD44 binding was found. *In vivo* experiments demonstrated the efficacy of this formulation after topical application to rabbit eyes [114]. Beside receptor-specific interactions, the general mucoadhesive properties of HA might promote NP uptake after

topical application. At therapeutic doses, *in vitro* toxicity of this delivery system is exceedingly low [116]. Tolerability and safety was further confirmed *in vivo* [112].

A key benefit of incorporating HA into this type of NP formulation is its influence on the mechanism of cellular entry and intracellular targeting [113]. Often, particles are trapped within endosomes and lysosomes after internalization. This might cause degradation of the NP cargo and a loss in functionality. However, HA-chitosan-oligomer NPs were internalized by a receptor-mediated, caveolin-dependent internalization process *in vitro*, bypassing the cellular compartments dedicated to degradation and resulting in high transfection efficiencies for ocular surface epithelial cells.

Macroscopic drug delivery systems

Beside working on eye drops and NPs, efforts have been made to develop drug delivery systems in order to achieve a sustained liberation and dissolution of drug substances to the cornea and conjunctiva.

Hume et al. succeeded in producing HA-based films for sustained delivery of the anti-inflammatory steroid prednisolone [125]. They esterified HA with varying amounts of benzyl alcohol to obtain polymers with different degrees of hydrophilicity that were suitable for producing drug-loaded films. Higher degrees of esterification resulted in enhanced hydrophobicity and diminished polymer swelling capacity. HA derivatives with the highest hydrophobicity (100 % of carboxyl groups esterified) enabled the best drug release characteristics, with constant lacrimal prednisolone levels of 45-72 µg/mL over 24 h in rabbits. The Calles group developed HA-itaconic acid films, crosslinked with polyethylene glycol diglycidyl ether, that show excellent material properties and good biocompatibility *in vitro* and *in vivo* [124]. Timolol, a substance which reduces the production of AH in the ciliary body and lowers IOP, was physically incorporated into the film during manufacturing. A therapeutic effect on IOP could be observed for more than ten hours, as opposed to eight hours for the conventional eye drop formulation (Figure 12). Since this finding is significant but clinically not relevant, it remains to be seen whether the lengthened time of therapeutic impact is worth the difficult handling of the insert in this specific case.
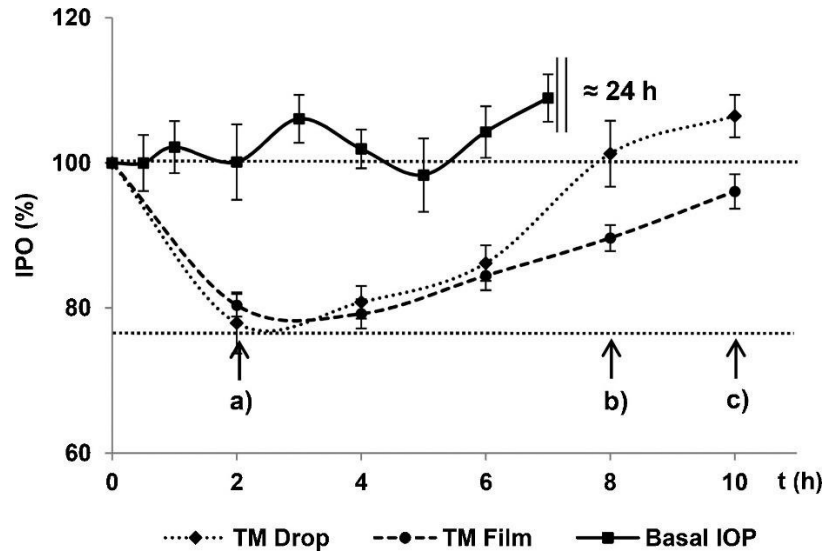
Figure 12. IOP of rabbits after the administration of timolol as an eye drop formulation (TM Drop) or as an ocular insert (TM Film). The lowest IOP was observed two hours after application for both formulations (a). After eight hours, IOP reached the baseline value in the eye drop group (b) whereas it took additional two hours in the insert group (c). With permission taken from [124].

Possibly more common – as already known and applied by millions of people for vision correction - are contact lenses (CL). It has been shown that this approach is not only suitable for the sustained delivery of small MW drugs but also for polymers such as HA [121,122]. An example is the strategy of biomimetic, molecular imprinting as shown in Figure 13A [123]. Here, modified Nelficon A – a polyvinyl alcohol derivative – was crosslinked with UV-crosslinking monomers. The particular monomers used were chosen because of their chemical similarity to amino acids found at the HA-binding site of CD44. The hypothesis was that these monomers would generate a template for directed interactions between the hydrogel scaffold and the HA-polymer within the CL when the crosslinking reaction takes place in presence of HA. HA would have higher affinity for such "memory sites", which would slow down release. Using this approach, CL with an HA dissolution profile of 6 μg/hour over 24 hours was achieved, matching therapeutic doses. While such CL are suitable for long-term supply of the ocular surface with HA, incorporation of HA into CL can be applied more generally to improve wettability of the lens material and increase the comfort to wear. Other groups pursued this goal and fixed HA within the CL material, either by creating a crosslinked HA network within the CL, as in Figure 13B [117,120], or by covalent grafting of HA to the polymeric CL compounds, as in Figure 13C [118]. Beside higher hydrophilicity and wettability, this resulted in decreased adsorption and denaturation of proteins on the CL surface. Depending on the strategy of HA functionalization, the sorption of lysozyme was reduced to only 5 to 70 % compared to that of the unmodified

control. This reduces the risk of developing inflammatory eye diseases [119] and provides for the opportunity of an extended wearing time.
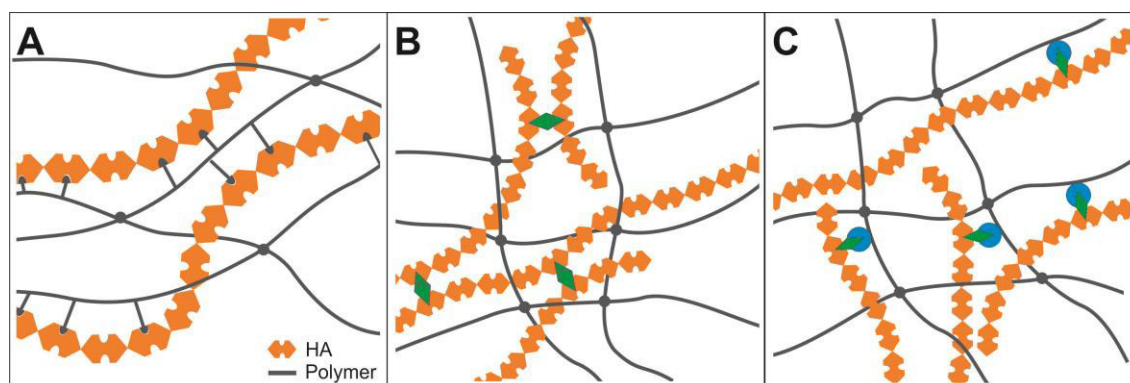

Figure 13. Immobilization of HA in CL material. A) Molecular imprinting; directed interactions between HA and "memory sites" of the hydrogel scaffold. B) HA-crosslinking; fixation of HA due to convolution of individually crosslinked HA- and polymer network. C) Covalent linkage; immobilization of HA by covalent grafting to the polymer.

4.2　Intracameral administration

Related to the aforementioned CL, Wang et al. extended HA incorporation to produce modified intraocular lenses (IOL), which are used for cataract patients [126]. IOLs are artificial lenses that substitute the natural lens if it becomes cloudy or damaged. Common side effects of the surgical implantation procedure are opacification of the new lens as well as inflammation and infection. To overcome these effects, Wang et al. covalently grafted an HA-lysozyme composite to the surface of the IOL, providing it with anti-adhesive and antibacterial properties. HA modification appeared to reduce adsorption of lens epithelial cells and prevented opacification. Additionally, fewer bacteria adhered to the implant compared with the unmodified lenses. Lysozyme, a lytic enzyme which is naturally present in tear fluid, kills remaining bacteria and therefore prevents the spread of microorganisms, reducing the risk of developing sight-threatening infections. The efficacy of this approach was measured via fluorescence microscopy.

4.3　Intravitreal administration

Vitreous substitution

HA has also been extensively investigated as a vitreous substitute. Vitreous substitution is required during vitro-retinal surgery or in cases where the retina detaches from the RPE, as

in DR. Conventional tamponade agents are inert gases, silicon oil or perfluorocarbon liquids [146–148]. However, these materials have significant disadvantages. Gases work for just a short period during and after surgery as they are rapidly absorbed by the bloodstream. Additionally, they might cause sight-threatening elevations of IOP under certain conditions. Due to their toxicity, perfluorocarbon liquids are used only during the surgical intervention itself, and not afterward. Silicon oils are suitable for long-term vitreous replacement but must eventually be removed, as glaucoma, cataracts and other complications have been reported. During this procedure, retinal re-detachment can also be induced. HA is a promising substitute as a result of its good biocompatibility – it is the principal component of the vitreous humor – its easy injectability and its biodegradability. Unfortunately, the process of degradation happens very rapidly, as total vitreal HA is replaced every 10 to 70 days (see "anatomy section") [78]. In response, HA derivatives with slower biodegradation kinetics were developed.

Crosslinking of HA with adipic dihydrazide or N-vinyl-pyrrolidinone / UV light reduced biodegradation *in vitro* to 10 % within the first four weeks, and with even slower degradation kinetics after that point [12]. UV-crosslinked hydrogels did not show any signs of toxicity in cell culture experiments and were well-tolerated after implantation in the vitreous cavity of rabbits. The vitreous substitutes were stable for more than six weeks and their optical and mechanical properties remained almost unchanged. Grafting of a thermogelling poloxamer F127 to HA resulted in a vitreous substitute that was readily injectable at room temperature and with properties reasonably well-matched to those of the vitreous upon gelation at 37 °C [127]. However, these graft copolymers were unable to provide the needed rheological and mechanical characteristics nor to slow degradation kinetics required for long term use [146].

As already outlined, a general problem of all biomaterials of natural origin – including HA-based vitreous substitutes - is a significant batch-to-batch variation. Therefore, synthetic polymers such as polyethylene glycol (PEG) derivatives, polymethacrylates and polyurethanes have been developed for this purpose. They combine reasonable rheological and refractive properties with high reproducibility and consistent quality.

NP formulations

If therapeutics must reach the posterior segment of the eye, application via eye drops is unsatisfactory, as the drug is required to cross several barriers and traverse relatively long distances [149]. Intravitreal injection represents one possibility for specific administration to this difficult to access area of the eye. Even then, applied substances must diffuse through

the vitreous cavity to reach their target. Xu et al. investigated the general factors influencing NP mobility in the vitreous body by multiple particle tracking on a fluorescence microscope [150] and found dependencies on NP colloidal stability, particle size, surface charge and concentration. Neutral, PEGylated NPs that tend not to interact with components of the vitreous humor are able to diffuse freely up to a size of 510 nm (Figure 14). Negatively charged NPs are hampered in their mobility if they are larger than 200 nm or if the concentration exceeds a certain threshold. Cationic particles in turn are fully immobile, independent of size or concentration. They stick to anionic vitreal collagen fibrils via electrostatic interactions and might only be considered therapeutically if drug release at the site of injection is required.
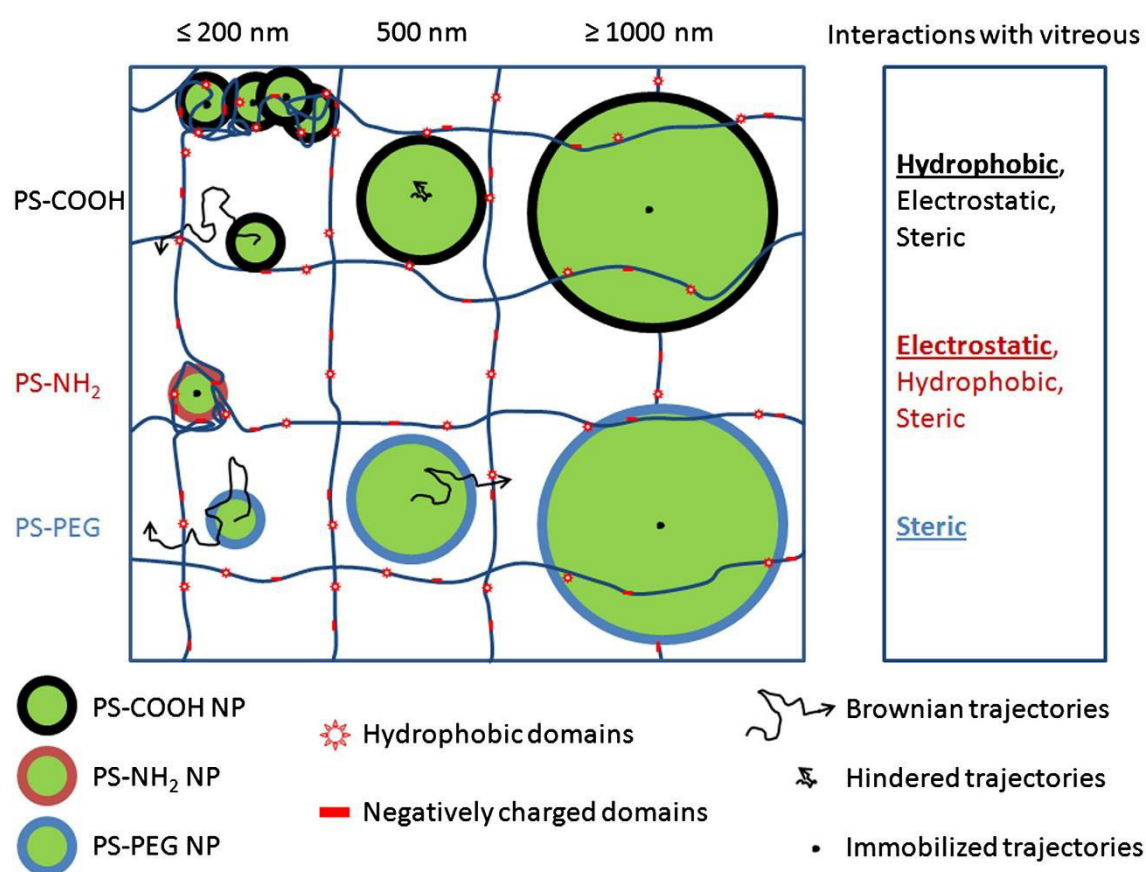

Figure 14. Influence of surface charge, size and concentration of NPs on their mobility in the vitreous body. Electrostatic, steric and hydrophobic effects influence the diffusivity of NPs in the vitreous gel. PEGylated particles (PS-PEG) are able to diffuse freely up to a size of 500 nm. Anionic NPs (PS-COOH) smaller than 200 nm move unimpeded. If their size or concentration increases, diffusivity is reduced due to steric and hydrophobic effects. Cationic polystyrene-amine NPs (PS-NH2) interact electrostatically and aggregate within the vitreous. With permission taken from [150].

PEGylation of NPs reduces aggregation and nonspecific binding to ECM components and enhances the diffusivity of particles in the vitreous [151]. Unfortunately, in addition to reducing undesirable interactions, interactions with target cells and tissues are also reduced [152]. A possible solution could be the modification or coating of nanostructures with HA to enhance NP mobility in the vitreous without reducing cellular uptake or transfection efficiency. The movement of different types of NPs through the vitreous and retina was investigated by Koo et al. [130]. HA-NPs of about 200 nm in size with a negative surface charge of -26 mV diffused through the vitreal gel and accumulated in deeper regions of the retina following intravitreal injection. PEI-modified NPs (+ 33 mV) with a slightly larger size were almost completely immobile. Interestingly, the HA-NPs seemed to be eliminated from the posterior segment within a few days, which might be a beneficial property for candidate therapeutics. Further detailed investigations concerning the mobility and functionality of polyplexes were carried out by Martens et al. [129]. Martens determined the diffusion coefficients of polyplexes functionalized with HA of varying molecular weight by fluorescent particle tracking microscopy in excised bovine eyes. The unmodified probe (108 nm, +29 mV) reflects the reduced mobility of positively charged complexes in the vitreous (Figure 15). Diffusivity increased upon functionalization with HA and displayed the most improvement when modified with 137 kDa HA. Although the particles became larger (343 nm), the negative surface charge of -30 mV and the antifouling properties of HA seem to adequately compensate for the increase in size. HA 2700 kDa was not suitable as a diffusivity enhancer here, as the resulting particles became too large and aggregated.
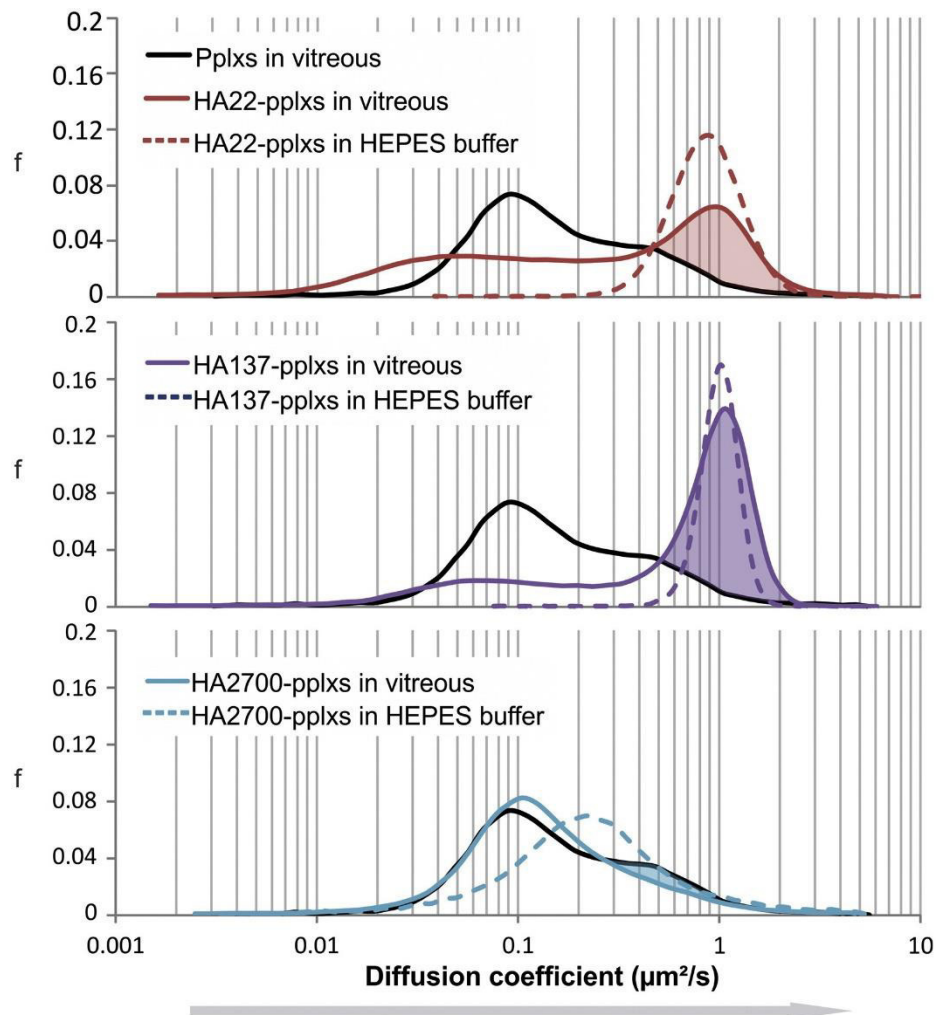
Figure 15. Diffusion coefficients of polyplexes obtained by single particle tracking analysis in intact bovine vitreous. The strongest increase in diffusivity was found for polyplexes coated with HA 137 kDa (HA137-pplxs); no improvement was achieved with HA 2700 kDa (HA2700-pplxs). The black, solid line represents the bimodal distribution of diffusion coefficients of uncoated, cationic polyplexes. The mobilities of the respective NP in HEPES-buffer are shown as dotted lines. With permission taken from [129].

Further *in vitro* experiments confirmed both the polyplexes' ability to enter RPE cells via interactions with CD44 and their superlative cell transfection capabilities. Similar results were achieved by Gan et al. [128], who modified chitosan-lipo-NP (chitosan-NP capped with a lipid bilayer) with HA of different MW. The modified NP were able to diffuse freely through the vitreous and accumulated on the inner limiting membrane following intravitreal injection. In a model of retinal damage – experimental autoimmune uveitis – the group found that these HA-modified chitosan-lipo-NP were even able to specifically target the RPE, as CD44 is upregulated in this disease.

4.4   Retinal administration

Retinal patches

During aging, compounds of the vitreous body become liquefied and collagen fibrils change their structure, forming bundles and becoming stiffer [153]. The tension on the retina increases and begins to peel the sensitive structure from the back of the eye, which may lead to impaired vision or blindness. Patients suffering from diabetes typically show faster liquefaction and run a higher risk of retinal detachment [154]. Holes and breaks in the retina accelerate the shedding, allowing vitreous fluid to leak into the subretinal space [155]. Therefore, it is critically important to seal retinal breaks and prevent the accumulation of fluids. Common options for the treatment of such breaks are laser-induced retinal fixation or the administration of anti-inflammatory steroids. Another possibility is the application of gel-like retinal patches. Sueda et al. developed an absorbable material based on HA and carboxymethylcellulose to close retinal breaks [132]. The patch was liquid-tight and stayed in place for 30 days on retinas of excised bovine eyes. No signs of toxicity were observed *in vivo*. Unfortunately, its application during vitrectomy surgery is quite difficult. In order to enhance the therapeutic effectiveness of retinal patches, 1,2,3,4-diepoxybutane crosslinked HA gels were prepared and loaded with triamcinolone acetonide [131]. This combined the retina stabilizing effect of a self-adhesive patch with the local delivery of an anti-inflammatory agent. The gel was directly applied to the retinal injury via an injector system, a special kind of syringe. While the application process was still challenging, the patch was well-tolerated during initial trials and the approach is a promising therapeutic option to reduce retinal inflammation and accelerate healing.

Hydrogels for protein and stem cell delivery

Aside from small molecule drugs and genetic material, proteins represent a further opportunity in the treatment of ocular diseases. This therapeutic option has garnered intense interest, especially for CNV. Vascular endothelial growth factor (VEGF) contributes decisively to the development and progress of this disease, as it is known to boost proliferation of vascular endothelial cells and formation of new blood vessels [156]. Perhaps the most well-known of therapeutics in this field are biologics which inhibit the binding of VEGF to its receptor, such as the antibodies ranibizumab (Lucentis®) and bevacizumab (Avastin® - off label), or the recombinant fusion protein aflibercept (Eylea®). Anti-Flt1-peptide is another candidate, a short, non-immunogenic hexapeptide that acts because of an

antagonistic effect on VEGF receptor 1 (VEGFR1). By chemical conjugation of HA to this peptide, its potency could be improved [157], possibly due to the formation of micelle-like NP in aqueous solution and improved solubility. After a single intravitreal injection, the severity of CNV lesions was reduced by 20 percent, the effect on the reduction of vascular hyperpermeability was even stronger compared to the unmodified peptide.

Kontturi et al. extended this approach a step further by incorporating genetically modified RPE cells (ARPE-19), which secrete soluble VEGFR1, into a hydrogel of cross-linked collagen and HA [135]. This matrix promoted cellular survival and protein secretion for at least 50 days and may prevent the need for frequent application of the therapeutic protein. However, even if delivery of anti-VEGF-therapeutics slows down the progress of the disease, damaged cells are not replaced. Retinal stem-progenitor cells can differentiate into many kinds of retinal cells, including neurons and pigment epithelial cells. Ballios et al. developed an injectable, biodegradable hydrogel scaffold consisting of HA and methylcellulose (MC) for the successful delivery of stem cells to the sub-retinal space [134]. The polymers combine biocompatibility and anti-inflammatory properties with sufficient stability to support the application. In this way, applied stem cells distributed well in the sub-retinal space, overcoming previous obstacles. To refine this approach, the HA-MC hydrogel was modified to serve as a delivery system for insulin-like growth-factor 1 (IGF-1) and cells at the same time [133]. Following a molecular imprinting strategy, two different peptides with weak and strong binding affinity to IGF-1 were conjugated covalently to the hydrogel. Thus, a sustained release of the growth factor was achieved and the viability of embedded RPE cells promoted *in vitro*. However, it was not reported whether or not IGF-1 promotes further neovascularization, an open question that must be subject of future investigations.

5 Summary and conclusion

Taken together, HA is an extremely promising polymer for a wide array of biomedical applications. HA combines a number of unique biochemical properties: the ability to bind enormous amounts of water because of its extraordinary hydrophilicity, viscosity enhancement of aqueous solutions at low concentration, pseudoplastic flow characteristics, and accessible reactive groups along the polysaccharide chain for easy crosslinking and/or grafting to other compounds [158]. Since HA is an endogenous component present in most tissues of the body, it is well tolerated and toxicity issues are largely unheard of.

In this review we have focused on the ophthalmic applications of HA – an exceptionally promising area of clinical use. HA is thought to be an ideal excipient for this purpose, as given its naturally high concentration in the eye, and concomitantly good ocular tolerability. Furthermore, its transparency and other optical properties are suitable for use in the optical path. Topically applied, HA is used in eye drops as either a therapeutic ingredient itself or to increase the tolerability and efficacy of other drugs. When incorporated into CL, ocular comfort was enhanced and wearing time was extended. As the principal component of the vitreous humor, the polymer was additionally investigated for suitability as a vitreous substitute. In this special case, the fact that HA is an endogenous compound was unfortunately counterproductive, as biodegradation by hyaluronidases occurred too rapidly for long-term use. HA-modified NPs were also investigated for their therapeutic potential in the ocular environment after extensive investigation regarding their potential for cancer therapy. The mucoadhesive properties of the polymer are paramount if NPs are applied topically to the ocular surface. However, after intravitreal injection, HA's capability to inhibit protein adsorption, promote high mobility through the collagen matrix and target cells in the posterior segment of the eye are of greater interest. HA has also been assessed in a variety of forms for its ability to deliver therapeutic proteins or cells.

In some clinical applications, HA has been employed to relieve debilitating symptoms for many years, and presently forms an integral part of the standard treatment regime. Other approaches proposed are more speculative in nature; significant work must still occur to bring these ideas from bench to bedside. Nevertheless, with increasing scientific interest – and consequently, a steady uptick in the accumulated knowledge surrounding HA's properties and multiform modes of use – it is becoming increasingly apparent that both novel HA-based therapeutics and HA-mediated refinements of existing approaches deserve to be pursued into the clinic.

References

[1] Zhang K, Zhang L, Weinreb RN (2012), Ophthalmic drug discovery: novel targets and mechanisms for retinal diseases and glaucoma, Nat Rev Drug Discov 11 541–559.

[2] Abdelkader H, G. Alany R (2012), Controlled and Continuous Release Ocular Drug Delivery Systems: Pros and Cons, CDD 9 421–430.

[3] Eandi CM, Alovisi C, Sanctis U de, Grignolo FM (2016), Treatment for neovascular age related macular degeneration: The state of the art, Eur J Pharmacol

[4] Kirchhof S, Goepferich AM, Brandl FP (2015), Hydrogels in ophthalmic applications, Eur J Pharm Biopharm 95 227–238.

[5] Solinís MÁ, del Pozo-Rodríguez A, Apaolaza PS, Rodríguez-Gascón A (2015), Treatment of ocular disorders by gene therapy, Eur J Pharm Biopharm 95 331–342.

[6] Kim YC, Chiang B, Wu X, Prausnitz MR (2014), Ocular delivery of macromolecules, J Control Release 190 172–181.

[7] Carvalho IM, Marques CS, Oliveira RS, Coelho PB, Costa PC, Ferreira DC (2015), Sustained drug release by contact lenses for glaucoma treatment—A review, J Control Release 202 76–82.

[8] Delplace V, Payne S, Shoichet M (2015), Delivery strategies for treatment of age-related ocular diseases: From a biological understanding to biomaterial solutions, J Control Release 219 652–668.

[9] Sze JH, Brownlie JC, Love CA (2016), Biotechnological production of hyaluronic acid: a mini review, 3 Biotech 6.

[10] Liu L, Liu Y, Li J, Du G, Chen J (2011), Microbial production of hyaluronic acid: current state, challenges, and perspectives, Microb Cell Fact 10 99.

[11] Clegg TE, Caborn D, Mauffrey C (2013), Viscosupplementation with hyaluronic acid in the treatment for cartilage lesions: a review of current evidence and future directions, Eur J Orthop Surg Tr 23 119–124.

[12]   Schramm C, Spitzer MS, Henke-Fahle S, Steinmetz G, Januschowski K, Heiduschka P, Geis-Gerstorfer J, Biedermann T, Bartz-Schmidt KU, Szurman P (2012), The Cross-linked Biopolymer Hyaluronic Acid as an Artificial Vitreous Substitute, Invest Ophth Vis Sci 53 613–621.

[13]   Collins MN, Birkinshaw C (2013), Hyaluronic acid based scaffolds for tissue engineering—A review, Carbohyd Pol 92 1262–1279.

[14]   Ossipov DA (2010), Nanostructured hyaluronic acid-based materials for active delivery to cancer, Expert Opin Drug Del 7 681–703.

[15]   Dosio F, Arpicco S, Stella B, Fattal E (2016), Hyaluronic acid for anticancer drug and nucleic acid delivery, Adv Drug Deliver Rev 97 204–236.

[16]   Xu K, Lee F, Gao SJ, Chung JE, Yano H, Kurisawa M (2013), Injectable hyaluronic acid-tyramine hydrogels incorporating interferon-α2a for liver cancer therapy, J Control Release 166 203–210.

[17]   Ueda K, Akiba J, Ogasawara S, Todoroki K, Nakayama M, Sumi A, Kusano H, Sanada S, Suekane S, Xu K, Bae KH, Kurisawa M, Igawa T, Yano H (2016), Growth inhibitory effect of an injectable hyaluronic acid–tyramine hydrogels incorporating human natural interferon-α and sorafenib on renal cell carcinoma cells, Acta Biomater 29 103–111.

[18]   Xu K, Lee F, Gao S, Tan M-H, Kurisawa M (2015), Hyaluronidase-incorporated hyaluronic acid–tyramine hydrogels for the sustained release of trastuzumab, J Control Release 216 47–55.

[19]   Lei Y, Rahim M, Ng Q, Segura T (2011), Hyaluronic acid and fibrin hydrogels with concentrated DNA/PEI polyplexes for local gene delivery, J Control Release 153 255–261.

[20]   Mero A, Campisi M (2014), Hyaluronic Acid Bioconjugates for the Delivery of Bioactive Molecules, Polymers 6 346–369.

[21]   Meyer K, Palmer, John, W. (1934), The Polysaccharide of the Vitrous Humor, J Biol Chem 107 629–634.

[22]   Stern R (2004), Hyaluronan catabolism: a new metabolic pathway, Eur J Cell Biol 83 317–325.

[23]   Tripodo G, Trapani A, Torre ML, Giammona G, Trapani G, Mandracchia D (2015), Hyaluronic acid and its derivatives in drug delivery and imaging: Recent advances and challenges, Eur J Pharm Biopharm 97 400–416.

[24]   Liao Y-H, Jones SA, Forbes B, Martin GP, Brown MB (2008), Hyaluronan: Pharmaceutical Characterization and Drug Delivery, Drug Deliv 12 327–342.

[25]   Toole BP (2004), Hyaluronan: from extracellular glue to pericellular cue, Nat Rev Cancer 4 528–539.

[26]   Karbownik MS, Nowak, Jerzy, Z. (2013), Hyaluronan: Towards novel anti-cancer therapeutics, Pharmacol Rep 65 1056–1074.

[27]   Fouissac E, Milas M, Rinaudo M (1993), Shear-rate, concentration, molecular weight, and temperature viscosity dependences of hyaluronate, a wormlike polyelectrolyte, Macromolecules 26 6945–6951.

[28]   Laurent TC, Laurent UBG, Fraser, J Robert E (1996), The structure and function of hyaluronan: An overview, Immunol Cell Biol 74 A1-A7.

[29]   Arpicco S, Milla P, Stella B, Dosio F (2014), Hyaluronic Acid Conjugates as Vectors for the Active Targeting of Drugs, Genes and Nanocomposites in Cancer Treatment, Molecules 19 3193–3230.

[30]   Girish KS, Kemparaju K (2007), The magic glue hyaluronan and its eraser hyaluronidase: A biological overview, Life Sci 80 1921–1943.

[31]   Day AJ, Prestwich GD (2002), Hyaluronan-binding Proteins: Tying Up the Giant, J Biol Chem 277 4585–4588.

[32]   Goodison S, Urquidi V., Tarin D (1999), CD44 cell adhesion molecules, Mol Pathol 52 189–196.

[33]   Banerji S, Wright AJ, Noble M, Mahoney DJ, Campbell ID, Day AJ, Jackson DG (2007), Structures of the Cd44–hyaluronan complex provide insight into a fundamental carbohydrate-protein interaction, Nat Struct Mol Biol 14 234–239.

[34]   Lesley J (2000), Hyaluronan Binding by Cell Surface CD44, J Biol Chem 275 26967–26975.

[35]   Mizrahy S, Raz SR, Hasgaard M, Liu H, Soffer-Tsur N, Cohen K, Dvash R, Landsman-Milo D, Bremer MG, Moghimi SM, Peer D (2011), Hyaluronan-coated nanoparticles: The influence of the molecular weight on CD44-hyaluronan interactions and on the immune response, J Control Release 156 231–238.

[36]   Knudson W, Chow G, Knudson CB (2002), CD44-mediated uptake and degradation of hyaluronan, Matrix Biology 21 15–23.

[37]   Platt VM, Szoka FC (2008), Anticancer Therapeutics: Targeting Macromolecules and Nanocarriers to Hyaluronan or CD44, a Hyaluronan Receptor, Mol Pharm 5 474–486.

[38]   Toole BP (2009), Hyaluronan-CD44 Interactions in Cancer: Paradoxes and Possibilities, Clin Cancer Res 15 7462–7468.

[39]   Choi KY, Saravanakumar G, Park JH, Park K (2012), Hyaluronic acid-based nanocarriers for intracellular targeting: Interfacial interactions with proteins in cancer, Colloid Surface B 99 82–94.

[40]   Xu X, Jha AK, Harrington DA, Farach-Carson MC, Jia X (2012), Hyaluronic Acid-Based Hydrogels: from a Natural Polysaccharide to Complex Networks, Soft Matter 8 3280–3294.

[41]   Kogan G, Šoltés L, Stern R, Gemeiner P (2006), Hyaluronic acid: a natural biopolymer with a broad range of biomedical and industrial applications, Biotechnol Lett 29 17–25.

[42]   Streilein JW (2003), Ocular immune privilege: therapeutic opportunities from an experiment of nature, Nat Rev Immunol 3 879–889.

[43]   Cholkar K, Patel SP, Vadlapudi AD, Mitra AK (2013), Novel Strategies for Anterior Segment Ocular Drug Delivery, J Ocul Pharm Th 29 106–123.

[44]   Remington LA (Ed.), Clinical Anatomy and Physiology of the Visual System: Chapter 6: Aqueous and Vitreous Chambers, Second Edition ed., Elsevier Inc., 2005.

[45]   Goel M, Picciani RG, Lee RK, Bhattacharya SK (2010), Aqueous Humor Dynamics: A Review, The Open Ophthal J 4 52–59.

[46]   Nickerson CS, Park J, Kornfield JA, Karageozian H (2008), Rheological properties of the vitreous and the role of hyaluronic acid, J Biomech 41 1840–1846.

[47]   Remington LA (Ed.), Clinical Anatomy and Physiology of the Visual System: Chapter 4: Retina, Second Edition ed., Elsevier Inc., 2005.

[48]   Bringmann A, Pannicke T, Grosche J, Francke M, Wiedemann P, Skatchkov S, Osborne N, Reichenbach A (2006), Müller cells in the healthy and diseased retina, Prog Retin Eye Res 25 397–424.

[49]   Strauss O (2005), The Retinal Pigment Epithelium in Visual Function, Physiolog Rev 85 845–881.

[50]   Zhu S-N, Nölle B, Duncker G (1997), Expression of adhesion molecule CD44 on human corneas, Brit J Ophthalmol 81 80–84.

[51]   Lerner LE, Schartz Daniel M., Hwang DG, Howes EL, Stern R (1998), Hyaluronan and CD44 in the Human Cornea and Limbal Conjunctiva, Exp Eye Res 67 481–484.

[52]   Yu FX, Guo J, Zhang Q (1998), Expression and Distribution of Adhesion Molecule CD44 in Healing Corneal Epithelia, Invest Ophthal Vis Sci 39 710–717.

[53]   García-Posadas L, Contreras-Ruiz L, López-García A, Villarón Álvarez S, Maldonado MJ, Diebold Y (2012), Hyaluronan receptors in the human ocular surface: a descriptive and comparative study of RHAMM and CD44 in tissues, cell lines and freshly collected samples, Histochem Cell Biol 137 165–176.

[54]   García-Posadas L, Contreras-Ruiz L, Arranz-Valsero I, López-García A, Calonge M, Diebold Y (2014), CD44 and RHAMM hyaluronan receptors in human ocular surface inflammation, Graefes Arch Clin Exp Ophthalmol 252 1289–1295.

[55]   Nishida T, Nakamura M, Mishima H, Otori T (1991), Hyaluronan Stimulates Corneal Epithelial Migration, Exp Eye Res 53 753–758.

[56]   Gomes, J A P (2004), Sodium hyaluronate (hyaluronic acid) promotes migration of human corneal epithelial cells in vitro, Brit J Ophthalmol 88 821–825.

[57]   Pauloin T, Dutot M, Joly F, Warnet J-M, Rat P (2009), High molecular weight hyaluronan decreases UVB-induced apoptosis and inflammation in human epithelial corneal cells, Mol Vis 15 577–583.

[58]   Miyauchi S, Morita M, Kuramoto K, Horie K (1996), Hyaluronan and chondroitin sulfate in rabbit tears, Curr Eye Res 15 131–135.

[59]   Frescura M, Berry M, Corfield A, Carrington S, Easty DL (1994), Evidence of hyaluronan in human tears and secretions of conjunctival cultures, Biochm Soc Trans 22 228S.

[60]   Laurent UB (1981), Hyaluronate in aqueous humour, Exp Eye Res 33 147–155.

[61]   Acott TS, Kelley MJ (2008), Extracellular matrix in the trabecular meshwork, Exp Eye Res 86 543–561.

[62]   Lerner LE, Polansky JR, Howes EL, Stern R (1997), Hyaluronan in the Human Trabecular Meshwork, Invest Ophthalmol Vis Sci 38 1222–1228.

[63]   Gong H, Underhill CB, Freddo TF (1994), Hyaluronan in the Bovine Ocuar Anterior Segment, With Emphasis on the Outflow Pathways, Invest Ophthalmol Vis Sci 35 4328–4332.

[64]   Navajas EV, Martins, João Roberto Maciel, Melo, Luiz Alberto S., Saraiva VS, Dietrich CP, Nader HB, Belfort R (2005), Concentration of hyaluronic acid in primary open-angle glaucoma aqueous humor, Exp Eye Res 80 853–857.

[65]   Jumper JM, Chang DF, Hoyt CS, Hall JL, Stern R, Schwartz DM (1997), Aqueous hyaluronic acid concentration: comparison in pediatric and adult patients, Curr Eye Res 16 1069–1071.

[66]   Budak YU, Akdogan M, Huysal K (2009), Aqueous humor level of sCD44 in patients with degenerative myopia and primary open-angle glaucoma, BMC Res Notes 2 224.

[67]   Knepper PA, Miller AM, Choi J, Wertz RD, Nolan MJ, Goossens W, Whitmer S, Yue, Beatrice Y. J. T., Ritch R, Liebmann JM, Allingham RR, Samples JR (2005), Hypophosphorylation of Aqueous Humor sCD44 and Primary Open-Angle Glaucoma, Invest Ophthalmol Vis Sci 46 2829–2837.

[68]   Nolan MJ, Giovingo MC, Miller AM, Wertz RD, Ritch R, Liebmann JM, Allingham RR, Herndon LW, Wax MB, Smolyak R, Hasan F, Barnett EM, Samples JR, Knepper PA (2007), Aqueous Humor sCD44 Concentration and Visual Field Loss in Primary Open-angle Glaucoma, J Glaucoma 16 419–429.

[69]   Koralewska-Makar A, Molander N, Madsen K, Lind M-L, Stenevi U, Ehinger B (1998), Endogenous hyaluronan in the normal and traumatized rabbit iris, Acta Ophthalmol Scand 76 391–395.

[70]   Desai VD, Wang Y, Simirskii VN, Duncan MK (2010), CD44 expression is developmentally regulated in the mouse lens and increases in the lens epithelium after injury, Differentiation 79 111–119.

[71]   Kulyk WM, Zalik SE, Dimitrov E (1987), Hyaluronic Acid Production and Hyaluronidase Activity in the Newt Iris during Lens Regeneration, Exp Cell Res 172 180–191.

[72]   Koralewska-Makár A, Johnsson C, Bruun A, Stenevi U, Ehinger B (2003), COX-2 Inhibitors Prolong Trauma-Induced Elevations of Iris Hyaluronan, J Ocul Pharmacol Th 19 385–395.

[73]   Nishi O, Nishi K, Akaishi T, Shirasawa E (1997), Detection of Cell Adhesion Molecules in Lens Epithelial Cells of Human Cataracts, Invest Ophthalmol Vis Sci 38 579–585.

[74]   Bishop PN (2000), Structural macromolecules and supramolecular organisation of the vitreous gel, Prog Ret Eye Res 19 323–344.

[75]   Kuppermann BD, Thomas EL, Smet MD de, Grillone LR (2005), Pooled efficacy results from two multinational randomized controlled clinical trials of a single intravitreous injection of highly purified ovine hyaluronidase (Vitrase) for the management of vitreous hemorrhage, Am J Ophthalmol 140 573–584.

[76]   Filas BA, Zhang Q, Okamoto RJ, Shui Y-B, Beebe DC (2014), Enzymatic Degradation Identifies Components Responsible for the Structural Properties of the Vitreous Body, Invest Ophthalmol Vis Sci 55 55.

[77]   Schwartz DM, Shuster S, Jumper MD, Chang A, Stern R (1996), Human vitreous hyaluronidase: isolation and characterization, Curr Eye Res 15 1156–1162.

[78]   Laurent UB, Reed RK (1991), Turnover of hyaluronan in the tissues, Adv Drug Deliver Rev 7 237–256.

[79]   Normand G, Hicks D, Dreyfus H (1998), Neurotrophic growth factors stimulate glycosaminoglycan synthesis in identified retinal cell populations in vitro, Glycobiol 8 1227–1235.

[80]   Clark SJ, Keenan, Tiarnan D. L., Fielder HL, Collinson LJ, Holley RJ, Merry, Catherine L. R., van Kuppevelt, Toin H., Day AJ, Bishop PN (2011), Mapping the Differential Distribution of Glycosaminoglycans in the Adult Human Retina, Choroid, and Sclera, Invest Ophthalmol Vis Sci 52 6511.

[81]   Des Senanayake P, Calabro A, Nishiyama K, Hu JG, Bok D, Hollyfield JG (2000), Glycosaminoglycan synthesis and secretion by the retinal pigment epithelium: polarized delivery of hyaluronan from the apical surface, J Cell Sci 114 199–205.

[82]   Gross-Jendroska M, Lui G-M, Stern R (1992), Retinal Pigment Epithelium-Stromal Interactions Modulate Hyaluronic Acid Deposition, Invest Ophthalmol Vis Sci 33 3394–3399.

[83]   Chaitin MH, Wortham HS, Brun-Zinkernagel A-M (1994), Immunocytochemical Localization of CD44 in the Mouse Retina, Exp Eye Res 58 359–366.

[84]   Shinoe T, Kuribayashi H, Saya H, Seiki M, Aburatani H, Watanabe S (2010), Identification of CD44 as a cell surface marker for Müller glia precursor cells, J Neurochem 115 1633–1642.

[85]   Nishina S, Hirakata A, Hida T, Sawa H, Azuma N (1997), CD44 expression in the developing human retina, Graefe's Arch Clin Exp Ophthalmol 235 92–96.

[86]   Ishikawa M, Sawada Y, Yoshitomi T (2015), Structure and function of the interphotoreceptor matrix surrounding retinal photoreceptor cells, Exp Eye Res 133 3–18.

[87]   Hollyfield JG, Rayborn Mary E., Tammi M, Tammi RH (1998), Hyaluronan in the Interphotoreceptor Matrix of the Eye: Species Differences in Content, Distribution, Ligand Binding and degradation, Exp Eye Res 66 241–248.

[88]   Liu N-P, Roberts WL, Hale LP, Levesque MC, Patel DD, Lu C-L, Jaffe GJ (1997), Expression of CD44 and Variant Isoforms in Cultured Human Retinal Pigment Epithelial Cells, Invest Ophthalmol Vis Sci 38 2027–2037.

[89]   Kuhrt H, Härtig W, Grimm D, Faude F, Kasper M, Reichenbach A (1997), Changes in CD44 and ApoE immunoreactivities due to retinal pathology of man and rat, J Hirnforsch. 38 223–229.

[90]   Krishnamoorthy R, Agarwal N, Chaitin MH (2000), Upregulation of CD44 expression in the retina during the rds degeneration, Mol Brain Res 77 125–130.

[91]   Mochimaru H, Takahashi E, Tsukamoto N, Miyazaki J, Yaguchi T, Koto T, Kurihara T, Noda K, Ozawa Y, Ishimoto T, Kawakami Y, Tanihara H, Saya H, Ishida S, Tsubota K (2009), Involvement of Hyaluronan and Its Receptor CD44 with Choroidal Neovascularization, Invest Ophthalmol Vis Sci 50 4410.

[92]   Schroedl F, Brehmer A, Neuhuber WL, Kruse FE, May CA, Cursiefen C (2008), The Normal Human Choroid Is Endowed with a Significant Number of Lymphatic Vessel Endothelial Hyaluronate Receptor 1 (LYVE-1)–Positive Macrophages, Invest Ophthalmol Vis Sci 49 5222.

[93]   Xu H, Manivannan A, Liversidge J, Sharp PF, Forrester JV, Crane IJ (2002), Involvement of CD44 in leukocyte trafficking at the blood-retinal barrier, J Leuko Biol 72 1133–1141.

[94]   Wallman J, Wildsoet C, Xu A, Gottlieb MD, Nickla DL, Marran L, Krebs W, Christensen AM (1995), Moving the retina: Choroidal modulation of refractive state, Vis Res 35 37–50.

[95]   Summers JA (2013), The choroid as a sclera growth regulator, Exp Eye Res 114 120–127.

[96]   Rada, Summers JA, Wiechmann AF, Hollaway LR, Baggenstoss BA, Weigel PH (2010), Increased Hyaluronan Synthase-2 mRNA Expression and Hyaluronan Accumulation with Choroidal Thickening: Response during Recovery from Induced Myopia, Invest Ophthalmol Vis Sci 51 6172.

[97]   Camilieri G, Bucolo C, Rossi S, Drago F (2004), Hyaluronan-Induced Stimulation of Corneal Wound Healing is a Pure Pharmacological Effect, J Ocul Pharm Th 20 548–553.

[98]   Nakamura M, Sato N, Chikama TI, Hasegawa Y, Nishida T (1997), Hyaluronan Facilitates Corneal Epithelial Wound Healing in Diabetic Rats, Exp Eye Res 64 1043-1050.

[99]   Troiano P, Monaco G (2008), Effect of Hypothonic 0.4% Hyaluronic Acid Drops in Dry Eye Patients: A Cross-Over Study, Cornea 27 1126–1130.

[100]   Kaya S, Schmidl D, Schmetterer L, Witkowska KJ, Unterhuber A, Aranha dos Santos, Valentin, Baar C, Garhöfer G, Werkmeister RM (2015), Effect of hyaluronic acid on tear film thickness as assessed with ultra-high resolution optical coherence tomography, Acta Ophthalmol 93 439–443.

[101] Schmidl D, Schmetterer L, Witkowska KJ, Unterhuber A, Aranha dos Santos, Valentin, Kaya S, Nepp J, Baar C, Rosner P, Werkmeister RM, Garhofer G (2015), Tear Film Thickness After Treatment With Artificial Tears in Patients With Moderate Dry Eye Disease, Cornea 34 421–426.

[102] Camber O, Edman P, Gurny R (1987), Influence of sodium hyaluronate on the meiotic effect of pilocarpine in rabbits, Curr Eye Res 6 779–784.

[103] Herrero-Vanrell R, Fernandez-Carballido A, Frutos G, Cadórniga R (2000), Enhancement of the Mydriatic Response to Tropicamide by Bioadhesive Polymers, J Ocul Pharmacol Th 16 419–428.

[104] Cho K (2003), Release of ciprofloxacin from poloxamer-graft-hyaluronic acid hydrogels in vitro, Int J Pharm 260 83–91.

[105] Bernatchez SF, Tabatabay C, Gurny R (1993), Sodium hyaluronate 0.25% used as a vehicle increases the bioavailability of topically administered gentamicin, Graefe's Arch Clin Exp Ophthalmol 231 157–161.

[106] Gurny R, Ibrahim H, Aebi A, Buri P, Wilson CG, Washington N, Edman P, Camer O (1987), Design and evaluation of controlled relese systems for the eye, J Control Release 6 367–373.

[107] Saettone MF, Giannaccini B, Chetoni P, Torracca MT, Monti D (1991), Evaluation of high- and low-molecular-weight fractions of sodium hyaluronate and an ionic complex as adjuvants for topical ophthalmic vehicles containing pilocarpine, Int J Pharm 72 131–139.

[108] Camber O, Edman P (1989), Sodium hyaluronate as an ophthalmic vehicle: Some factors governing its effect on the ocular absorption of pilocarpine, Curr Eye Res 8 563–567.

[109] Ibrahim HK, El-Leithy IS, Makky AA (2010), Mucoadhesive Nanoparticles as Carrier Systems for Prolonged Ocular Delivery of Gatifloxacin/Prednisolone Bitherapy, Mol Pharm 7 576–585.

[110] Yao J, Wu, Zhou, Dahmani FZ (2013), Enhanced and sustained topical ocular delivery of cyclosporine A in thermosensitive hyaluronic acid-based in situ forming microgels, Int J Nanomed 8 3587–3601.

[111] Yenice İ, Mocan MC, Palaska E, Bochot A, Bilensoy E, Vural İ, İrkeç M, Atilla Hıncal A (2008), Hyaluronic acid coated poly-ε-caprolactone nanospheres deliver high concentrations of cyclosporine A into the cornea, Exp Eye Res 87 162–167.

[112] Contreras-Ruiz L, de la Fuente M, García-Vázquez C, Sáez V, Seijo B, Alonso MJ, Calonge M, Diebold Y (2010), Ocular Tolerance to a Topical Formulation of Hyaluronic Acid and Chitosan-Based Nanoparticles, Cornea 29 550–558.

[113] Contreras-Ruiz L, de la Fuente M, Párraga JE, López-García A, Fernández I, Seijo B, Sánchez A, Calonge M, Diebold Y (2011), Intracellular trafficking of hyaluronic acid-chitosan oligomer-based nanoparticles in cultured human ocular surface cells, Mol Vis 17 279–290.

[114] de la Fuente M, Seijo B, Alonso MJ (2008), Bioadhesive hyaluronan-chitosan nanoparticles can transport genes across the ocular mucosa and transfect ocular tissue, Gene Ther 15 668–676.

[115] Hornof M, de la Fuente M, Hallikainen M, Tammi RH, Urtti A (2008), Low molecular weight hyaluronan shielding of DNA/PEI polyplexes facilitates CD44 receptor mediated uptake in human corneal epithelial cells, J Gene Med 10 70–80.

[116] de la Fuente, M, Seijo B, Alonso MJ (2008), Novel Hyaluronic Acid-Chitosan Nanoparticles for Ocular Gene Therapy, Invest Ophthalmol Vis Sci 49 2016–2024.

[117] Weeks A, Luensmann D, Boone A, Jones L, Sheardown H (2012), Hyaluronic acid as an internal wetting agent in model DMAA/TRIS contact lenses, J Biomat App 27 423–432.

[118] Weeks A, Morrison D, Alauzun JG, Brook MA, Jones L, Sheardown H (2012), Photocrosslinkable hyaluronic acid as an internal wetting agent in model conventional and silicone hydrogel contact lenses, J Biomed Mater Res 100A 1972–1982.

[119] Brennan NA, Coles M-L (2000), Deposits and symptomatology with soft contact lens wear, Int Cont Lens Clin 27 75–100.

[120] Vanbeek M, Jones L, Sheardown H (2008), Hyaluronic acid containing hydrogels for the reduction of protein adsorption, Biomaterials 29 780–789.

[121] Maulvi FA, Soni TG, Shah DO (2015), Extended release of hyaluronic acid from hydrogel contact lenses for dry eye syndrome, J Biomater Sci Polym E 26 1035–1050.

[122] Weeks A, Subbaraman LN, Jones L, Sheardown H (2013), Physical entrapment of hyaluronic acid during synthesis results in extended release from model hydrogel and silicone hydrogel contact lens materials, Eye Contact Lens 39 179–185.

[123] Ali M, Byrne ME (2009), Controlled Release of High Molecular Weight Hyaluronic Acid from Molecularly Imprinted Hydrogel Contact Lenses, Pharm Res 26 714–726.

[124] Calles JA, Tártara LI, Lopez-García A, Diebold Y, Palma SD, Vallés EM (2013), Novel bioadhesive hyaluronan–itaconic acid crosslinked films for ocular therapy, Int J Pharm 455 48–56.

[125] Hume LR, Lee HK, Benedetti L, Sanzgiri YD, Topp EM, Stella VJ (1994), Ocular sustained delivery of prednisolone using hyaluronic acid benzyl ester films, Int J Pharm 111 295–298.

[126] Wang B, Lin Q, Jin T, Shen C, Tang J, Han Y, Chen H (2015), Surface modification of intraocular lenses with hyaluronic acid and lysozyme for the prevention of endophthalmitis and posterior capsule opacification, RSC Adv 5 3597–3604.

[127] Lin Y-K, Chen K-H, Kuan C-Y (2013), The synthesis and characterization of a thermally responsive hyaluronic acid/ Pluronic copolymer and an evaluation of its potential as an artificial vitreous substitute, J Bioact and Compat Pol.

[128] Gan L, Wang J, Zhao Y, Chen D, Zhu C, Liu J, Gan Y (2013), Hyaluronan-modified core–shell liponanoparticles targeting CD44-positive retinal pigment epithelium cells via intravitreal injection, Biomaterials 34 5978–5987.

[129] Martens TF, Remaut K, Deschout H, Engbersen JF, Hennink WE, van Steenbergen, Mies J., Demeester J, De Smedt, Stefaan C., Braeckmans K (2015), Coating nanocarriers with hyaluronic acid facilitates intravitreal drug delivery for retinal gene therapy, J Control Release 202 83–92.

[130] Koo H, Moon H, Han H, Na JH, Huh MS, Park JH, Woo SJ, Park KH, Chan Kwon I, Kim K, Kim H (2012), The movement of self-assembled amphiphilic polymeric nanoparticles in the vitreous and retina after intravitreal injection, Biomaterials 33 3485–3493.

[131] Neffe AT, Kobuch KA, Maier M, Feucht N, Lohmann CP, Wolfstein A, Streufert D, Kamlage S, Lendlein A (2011), In Vitro and In Vivo Evaluation of a Multifunctional Hyaluronic acid Based Hydrogel System for Local Application on the Retina, Macromol Symp 309-310 229–235.

[132]   Sueda J, Sakuma T, Nakamura H, Usumoto N, Okuno T, Arai M, Hirose T (2006), In Vivo and In Vitro Feasibility Studies of Intraocular Use of Seprafilm to Close Retinal Breaks in Bovine and Rabbit Eyes, Invest Ophthalmol Vis Sci 47 1142.

[133]   Parker J, Mitrousis N, Shoichet MS (2016), Hydrogel for Simultaneous Tunable Growth Factor Delivery and Enhanced Viability of Encapsulated Cells in Vitro, Biomacromol 17 476-484.

[134]   Ballios BG, Cooke MJ, van der Kooy, Derek, Shoichet MS (2010), A hydrogel-based stem cell delivery system to treat retinal degenerative diseases, Biomaterials 31 2555–2564.

[135]   Kontturi L-S, Collin EC, Murtomäki L, Pandit AS, Yliperttula M, Urtti A (2015), Encapsulated cells for long-term secretion of soluble VEGEF receptor 1: Material optimization and simulation of ocular response, Eur J Pharm Biopharm 95 387-97.

[136]   Barar J, Javadzadeh AR, Omidi Y (2008), Ocular novel drug delivery: impacts of membranes and barriers, Exp Opin Drug Del 5 567–581.

[137]   Valim V, Trevisani, Virginia Fernandes Moça, de Sousa, Jacqueline Martins, Vilela VS, Belfort R (2015), Current Approach to Dry Eye Disease, Clinic Rev Allerg Immunol 49 288–297.

[138]   Baudouin C (2001), The Pathology of Dry Eye, Survey of Ophthalmology 45 S211-S220.

[139]   Lee HS, Ji YS, Yoon KC (2014), Efficacy of Hypotonic 0.18% Sodium Hyaluronate Eye Drops in Patients With Dry Eye Disease, Cornea 33 946–951.

[140]   Doughty MJ, Glavin S (2009), Efficacy of different dry eye treatments with artificial tears or ocular lubricants: a systematic review, Ophthal Phyl Opt 29 573–583.

[141]   Aragona P, Papa V, Micali A, Santocono M, Milazzo G (2002), Long term treatment with sodium hyaluronate-containing artificial tears reduces ocular surface damage in patients with dry eye, Brit J Ophthalmol 86 181–184.

[142]   Paugh JR, Nguyen AL, Ketelson HA, Christensen MT, Meadows DL (2008), Precorneal residence time of artificial tears measured in dry eye subjects, Optometry Vision Sci 85 725–731.

[143]   Ludwig A (2005), The use of mucoadhesive polymers in ocular drug delivery, Adv Drug Deliver Rev 57 1595–1639.

[144] Zignani M, Tabatabay C, Gurny R (1995), Topical semi-solid drug delivery: kinetics and tolerance of ophthalmic hydrogels, Adv Drug Deliver Rev 16 51–60.

[145] Jeong B, Kim SW, Bae YH (2002), Thermosensitive sol–gel reversible hydrogels, Adv Drug Deliver Rev 54 37–51.

[146] Su X, Tan MJ, Li Z, Wong M, Rajamani L, Lingam G, Loh XJ (2015), Recent Progress in Using Biomaterials as Vitreous Substitutes, Biomacromolecules 16 3093–3102.

[147] Kleinberg TT, Tzekov RT, Stein L, Ravi N, Kaushal S (2011), Vitreous Substitutes: A Comprehensive Review, Surv Ophthalmol 56 300–323.

[148] Baino F (2011), Towards an ideal biomaterial for vitreous replacement: Historical overview and future trends, Acta Biomater 7 921–935.

[149] Thrimawithana TR, Young S, Bunt CR, Green C, Alany RG (2011), Drug delivery to the posterior segment of the eye, Drug Discov Today 16 270–277.

[150] Xu Q, Boylan NJ, Suk JS, Wang Y-Y, Nance EA, Yang J-C, McDonnell PJ, Cone RA, Duh EJ, Hanes J (2013), Nanoparticle diffusion in, and microrheology of, the bovine vitreous ex vivo, J Control Release 167 76–84.

[151] Peeters L (2005), Vitreous: A Barrier to Nonviral Ocular Gene Therapy, Invest Ophthalmol Vis Sci 46 3553–3561.

[152] Naik R, Mukhopadhyay A, Ganguli M (2009), Gene delivery to the retina: focus on non-viral approaches, Drug Discov Today 14 306–315.

[153] Tozer K, Johnson MW, Sebag J, II.C. Vitreous Aging and Posterior Vitreous Detachment, pp. 131–150.

[154] Deguine V, Menasche M, Ferrari P, Fraisse L, Pouliquen Y, Robert L (1998), Free radical depolymerization of hyaluronan by maillard reaction products, Int J Biol Macromol 22 17–22.

[155] Lane JI, Watson RE, Witte RJ, McCannel CA (2003), Retinal Detachment: Imaging of Surgical Treatments and Complications1, RadioGraphics 23 983–994.

[156] Amadio M, Govoni S, Pascale A (2016), Targeting VEGF in eye neovascularization: What's new?, Pharmacol Res 103 253–269.

[157]   Oh EJ, Choi J-S, Kim H, Joo C-K, Hahn SK (2011), Anti-Flt1 peptide – Hyaluronate conjugate for the treatment of retinal neovascularization and diabetic retinopathy, Biomater 32 3115–3123.

[158]   Highley CB, Prestwich GD, Burdick JA (2016), Recent advances in hyaluronic acid hydrogels for biomedical applications, Curr Opin Biotechnol 40 35–40.

Chapter 2

Goals of the Thesis

Glaucoma is a progressive neurodegenerative disease of the optic nerve and is one of the leading causes of blindness along with cataracts, age-related macular degeneration and diabetic retinopathy [1]. Estimations predict that more than 110 million people will be affected worldwide by 2040, with African and Asian population bearing a higher risk of developing the disease [2]. The pathology of glaucoma is not fully understood yet but there are some risk factors such as genetic predisposition, ethnicity and age [3]. An elevated intraocular pressure (IOP) is evaluated as the most critical aspect. Therefore, current therapies focus on lowering the IOP by topically or systemically applied drugs or surgery. Table 1 summarizes substances frequently used in glaucoma therapy. They all result in the same pharmacological effect which relies on reducing the production or increasing the outflow of aqueous humor (AH). At a first glance, glaucoma therapy with eye drops appears to be a reasonable, non-invasive treatment method, but the need for application several times a day reduces patient adherence. Furthermore, mistakes in administration, like the application of too many drops, are common[4,5] and studies have shown that nine out of ten patients were unable to apply their eye drops correctly [6]. Consequently, undesired systemic side effects or insufficient therapeutic benefits result. Surgical procedures (summarized in Table 2) are reserved for more severe cases. During surgery, parts of the trabecular meshwork (TM) are removed or other drainage pathways are opened to improve AH outflow using incisional or minimally invasive techniques. However, achieved outcomes decrease over time and surgery always carries risks like scarring, fibrosis, the development of cataracts or sight-threatening infections [7,8].

Table 1. Frequently used drugs in glaucoma therapy. As an elevated intraocular pressure is regarded as most critical for the progression of the disease, current medications rely on lowering the intraocular pressure by topically applied eye drops. Adapted from [9].

drug type	examples	mechanism of action
prostaglandin analogues	latanoprost, travoprost, tafluprost, unoprostone, bimatoprost	increase in aqueous humor (AH) outflow
beta-adrenergic blockers	betaxolol, carteolol, levobunolol, timolol	reduction of AH production
carbonic anhydrase inhibitors	acetazolamide (oral), brinzolamide, dorzolamide,	reduction of AH production
alpha-adrenergic agonists	brimonidine, apraclonidine	reduction of AH production, increase in AH outflow
cholinergic agonists	pilocarpine, carbachol	increase in AH outflow

Table 2. Surgical options to reduce intraocular pressure. Trabeculectomy is the most frequently used procedure. However, newer minimally invasive techniques might become more important due to the reduced risk of side effects. Compiled from [10,11].

	method	description	mechanism of action
incisional			
surgery	trabeculectomy	removal of parts of the trabecular meshwork (TM) and adjacent tissues	subconjunctival filtration
implant	aqueous tube shunt, glaucoma drainage device	shunt from anterior chamber to external reservoir	external aqueous humor (AH) drainage
minimal invasive			
surgery	Trabectome	electrocautery TM ablation, removal of angle tissue barrier	increasing trabecular outflow
	gonioscopy-assisted transluminal trabeculotomy	circumferential trabeculotomy, removal of TM and adjacent structures	increasing trabecular outflow
stents	iStent, iStent inject	trabecular micro-bypass, connection between anterior chamber and Schlemm's channel (SC)	increasing trabecular outflow
	Hydrus Microstent	dilatation of SC	increasing trabecular outflow
	XEN Gel Implant, MicroShunt	shunt from anterior chamber to subconjunctival space	subconjunctival filtration
	Cypass Micro-Stent	fenestrated tube implanted between ciliary body and sclera	suprachoroidal shunts
laser	excimer laser trabeculotomy	photoablation of TM	increasing trabecular outflow
	Electrophoto-coagulation	blanching of ciliary processes	reduction of AH production

The IOP is generated by the circulation and hindered outflow of AH in the anterior segment of the eye as demonstrated in Figure 1 [12]. Epithelial cells of the ciliary body produce AH and secrete it into the posterior chamber. It provides nutrients to lens, iris and cornea which are not supplied with blood vessels. A pressure gradient drives the fluid through the gap between lens and iris into the anterior chamber where it drains into the outflow pathways of the iridocorneal angle. Only a small portion of AH leaves the eye via the unconventional or uveocorneal outflow pathway and diffuses through intramuscular spaces of the ciliary body into capillaries and lymphatic vessels [13] while 85 to 95 % of AH use the conventional outflow pathway of the TM [3].

a	trabecular meshwork
b	Schlemm's canal
c	Schwalbe's line
d	scleral spur
e	ciliary body
f	longitudinal muscle
g	circular muscle
h	ciliary processes
i	cornea
j	iris
k	pupil
l	lens
m	anterior chamber
n	posterior chamber
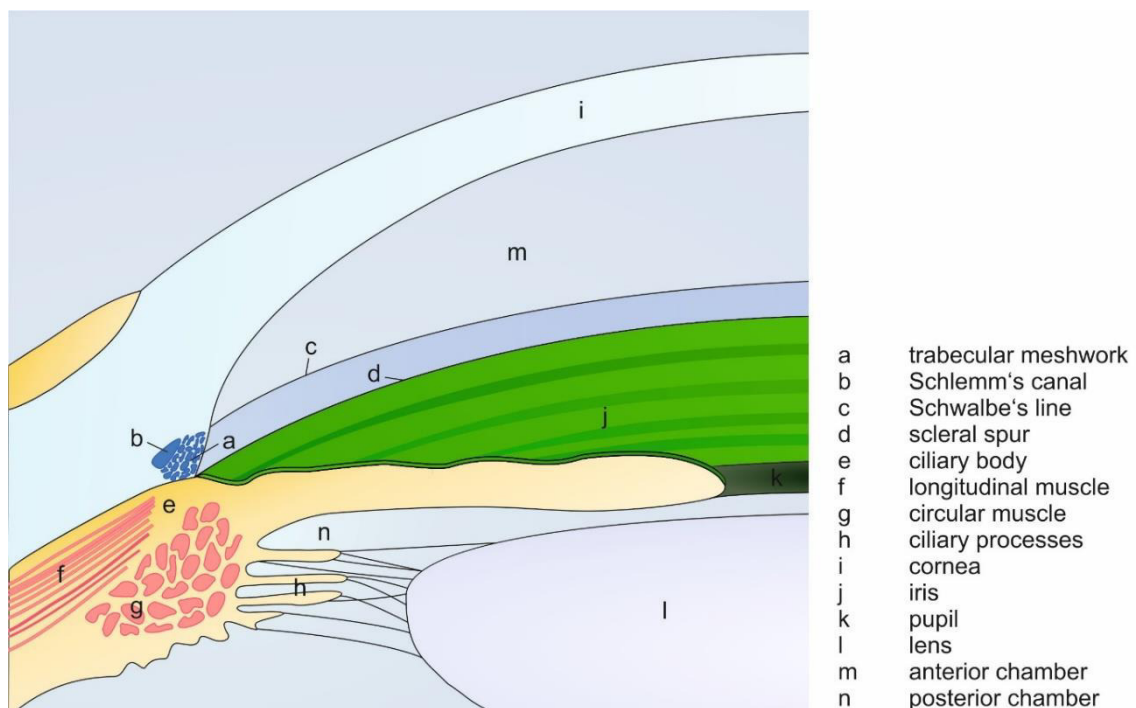
Figure 1. Anatomy of the anterior segment of the eye. Aqueous humor is produced in the ciliary body and secreted into the posterior chamber. The fluid passes the gap between lens and iris through the pupil into the anterior chamber and finally is drained into the trabecular meshwork, located in the iridocorneal angle.

The detailed anatomy of the TM is schematically represented in Figure 2. Its typical sponge-like structure results from connective tissue beams that span from Schwalbe's line, the anterior border of the TM, to the scleral spur which is attached to the ciliary body [13–15]. These lamellae consist of collagenous and elastic fibers and are covered by flat TM cells residing on a basement membrane. TM cells share properties with epithelial cells and macrophages. For example, they exhibit a flat morphology, produce antithrombotic substances and are capable of phagocytosis which is an important self-cleaning-mechanism

in the TM to keep the porous structure intact [16,17]. Connective tissue and cellular processes bridge adjacent beams and strengthen the network. AH first passes the uveal and corneoscleral meshwork which is characterized by this lamellae structure [13]. The juxtacanicular connective tissue (JCT) beneath contains star-shaped cells that are embedded in a loose connective tissue made up by fibrillar components and an amorphous ground substance. Finally, AH drains into Schlemm's channel (SC), a modified blood vessel with high permeability [13]. Large pores within SC endothelia and an incomplete basal lamina facilitate the perfusion of AH from the TM into the lumen.
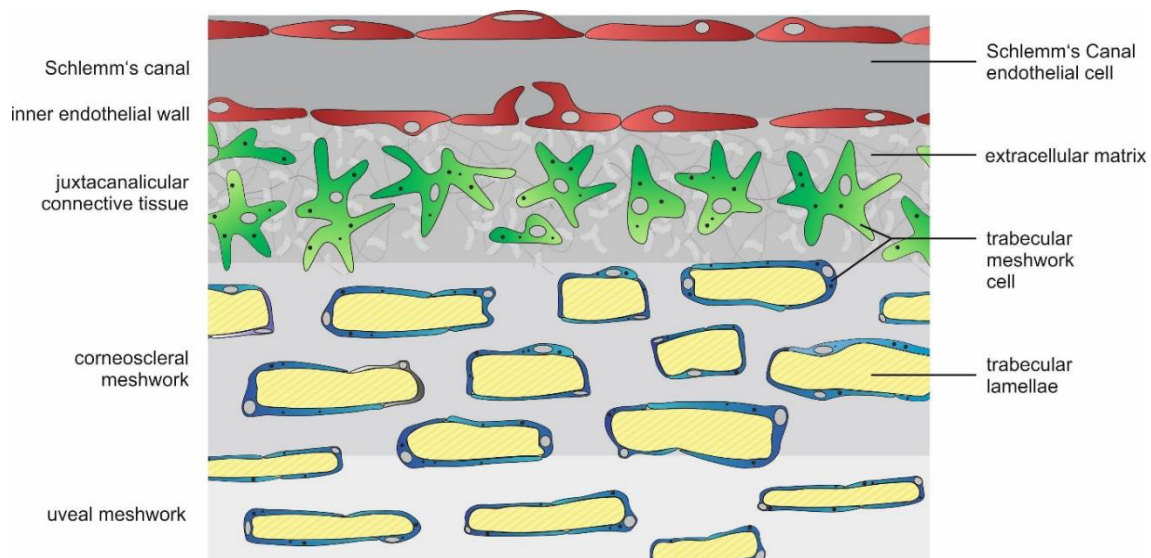
Figure 2. Detailed structure of the TM. AH first passes the sponge-like structure of the uveal and corneoscleral meshwork. Star-shaped cells and a dense extracellular matrix characterize the juxtacanicular connective tissue (JCT) beneath. Finally, AH drains into Schlemm's Channel (SC) and is transported to collector channels and the episcleral vein (not shown).

The loose network of the uveal and corneoscleral meshwork does not contribute to the buildup of IOP as the pore sizes are too wide to generate an outflow resistance [13]. However, spaces in the JCT region and the inner wall endothelium of SC are much smaller, and it is generally accepted that the outflow resistance to AH is generated in this region. The quality and quantity of extracellular matrix (ECM) in the JCT is highly regulated and strongly impacts AH flow [13,18]. Transforming growth factor (TGF)-β2 seems to be involved in this regulation as elevated levels in the AH of glaucoma patients were related to enhanced ECM deposition in the JCT. Furthermore, it was found that TGF-β2 stiffens the ECM by stimulation of fibronectin crosslinking and inhibition of ECM degrading enzymes. Some of these effects – especially ECM deposition - are transmitted by connective tissue growth

factor (CTGF). The system of TGF-β2 and CTGF also strengthens the contractile properties of the TM actin cytoskeleton, further increasing outflow resistance.

Interference with the TGF-β/CTGF-system presents an opportunity to reduce the massive ECM deposition within the TM and lower the enhanced contractility of the actin cytoskeleton. As TGF-β2 is a growth factor involved in many physiological and pathophysiological processes like proliferation, apoptosis, tumor growth and autoimmune diseases, complete depletion might cause unpredictable effects. Therefore, attenuation of CTGF, the downstream mediator of TGF-β2, is more reasonable. An enhanced expression of fibronectin and collagen I, III, IV and VI was shown *in vitro* after treating human TM cells with recombinant CTGF by Junglas et al. [19]. Additionally, an increase in IOP and a progressive loss of optic nerve axons was demonstrated in CTGF overexpressing transgenic mice [20]. Hence, reducing CTGF levels has the potential to prevent the progression of the disease.

A promising method to reduce the production of a protein is silencing gene expression with small interfering RNA (siRNA). siRNA are short, double stranded RNAs with a length of 21 to 23 base pairs and two nucleotides overhang at the 3' end [21]. The mechanism of gene knockdown is summarized in Figure 3. In the cytosol of a cell, siRNA interacts with a protein complex called RNA-induced silencing complex (RISC). Double-stranded siRNA is unwound and the antisense strand is incorporated into the complex. This antisense strand pairs with a complementary messenger RNA (mRNA) strand and mediates its cleavage.
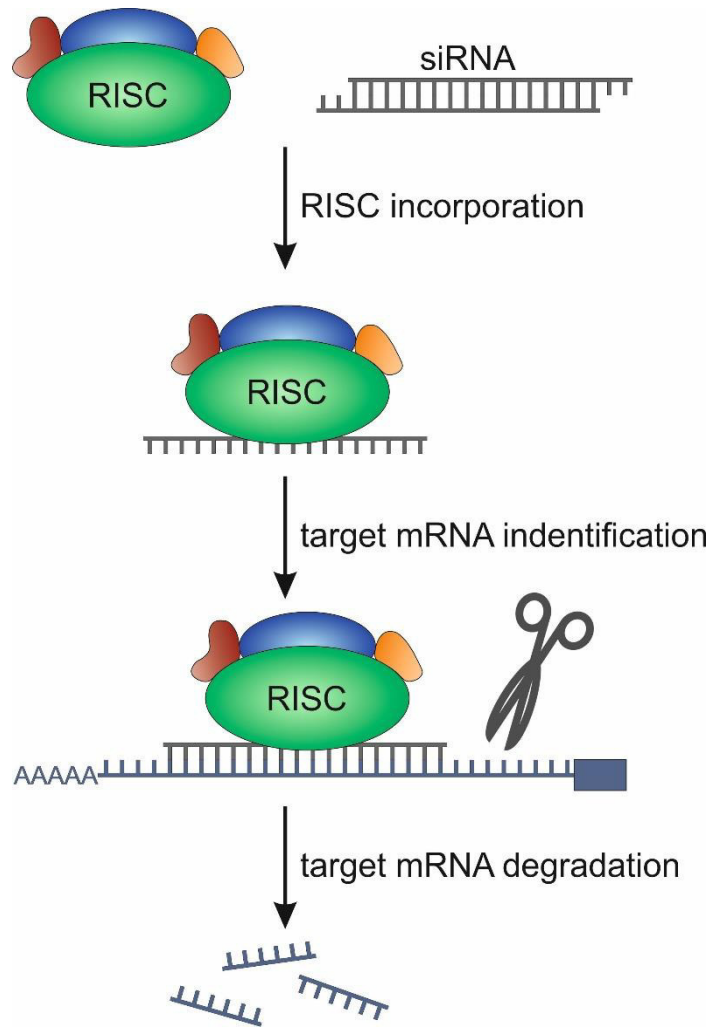
Figure 3. Mechanism of gene knockdown by small interfering RNA (siRNA). siRNA associates with the RNA induced silencing complex (RISC). Complementary messenger RNA (mRNA) is recognized by base paring and enzymatically cleaved by a RISC subunit with endonuclease activity.

RNA interference was identified as promising approach for the therapy of diseases caused by the overexpression of specific proteins. However, the delivery of siRNA is difficult. The polar nature of the molecule and the high molecular weight hinder cellular access [22]. Rapid degradation by endogenous nucleases occurs immediately after injection into the blood and is the biggest obstacle for siRNA gene therapy. Hence, a suitable delivery system must be applied, protecting siRNA from degradation and facilitating cellular entry.

The main goal of the thesis was the development of a nanoparticulate system for the delivery of siRNA to cells in the TM. These particles would be injected into the anterior chamber of the eye and follow the natural AH flow to the JCT where outflow resistance is generated. Therefore, the particles must comply with a number of requirements. First, the loading capacity has to be sufficiently high to have a therapeutic effect and siRNA must be protected

against degradation. Further, the nanoparticles (NPs) should move freely in the extracellular space but specifically interact with their target cells once they reach the inner TM. Layer-by-layer (LbL)-NPs as described by Elbakry et al. [23] meet all criteria. As siRNA is electrostatically attached to the surface of a nanoparticulate template, high loading is possible, and the fragile molecule can facilely be protected by covering it with an oppositely charged polyelectrolyte. An outer layer of hyaluronic acid (HA) is intended to enhance the NP mobility in the extracellular space, as this polysaccharide is a naturally present in the TM. At the same time, interactions of HA with receptors on TM cells are predicted to enhance the accumulation of NPs and cells.

In the first step, suitable NPs were designed and fabricated. A protocol was developed for the preparation of biodegradable poly(lactic-*co*-glycolic acid) (PLGA) nanoparticles and their coating with polyelectrolytes in a layer-by-layer process. Although the procedure of alternating deposition of oppositely charged polymers is easily feasible on planar substrates, the method is challenging to apply to colloidal templates because of their tendency to aggregate. PLGA was chosen as a template because of its thorough characterization and ability to encapsulate drugs. A freeze-drying method was established for long term storage and quantification of the particles. NPs were characterized with regard to size and surface charge before, during and after coating by scanning electron microscopy and dynamic light scattering (DLS). Colloidal stability and NP disassembly was investigated in different environments simulating conditions prior to and after administration into the AH by further DLS-studies and in an approach based on Foerster Resonance Energy Transfer (chapter 3).

Cluster of differentiation (CD) 44 receptors were identified as promising target for the LbL-NPs as this cell surface protein is overexpressed in the TM of glaucoma patients. Functionalization with HA, the natural ligand of CD44, is a widely used approach for directing drugs or drug delivery systems to CD44 producing cells. The efficacy of this method has been demonstrated in various types of cancer [24–27]. However, targeting the TM with HA-functionalized NPs has not been reported so far. *In vitro* studies using flow cytometry and confocal laser scanning microscopy demonstrated the participation of CD44 in and the impact of receptor density on the interactions of cells and HA-decorated NPs. Further, additional effects of HA, such as enhanced colloidal stability and permeation through the extracellular matrix were addressed in a 3D cell culture setup (chapter 4).

The challenge of siRNA delivery does not end with the NPs reaching the target cell. Intracellular bottlenecks must be overcome as well. Major issues in particular include the

ability of NPs to quickly escape endosomes and also release the siRNA cargo. To evaluate the performance of LbL-NPs as an siRNA delivery system, an *in vitro* assay was established. The reduction of green fluorescent protein expression in stably transfected immortalized TM cells was detected by flow cytometry and used to study the gene silencing effect of NPs of different compositions. To clearly visualize the intracellular fate of the particles, their colocalization with different intracellular compartments such as early and late endosomes or lysosomes was determined by optical sectioning using a confocal laser scanning microscope. Finally, different fluorescence-based techniques were used to analyze whether the NPs were exocytosed (chapter 5).

So far, general aspects like NP characterization, their interaction with cells and intracellular fate were discussed. In the last part of the thesis, however, the specific application of LbL-NPs for CTGF silencing in the TM was addressed. First, it was investigated whether pathological alterations in the TM also affect CD44. Quantitative real-time polymerase chain reaction (qRT-PCR), western blotting and immunohistochemistry were used to analyze samples obtained *in vitro*, *in vivo*, in transgenic mice and *ex vivo* from human donors. NP distribution in the outflow pathways of porcine and human eyes was evaluated after perfusion with either HA-functionalized or unfunctionalized NPs. Fluorescent images of whole outflow rings and confocal micrographs of sagital sections were taken and the colocalization of NPs with CD44 and CD31 was evaluated. Finally, the CTGF silencing efficacy of the NPs was addressed in primary human trabecular meshwork cells by qRT-PCR and western blotting (chapter 6).

References

[1]   Flaxman SR, Bourne RRA, Resnikoff S, Ackland P, Braithwaite T et al. (2017), Global causes of blindness and distance vision impairment 1990–2020: A systematic review and meta-analysis, Lancet Glob Health 5 e1221-e1234.

[2]   Tham Y-C, Li X, Wong TY, Quigley HA, Aung T, Cheng C-Y (2014), Global prevalence of glaucoma and projections of glaucoma burden through 2040: a systematic review and meta-analysis, Ophthalmology 121 2081–2090.

[3]   Doucette LP, Rasnitsyn A, Seifi M, Walter MA (2015), The interactions of genes, age, and environment in glaucoma pathogenesis, Survey Ophthalmol 60 310–326.

[4]   Stryker JE, Beck AD, Primo SA, Echt KV, Bundy L, Pretorius GC, Glanz K (2010), An exploratory study of factors influencing glaucoma treatment adherence, J Glaucoma 19 66–72.

[5]   Tatham AJ, Sarodia U, Gatrad F, Awan A (2013), Eye drop instillation technique in patients with glaucoma, Eye 27 1293–1298.

[6]   Gupta R, Patil B, Shah BM, Bali SJ, Mishra SK, Dada T (2012), Evaluating eye drop instillation technique in glaucoma patients, J Glaucoma 21 189–192.

[7]   Weinreb RN, Aung T, Medeiros FA (2014), The pathophysiology and treatment of glaucoma: a review, JAMA 311 1901–1911.

[8]   Weinreb RN, Khaw PT (2004), Primary open-angle glaucoma, Lancet 363 1711–1720.

[9]   Weinreb RN, Aung T, Medeiros FA (2014), The Pathophysiology and Treatment of Glaucoma, JAMA 311 1901.

[10]   Kerr NM, Wang J, Barton K (2017), Minimally invasive glaucoma surgery as primary stand-alone surgery for glaucoma, Clin Exp Ophthalmol 45 393–400.

[11]   Richter GM, Coleman AL (2016), Minimally invasive glaucoma surgery: current status and future prospects, Clin Ophthalmol 10 189–206.

[12]   Goel M, Picciani RG, Lee RK, Bhattacharya SK (2010), Aqueous humor dynamics: a review, Open Ophthalmol J 4 52–59.

[13]   Braunger BM, Fuchshofer R, Tamm ER (2015), The aqueous humor outflow pathways in glaucoma: A unifying concept of disease mechanisms and causative treatment, Eur J Pharm Biopharm 95 173–181.

[14]   Tamm ER, Braunger BM, Fuchshofer R (2015), Intraocular Pressure and the Mechanisms Involved in Resistance of the Aqueous Humor Flow in the Trabecular Meshwork Outflow Pathways, Prog Mol Biol Transl 134 301–314.

[15]   Tamm ER (2009), The trabecular meshwork outflow pathways: structural and functional aspects, Exp Eye Res 88 648–655.

[16]   Stamer WD, Clark AF (2017), The many faces of the trabecular meshwork cell, Exp Eye Res 158 112–123.

[17]   Tamm ER (2009), The trabecular meshwork outflow pathways: Structural and functional aspects, Exp Eye Res 88 648–655.

[18]   Tamm ER, Fuchshofer R (2007), What increases outflow resistance in primary open-angle glaucoma?, Surv Ophthalmol 52 Suppl 2 S101-4.

[19]   Junglas B, Yu AHL, Welge-Lussen U, Tamm ER, Fuchshofer R (2009), Connective tissue growth factor induces extracellular matrix deposition in human trabecular meshwork cells, Exp Eye Res 88 1065–1075.

[20]   Junglas B, Kuespert S, Seleem AA, Struller T, Ullmann S, Bosl M, Bosserhoff A, Kostler J, Wagner R, Tamm ER, Fuchshofer R (2012), Connective tissue growth factor causes glaucoma by modifying the actin cytoskeleton of the trabecular meshwork, Am J Phathol 180 2386–2403.

[21]   Wittrup A, Lieberman J (2015), Knocking down disease: a progress report on siRNA therapeutics, Nat Rev Genetics 16 543–552.

[22]   Williford J-M, Wu J, Ren Y, Archang MM, Leong KW, Mao H-Q (2014), Recent advances in nanoparticle-mediated siRNA delivery, Annu Rev Biomed Eng 16 347–370.

[23]   Elbakry A, Zaky A, Liebl R, Rachel R, Goepferich A, Breunig M (2009), Layer-by-Layer Assembled Gold Nanoparticles for siRNA Delivery, Nano Lett 9 2059–2064.

[24]   Skandalis SS, Gialeli C, Theocharis AD, Karamanos NK (2014), Advances and advantages of nanomedicine in the pharmacological targeting of hyaluronan-CD44 interactions and signaling in cancer, Adv Cancer Res 123 277–317.

[25]   Maiolino S, Moret F, Conte C, Fraix A, Tirino P, Ungaro F, Sortino S, Reddi E, Quaglia F (2015), Hyaluronan-decorated polymer nanoparticles targeting the CD44 receptor for the combined photo/chemo-therapy of cancer, Nanoscale 7 5643–5653.

[26]   Dosio F, Arpicco S, Stella B, Fattal E (2016), Hyaluronic acid for anticancer drug and nucleic acid delivery, Adv Drug Deliver Rev 97 204–236.

[27]   Tripodo G, Trapani A, Torre ML, Giammona G, Trapani G, Mandracchia D (2015), Hyaluronic acid and its derivatives in drug delivery and imaging: Recent advances and challenges, Eur J Pharm Biopharm 97 400–416.

Chapter 3

Layer-by-layer assembled nanoparticles for siRNA delivery

Parts of the shown results are accepted for publication in

Nanotechnology for Nucleic Acid Delivery: Methods and Protocols,

Second Edition

Abstract
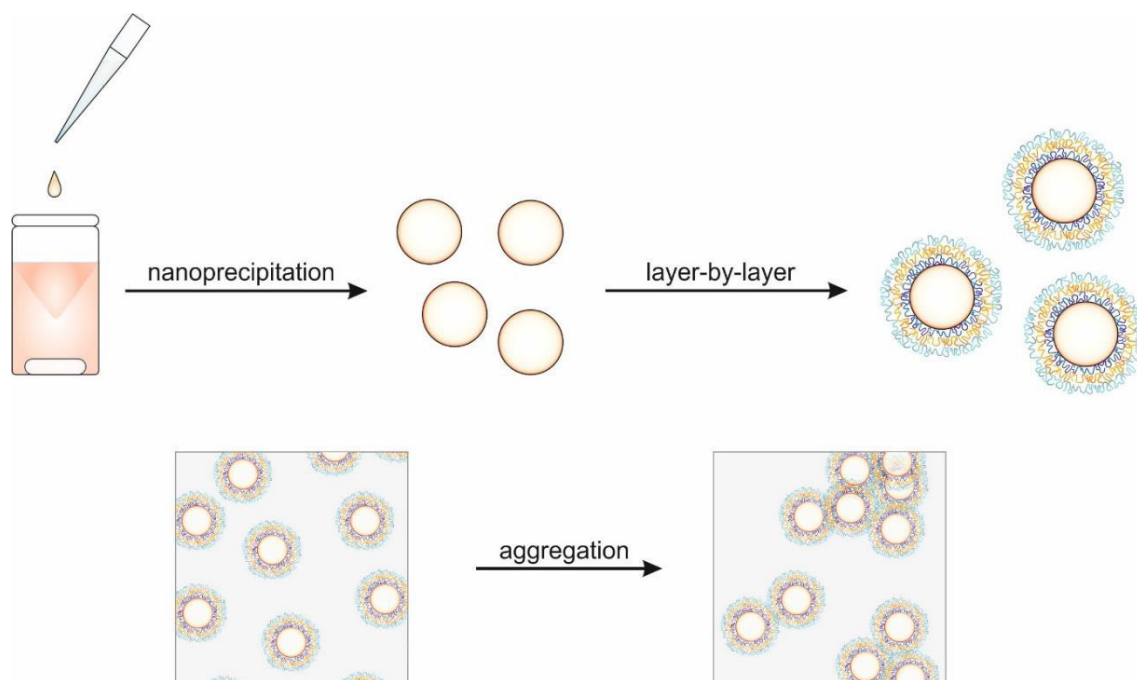
Nanoparticles (NPs) synthesized via layer-by-layer processes are promising candidates for successful drug and gene delivery. Widespread use of the layer-by-layer technique has resulted from its accessibility to every lab; to generate nanoscale structures, layer-by-layer processes require common lab equipment of only modest quality and do not involve the use of organic solvents. In addition, a wide range of different starting materials can be flexibly combined, enabling the production of a nearly unlimited number of different nanoparticles with various physicochemical properties. Here we describe the manufacturing of poly(lactic-*co*-glycolic acid) NPs coated with small interfering RNA for gene silencing. Positively charged polyethyleneimine and negatively charged nucleic acids form the polyelectrolyte shell. Finally, the nanoparticles are functionalized with hyaluronic acid, a polysaccharide which targets the CD44 receptor. The particles were characterized with regard to size and zeta potential before, during and after the layer-by-layer deposition of the polymers. Additionally, their colloidal stability in different dispersants was monitored via dynamic light scattering and Foerster Resonance Energy Transfer.

1   Introduction

"Layer-by-layer" (LbL) is a term used to describe film formation by depositing oppositely charged materials on a surface [1]. Decher was the first to characterize the underlying mechanism in 1991, assembling a 35-layer film, 170 nm in thickness, composed of alternating anionic and cationic bipolar amphiphiles on a planar surface [2]. Since then, the field has developed immensely. LbL techniques are now routinely leveraged for applications in material science, physical chemistry, electrochemistry and biomedical engineering [1]. In the fields of drug and gene delivery, LbL shell growth on nanoscale templates has emerged as an area of particular interest [3]. The structure of LbL-coated nanoparticles (NPs) allows the inclusion of therapeutics (e.g. small molecules or macromolecules like proteins and nucleic acids) into either the multilayer shell or the NP core. The technique is even suitable for extremely sensitive or labile molecules like RNA, as the layering process is performed under mild conditions without the need for harsh pH or elevated temperatures. The surface properties of the fully-assembled NPs can be tailored on a molecular level without significantly altering the shape and size of the particle as a whole, simply by selecting a suitable charged substance for the final layer. Substances with targeting functions can readily be attached to the nanoparticle surface by similar means. Additionally, inclusion of pH-sheddable, redox-sensitive or enzymatically degradable materials enable spatially and temporally controlled or triggered release [4]. Despite these significant advantages, high-quality LbL assembly is quite difficult, impeding broad application of the technique [5]. Of utmost importance is the complete removal of unbound polyelectrolyte after each layering cycle. Any oppositely charged polymers remaining in solution after a cycle will form complexes which are difficult to separate from coated particles. Purification processes must be thorough but gentle, as irreversible aggregation of particles poses a serious issue. Commonly applied strategies are repeated centrifugation and ultrafiltration.

We developed a LbL-based protocol for manufacturing poly(lactic-*co*-glycolic acid) (PLGA) NPs for small interfering RNA (siRNA) delivery. Figure 1 summarizes the composition of the particles. The NP core is composed of PLGA, an FDA-approved biodegradable polymer that is commercially available in high quality and a wide range of molecular weights. The synthesis of PLGA-NPs is well established in the literature [6]. During synthesis of the PLGA core particle, we utilize polyethyleneimine (PEI) instead of poly(vinyl alcohol) as a stabilizing agent. As a well-known and highly effective transfection agent [7], PEI is intended to enhance the particles' effectiveness as gene delivery vehicles. Further, PEI provides the NPs with the

cationic surface charge necessary for adsorption of an initial layer of negatively charged siRNA. To protect the siRNA from degradation, another layer of PEI was adsorbed on top of the siRNA. The negatively charged polysaccharide hyaluronic acid (HA) was used as a final, outermost layer. HA enhances the NP colloidal stability [8], increases NP mobility in the extracellular space [9] and serves as a targeting moiety [10]. As the main ligand of the cluster of differentiation (CD) 44-receptor, HA directs the NPs to cells with high receptor density, e. g. tumor cells [11] and others known to strongly interact with their extracellular matrix as for example in the trabecular meshwork [12]. References [13,14] are excellent review articles covering this topic.

Here, we describe a protocol for the preparation of LbL-based NPs. Changing the ratio of PLGA and stabilizer during the synthesis resulted in NPs of different sizes as demonstrated by scanning electron microscopy (SEM) and dynamic light scattering (DLS). A freeze-drying method was developed for storage and quantification of the NPs. The deposition of oppositely charged polymers on the core was monitored by DLS, and the siRNA loading was photometrically estimated. Finally, the colloidal stability of the NPs was investigated in different dispersants by DLS and Foerster Resonance Energy Transfer (FRET).
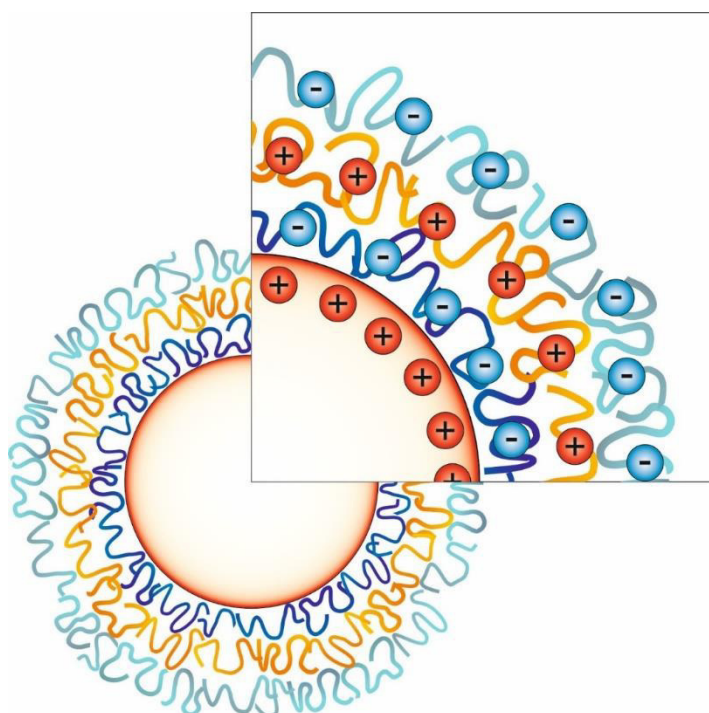
Figure 1. The LbL-based NP consists of a positively charged PLGA-PEI core and 3 subsequently deposited polyelectrolyte layers. The first layer consists of negatively charged siRNA (blue). This is coated and protected by a layer of polycationic PEI (orange). A final layer of anionic HA (light blue) is then deposited to enable targeting of CD44 receptors.

2 Materials and Methods

2.1 Materials

Acid terminated poly(D,L-lactide-*co*-gylcolide) (PLGA) (lactide/glycolide 50/50) with an average molecular weight of 38-54 kDa (PLGA) and branched poly(ethylenimine) 25 kDa (PEI) were bought from Sigma-Aldrich (Taufkirchen, Germany). Sucrose, microbiological grade, was purchased from Merck (Darmstadt, Germany). Rhodamine B endcapped PLGA (lactide/glycolide 50/50, average molecular weight 30 kDa) (RHOD-PLGA) was obtained from Polyscitech (West Lafayette, Indiana, United States). siSCRBL 5'-UUC UCC GAA CGU GUC ACG UdTdT-3' (with and without fluorescein-tag) and siCTGF 5'-AGA UUC CCA CCC AAU UCA ATT dTdT-3' were from Qiagen (Hilden, Germany) and Eurofins (Ebersberg, Germany). Sodium hyaluronate (13 kDa) (HA) was bought from Lifecore Biomedicals (Chaska, Minnesota, United States). Cell culture media, phosphate-buffered saline (PBS) and fetal calf serum were purchased from ThermoFisher Scientific (Darmstadt, Germany).

2.2 Methods

Working with RNA

RNAse-free working conditions were strictly applied. A separate work space that has been treated with RNAse-digesting substances was used and working in locations with turbulent airflow was avoided. A lab coat and gloves were worn at all times and changed on a regular basis. Barrier tips and other RNAse-free consumables from unopened boxes and bags were used exclusively. All glass ware was baked for at least 8 hours at 200°C prior to use. An extra set of chemicals and reagents was kept, and only RNAse-free equipment was used to remove them from their containers. RNAse-free water was obtained from a certified reverse osmosis facility. All solutions containing siRNA or siRNA-coated NPs were kept on ice if possible.

Preparation of LbL NPs

LbL-NP were prepared in a multi-stage process summarized in Figure 2.
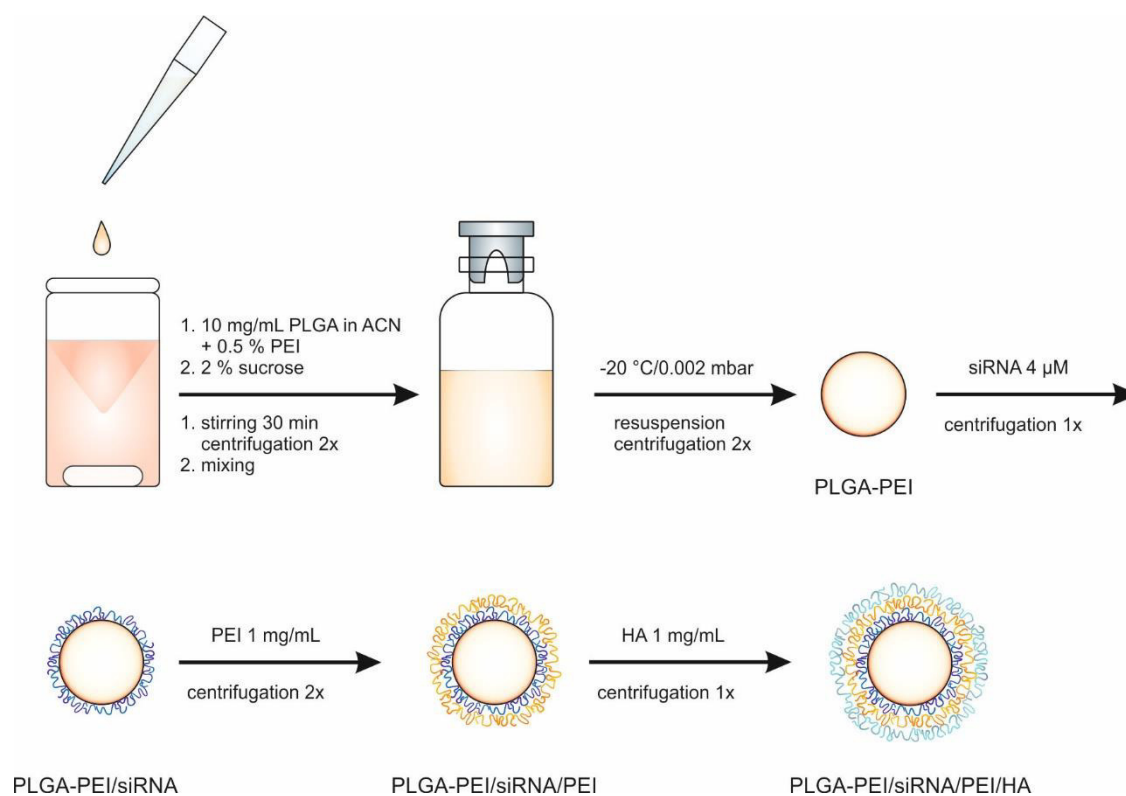
Figure 2. Schematic illustration of the synthesis and LbL coating procedures for PLGA-NPs. PLGA-NPs were prepared by nanoprecipitation and freeze dried for further storage. Resuspended NPs were coated with siRNA, PEI and HA, in that order. Each coating step was followed by purification of NPs from excess polyelectrolyte.

Synthesis of PLGA-NPs

8 mL of 0.5 % PEI were stirred in a snap cap vial to create a vortex and 2 mL PLGA solution (10 mg/mL in acetonitrile) was slowly injected. For the preparation of other sizes, PLGA and PEI concentrations were varied. The dispersion was stirred for at least 4 hours to guarantee the complete curing of the particles and evaporation of the organic solvent. For the preparation of rhodamine (RHOD)-labeled NP, a mixture of PLGA and RHOD-PLGA (50/50) was used.

NP purification

The NP dispersion was split into several Eppendorf tubes and centrifuged for 7 min at 4°C with a speed of 5,000 x g. The supernatant was removed. The pellet was resuspended in ultrapure water and the supernatant was centrifuged again for 7 min at 4°C with a velocity of 7,000 x g. To increase yield, the last step was repeated with a centrifugation speed of 9,000 x g. Supernatant of the last step was discarded and resuspended NPs were combined.

The entire process was repeated once. If the purified NPs were coated with siRNA, the final resuspension was performed in 10 mM sodium chloride.

Freeze drying and storage

Purified NPs were pooled, mixed with an equal volume of sucrose solution (4 % (w/v) in water) and filled into tared lyophilization vials. NPs were frozen at -80°C and dried for 5 days at -20°C and for two days at +20°C under vacuum using a Christ LMC-2 freeze-drying facility (Osterode am Harz, Germany). Dried samples were weight and the NP mass in the lyophilizate was calculated by subtracting the mass of sucrose added initially. NPs were resuspended in ultrapure water to a concentration of 1 mg/mL and purified as described above prior to coating.

Coating with polyelectrolytes

The polyelectrolyte solution was placed into a snap cap vial equipped with a stir bar. For the preparation of 1 mL of coated particles a) 200 μL siRNA 20 μM + 800 μL purified NPs; b) 10 μL PEI 100 mg/mL + 990 μL purified NPs; c) 100 μL HA 10 mg/mL + 900 μL purified NPs were used. Purified NPs were added dropwise into the gently stirred solution of polyelectrolyte and stirring was continued for approximately 30 min at room temperature. The concentration of the polymers during coating was 1 mg/mL in water or 4 μM in 10 mM NaCl for polymers (PEI and HA) and siRNA respectively. To monitor polyelectrolyte adsorption and NP aggregation, size and zeta potential measurements were carried out after every coating step.

Characterization by dynamic light scattering (DLS) and electrophoretic mobility

NPs were characterized in water by dynamic light scattering with a Zetasizer Nano ZS (Malvern Instruments, Herrenberg, Germany). 173° backward scatter and the general-purpose mode with automatic measurement position and attenuator selection at a temperature of 25°C was used. Z-average values were stated. Zeta potential measurements were conducted in monomodal mode.

Scanning electron microscopy

Purified NPs were added dropwise to conductive pads (Plano GmbH, Wetzlar, Germany) attached to aluminum specimen stubs (Agar Scientific, Stansted, Essex, UK) and air dried. The samples were sputtered with Au/Pd using a Polaron SC 515 SEM Sputter Coating System. Images were taken on a Zeiss DSM 950 scanning electron microscope (Jena, Germany). An acceleration voltage of 10 kV was used. The working distance was set to 24 mm and a magnification of 20,000 x was chosen.

Stability

To determine their stability, NPs were stored in Millipore water at 4°C for several weeks and DLS measurements were performed at least once a week after equilibrating the samples to room temperature. Short term stability studies at different pHs were performed by mixing the NPs with a 10 mM citrate or phosphate buffer of the respective pH, with PBS or with Leibovitz containing 0.35 % serum. Particles were diluted to a final concentration of 10 µg/mL. DLS measurements were initiated immediately after mixing the components. At least 40 measurement runs with a delay of 270 seconds were performed, covering a period of 5 hours.

FRET Measurements

For the preparation of NPs for FRET analysis, a RHOD-tagged PLGA core (RHOD-NP) and fluorescein-labeled siRNA (FITC-siRNA) were used. NPs were diluted to a final concentration of 10 µg/mL with PBS or serum containing Leibovitz media. siRNA concentration was set to 0.02 µM. Fluorescence emission spectra from 500 to 700 nm after excitation at 488 nm were recorded using a Perkin Elmer LS55 fluorescence spectrometer (Waltham, Massachusetts, United States). The slit width was set to 6 nm and the detector voltage to 700 V. Measurements were performed in triplicate, running 3 scans with 200 nm/min each.

3 Results and Discussion

3.1 Size variability of PLGA-NP

PLGA-NPs of different sizes were produced by varying the PLGA to PEI ratio during synthesis. Figure 3 shows a selection of scanning electron micrographs. While an increase in PLGA concentration resulted in larger particles, NPs became smaller if higher PEI concentrations were used. Similar findings were reported in literature [15,16]. These effects are related to the surface area of nascent NPs. If a high amount of stabilizer is available during NP formation, a large surface area can be stabilized and smaller particles form. If only few stabilizer molecules are present, larger particles are produced to keep the total surface area low. Dynamic light scattering measurements (Figure 4A) supported these findings.
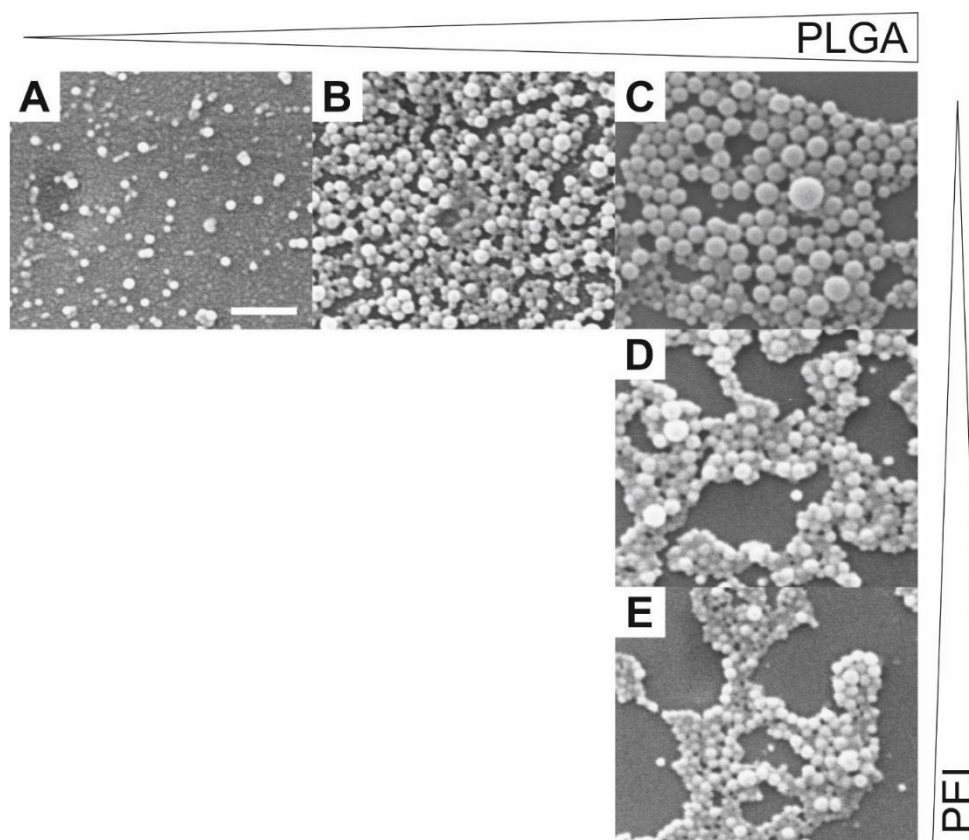
Figure 3. Scanning electron micrographs of NPs manufactured with different ratios of PLGA to PEI. The size of the NPs increased with PLGA concentration (from left to right) and with decreasing PEI concentration (from bottom to top). NPs were produced by combining 2 mL PLGA in acetonitrile and 8 mL of an aqueous PEI solution. A) 5 mg/mL PLGA + 0.5 % PEI. B) 10 mg/mL PLGA + 0.5 % PEI. C) 20 mg/mL PLGA + 0.5 % PEI. D) 20 mg/mL PLGA + 1 % PEI. E) 20 mg/mL PLGA + 2 % PEI. The scale bar represents 1 µm.

In addition to size, the zeta potential was also determined (Figure 4C). The zeta potential of the NPs was higher when more PLGA was used for the preparation and when the NP were larger, but decreased with PEI concentration. One explanation for these findings is that there is a link between the surface curvature of the particles and the zeta potential. Small NPs with higher curvature might have bound only a small number of PEI molecules. As PEI was highly hydrated and stretched over a large area, surface charge was low. Less curved, larger particles bound more PEI and surface charge was higher. The formulations also differed in terms of their polydispersity (Figure 4B). PDI was low when 0.5 or 1 % PEI and 10 mg/mL PLGA was used for the preparation of the particles. A PEI-concentration of 2 % resulted in inhomogeneous samples. To ensure sample uniformity, NPs synthesized with 0.5 % PEI and a 10 mg/mL solution of PLGA were used for all further studies.
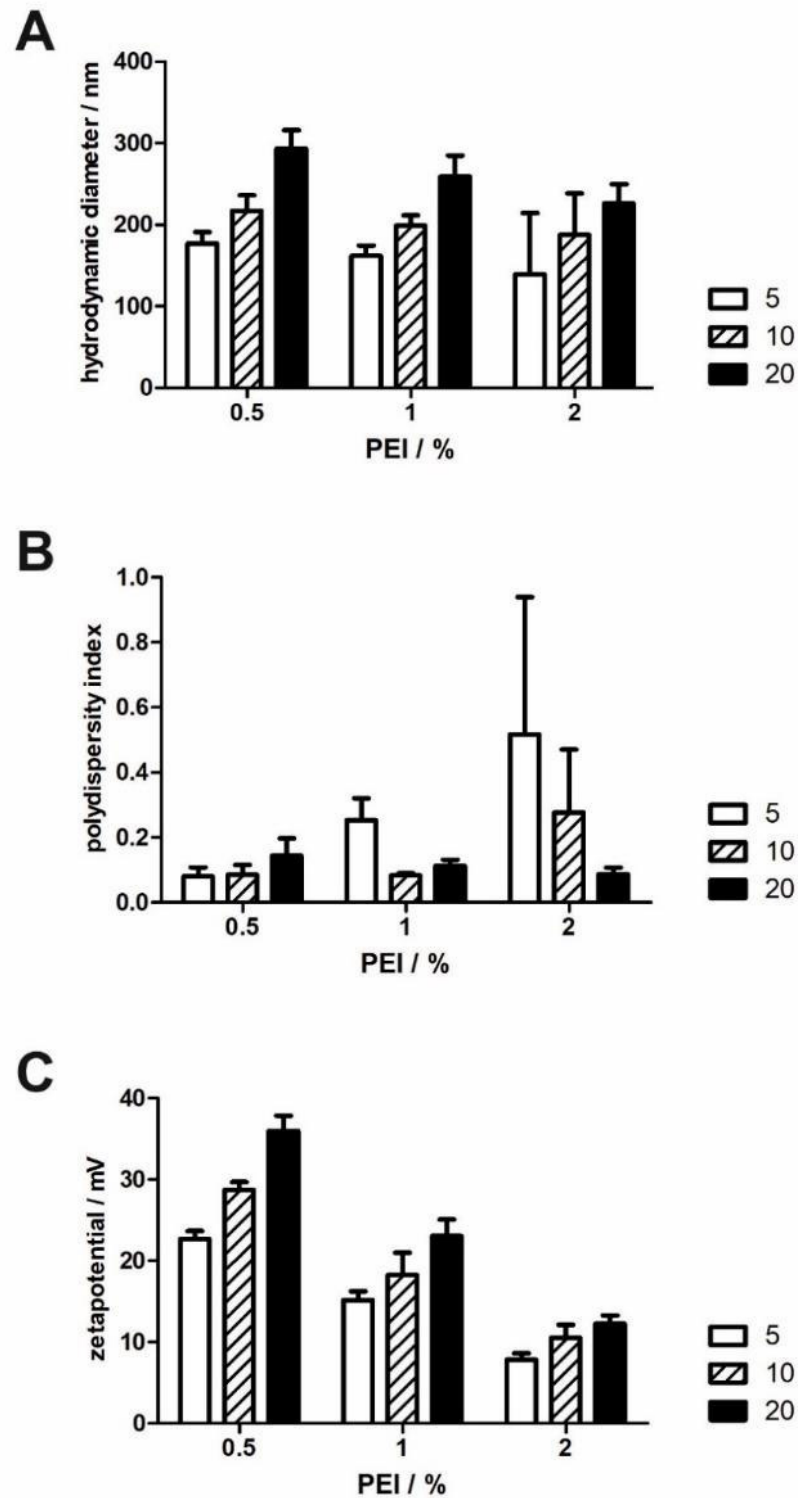
Figure 4. Characterization of PLGA-PEI-NP of different compositions by DLS and electrophoretic mobility. NPs were produced by mixing 2 mL of 5, 10 or 20 mg/mL PLGA in acetonitrile and 8 mL of a 0.5, 1 or 2 % aqueous PEI solution. A) The hydrodynamic diameter of the NP increased with PLGA concentration but decreased with PEI concentration. B) If low PGLA and PEI concentrations were used, polydispersity index was below 0.1. C) Higher concentrations of PLGA resulted in a higher surface charge whereas higher PEI concentrations led to lower values. Shown is the mean +/- SD of three independent experiments.

3.2 Freeze drying of PLGA-NPs

For storage and quantification of PLGA-NPs, a freeze-drying procedure was established. The addition of 1 to 3 % sucrose was sufficient to protect the NP from aggregation (Figure 5). Reconstituted NPs had a similar size and surface charge to the NPs before freeze drying (Figure 5A and C). Polydispersity index did not exceed 0.1 which indicates a narrow particle size distribution (Figure 5B) [17]. However, resuspension was not possible when NPs were frozen and dried without the addition of sucrose. Holzer et al. systematically investigated the influence of several cryoprotective agents on the reconstitution of freeze dried NPs [18]. They demonstrated that 1% sucrose or 2% trehalose is suitable for maintaining the colloidal stability of lyophilized PLGA-NPs stabilized with poly(vinyl alcohol). Here, this approach was applied to positively charged PEI-stabilized PLGA-NPs. Volume and mass of the lyophilization cake was considerably increased by the addition of sucrose. Thus, it was possible to gravimetrically determine the percentage of NPs of the lyophilizate. All NPs prepared made up 0.5 to 8 % of the lyophilized cake total mass (data not shown). The concentration of LbL-NPs after completed coating was determined by fluorescence intensity measurements in relation to a calibration curve of resuspended but unpurified NPs of known concentration (see supporting information).
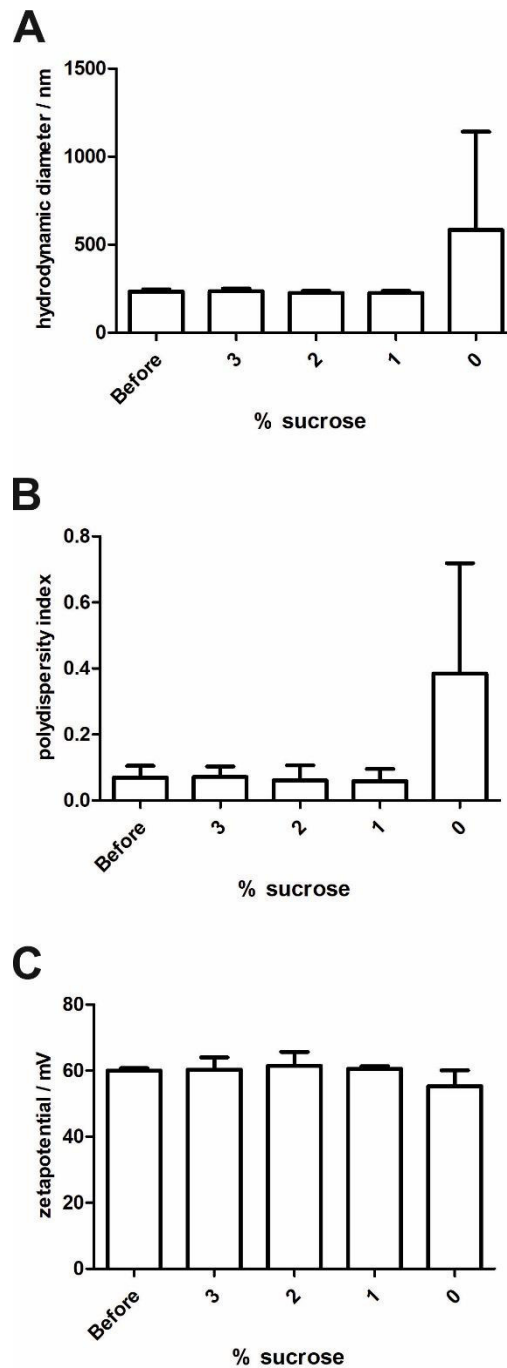
Figure 5. Effect of sucrose on the properties of resuspended PLGA-NP after freeze drying. A) The hydrodynamic diameter of the NPs remained unchanged after freeze drying and resuspension when 1 to 3 % sucrose was added. However, freeze drying without protective agent resulted in the aggregation of NPs. B) Polydispersity index after resuspension was <0.1 when sucrose was added during freeze drying. Complete resuspension was not possible without a lyoprotective agent. C) Zeta potential remained almost unchanged by the addition of sucrose for lyoprotection. Shown is the mean +/- SD of three independent experiments.

3.3   Layer-by-layer coating of PLGA-NPs and siRNA loading

The successful coating of PLGA-NPs with two different siRNA molecules, PEI and HA was demonstrated by DLS and zeta potential measurements (Figure 6). Throughout the entire process, particle size distribution was narrow. The polydispersity index (PDI), which is an indicator for the heterogeneity of particle sizes in a mixture, was < 0.1, an excellent value representing a highly monodisperse sample (Figure 6B). Though it is described in literature [10,19–21], no continuous increase in particle size was visible during the layer-by-layer deposition (Figure 6A). Hydrodynamic diameter decreased when negatively charged siRNA or HA was adsorbed and increased only if PEI was attached to the NP surface. A reversal of the surface charge (Figure 6C), however, proved the successful deposition of the respective polyelectrolyte. Interestingly, higher absolute zeta potential values were measured for PEI-terminated NPs than for those with a negatively charged terminal layer. As the zeta potential of a particle influences its hydrodynamic diameter [17], the formation of a thicker hydration shell around highly charged PEI-terminated NPs in comparison to less charged siRNA- or HA-NPs seems to be a rational explanation for the absence of size growth during the layer-by-layer formation process. The purification state of the NPs influenced the parameter size and zeta potential too. On the one hand, loosely bound polyelectrolytes were removed during purification, and size as well as zeta potential decreased. On the other hand, washing changed the pH and ionic strength of the dispersant. As a consequence, the zeta potential and hydrodynamic diameter of PEI-NPs increased after washing.
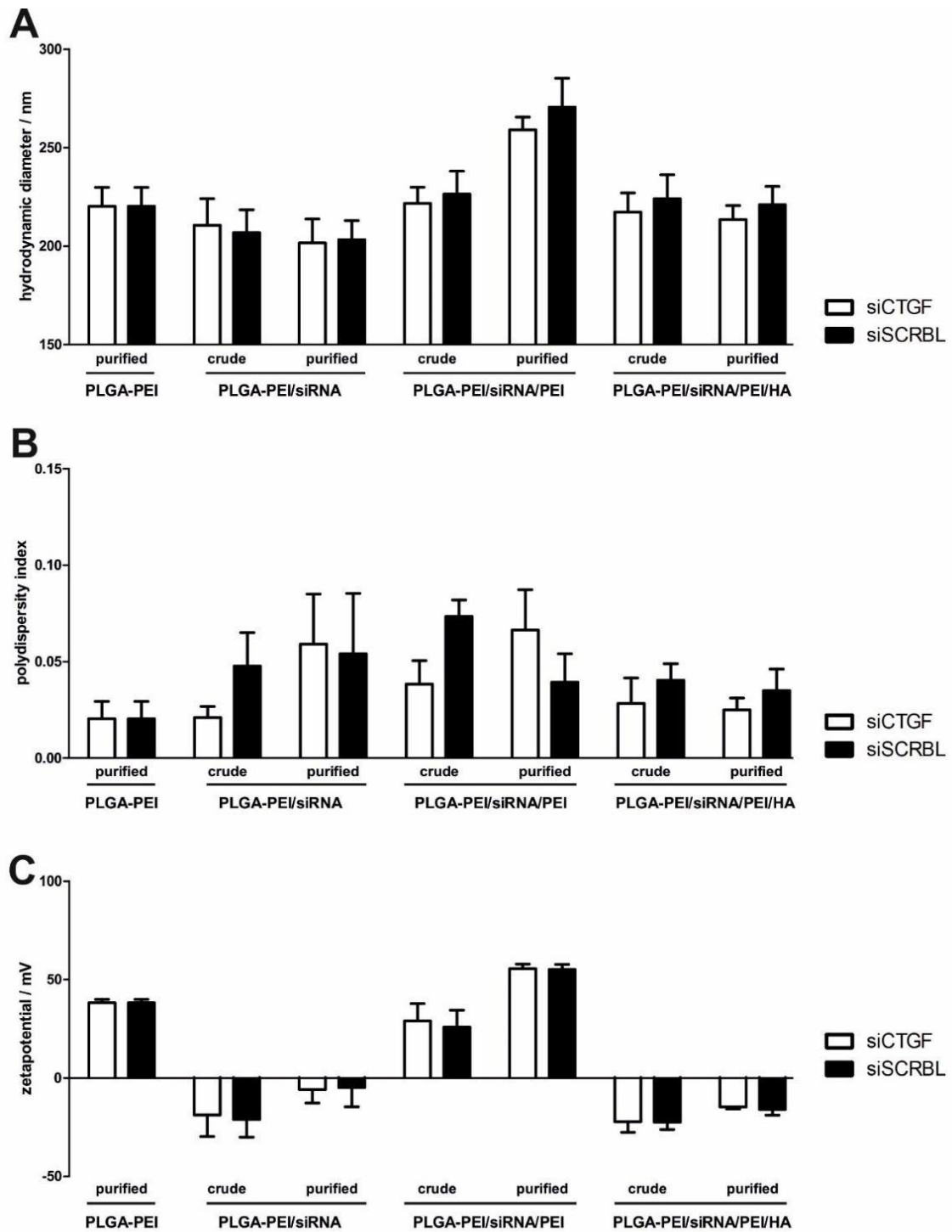
Figure 6. Characterization of the NPs during the LbL-process with two different siRNA (siCTGF and siSCRBL). A) Hydrodynamic diameter of the particles as determined by DLS. The NP size decreased after adsorption of negatively charged polymers but increased when PEI was deposited onto the NPs. Further, the purification from excessive polyelectrolyte led to an increase in diameter. B) A polydispersity index lower than 0.1 for all samples represented the absence of aggregates and a narrow particle size distribution. C) Electrophoretic mobility of the NPs. A reversal of zeta potential was determined after each coating step, indicating the successful deposition of the respective polyelectrolyte. Shown is the mean +/- SD of three independent experiments.

Calculations indicate that 7,500 to 60,000 siRNA molecules were bound to one individual NP (see supporting information). Based upon the number of bound siRNA molecules and the NP surface area, a single siRNA molecule occupied an area of 2.5 to 20 nm². This is a plausible range as the size of the siRNA is less than 10 nm [22,23]. A more precise indication may be the radius of gyration, which is the distance where the mass of a body may be assumed to be concentrated. As the radius of gyration was determined to be 2 nm [24], the area occupied by a sphere of this size would be approximately 12.5 nm² - which is perfectly within the calculated range.

3.4 Stability

While a delivery system for siRNA must protect the nucleic acid from degradation until it reaches the cell, it must also quickly release the therapeutic freight into the cytosol after endocytosis. Thus, LbL-NPs must show superior stability before application and in the extracellular space but disassemble quickly after successful uptake. During storage at 4°C, bare NP cores were stable in ultrapure water over several weeks (data not shown). However, NPs with siRNA coating were used within one week after preparation due to the fragility of the nucleic acid [25].

Changes in size of fully assembled LbL-NP by swelling or aggregation were evaluated in buffers of different pHs, in PBS and in cell culture media by DLS (Figure 7). Both types of NPs were stable in low ionic strength buffer, but PEI-terminated particles showed a steady increase in hydrodynamic diameter when the pH of the dispersant dropped to 5.5. Although the particles were stable in 10 mM phosphate buffer pH 7, HA-coated particles showed strong aggregation in PBS of the same pH. During a period of five hours, the size of both NP types increased in Leibovitz supplemented with 0.35 % serum. Whereas particle growth of PEI-NP started immediately after mixing with cell culture medium, HA-NPs were unchanged for at least one hour.
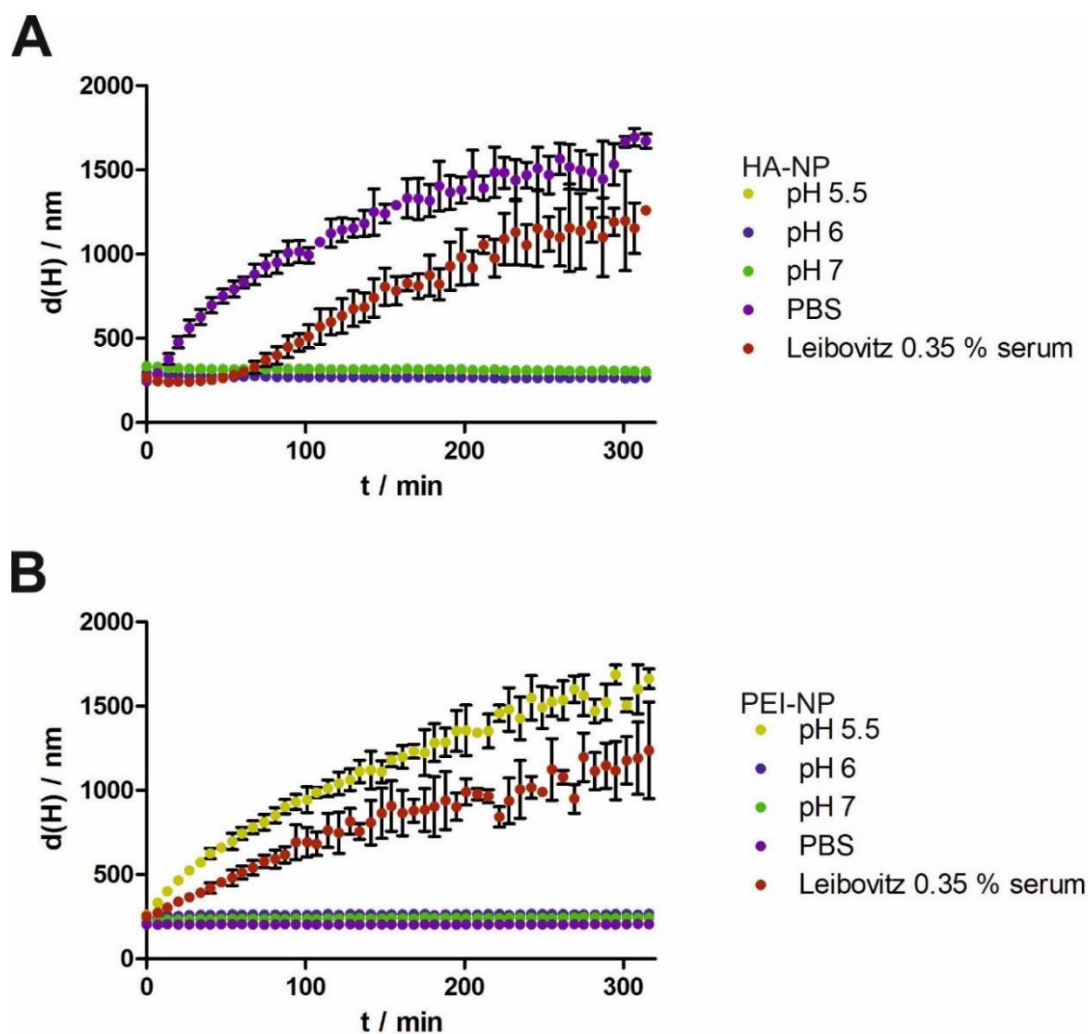
Figure 7. Colloidal stability of HA- (top) and PEI-terminated (bottom), fully assembled LbL-NP in 10 mM buffer of different pHs, PBS and Leibovitz with 0.35 % serum. Both NPs were stable in buffer of pH 6 and 7. However, aggregation occurred for both NPs in Leibovitz media with 0.35 % serum, for HA-NPs in PBS and for PEI-NPs in a buffer of pH 5.5.

The dispersion state of NPs is influenced by pH, ions and proteins since particles are stabilized by electrostatic interactions, steric hindrance or a combination of both [26]. Changing the pH of the dispersant might reduce the surface charge to values lower than an absolute value of 20 to 30 mV, which is critical for sufficient electrostatic repulsion and stabilization [27]. Findings for PEI-NPs in buffer of pH 5.5, however, seemed to contradict this theory as more positive surface charges were expected with the lower pH. In general, high concentrations of ions in the dispersant interfere with the colloidal stability of the NPs as the electrostatic double layer around them might be compressed and surface charges screened. Hence, aggregation is more likely. In our study, PEI-NPs tolerated high ion concentrations better than HA-coated NPs, possibly because of the higher charge density of PEI compared to HA. Results regarding the influence of proteins on the stability of NPs are

contradictory. Depending on protein concentration and composition of the NPs, a stabilizing or destabilizing effect can be observed [26]. DLS measurements reported here show an enhanced stability of HA-NPs in Leibovitz supplemented with 0.35 % serum compared to PEI-NPs. Leibovitz with 0.35 % serum was used to mimic the concentration of proteins in the aqueous humor in the eye, which is the intended application site of the NPs. As HA-NPs were dispersed for a longer time until aggregate formation began, these particles are more likely to reach their target cells well dispersed. An additional stability study of the NPs in cell culture and the influence of serum proteins will be detailly discussed in chapter 4.

The cohesion of the polymer shells of a LbL-NP can be monitored by FRET-studies [28]. FRET describes the radiation less energy-transfer of two fluorophores in close spatial proximity [29]. A donor chromophore transfers its energy by dipole-dipole coupling to another acceptor chromophore. As the FRET efficiency is irreversible proportional to the sixth power of distance, this method can be used to determine distances in the lower nanometer range. To observe this effect, an overlap of the emission spectra of the FRET donor and the extinction spectrum of FRET acceptor is required. Commonly used FRET fluorophores are fluorescein (FITC) and rhodamine (RHOD). We prepared NPs where the core was labeled with RHOD and siRNA with FITC (Figure 8A). Emission spectra of these particles were recorded after irradiation with light at a wavelength of 488 nm in PBS (Figure 8B) or Leibovitz with 0.35 % serum (Figure 8C). As expected, a prominent maximum was detectable for FITC-siRNA at 525 nm. Nanoparticles without siRNA carrying only the RHOD fluorophore did not show any fluorescence signal after irradiation with light at 488 nm. However, if RHOD-NP were coated with FITC-siRNA, fluorescence was detectable at 580 nm, the emission maximum of RHOD (see supporting information). Fluorophores seemed to be close enough for FRET energy transfer. As there was neither a difference between the HA- and PEI-terminated NPs nor between PBS and Leibovitz as a dispersant, it can be assumed that both NP types were stable in PBS and Leibovitz and no disassembly of the particles occurred during the investigated time frame.
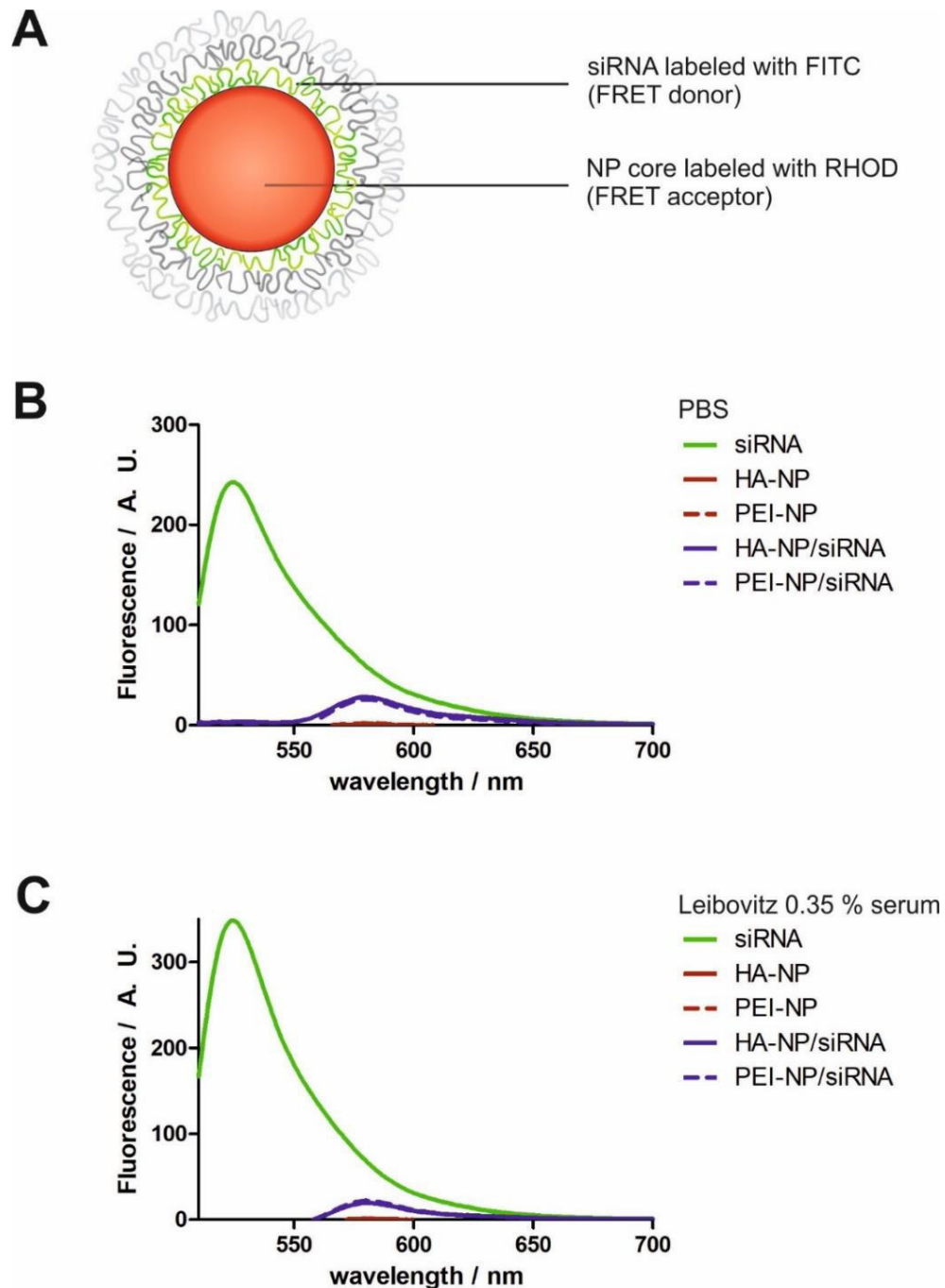
Figure 8. Stability and disassembly of multilayered NPs was determined in PBS (B) and Leibovitz with 0.35 % serum (C) by Foerster resonance energy transfer (FRET). The FRET donor FITC was conjugated to siRNA and the NP core was labeled with the FRET acceptor RHOD (A). FITC-siRNA (green) showed a characteristic fluorescence emission spectrum after irradiation with 488 nm laser light. The maximum was detected at 525 nm. RHOD-NPs without siRNA did not show any fluorescence (red, both lines very close to x-axis). However, fully assembled NPs with both fluorophores (blue) showed an emission maximum at 580 nm which corresponds to the maximum of RHOD when excited with light at 543 nm. The differences between particle types and dispersants were neglectable. Shown is the mean of three independent measurements. SD was not presented to achieve better visualization of the curves.

4   Conclusion

Here we demonstrated the development of a successful protocol for the preparation of LbL-NPs for siRNA delivery. By choosing appropriate amounts of PLGA and stabilizer, NPs in a wide range of sizes could be produced without major changes in the protocol. Hence, particle size could be easily tailored to individual requirements. The addition of sucrose for lyoprotection enabled the complete resuspension of the particles after freeze drying without impeding their quality. By the establishment of this procedure, the quantification of the particles also became possible. With our coating strategy, we were able to produce NPs with a multilayered shell for siRNA delivery. During the process, the method of stepwise centrifugation was effective in removing all unbound polyelectrolytes without inducing aggregation before adsorption of the next polyelectrolyte shell. DLS stability studies showed an advantage of the HA-coating over uncoated NPs with regard to aggregation in an environment mimicking physiologic conditions. Further benefits of the HA coating will be discussed in the next chapters.

References

[1] Ariga K, Yamauchi Y, Rydzek G, Ji Q, Yonamine Y, Wu KC-W, Hill JP (2014), Layer-by-layer Nanoarchitectonics: Invention, Innovation, and Evolution: Invention, Innovation, and Evolution, Chem Lett 43 36–68.

[2] Decher G, Hong J-D (1991), Buildup of ultrathin multilayer films by a self-assembly process, 1 consecutive adsorption of anionic and cationic bipolar amphiphiles on charged surfaces, Makromol Chem Macromol Symp 46 321–327.

[3] Yan Y, Such GK, Johnston APR, Lomas H, Caruso F (2011), Toward therapeutic delivery with layer-by-layer engineered particles, ACS Nano 5 4252–4257.

[4] Wohl BM, Engbersen JFJ (2012), Responsive layer-by-layer materials for drug delivery, J Control Release 158 2–14.

[5] Elbakry A, Zaky A, Liebl R, Rachel R, Goepferich A, Breunig M (2009), Layer-by-Layer Assembled Gold Nanoparticles for siRNA Delivery, Nano Lett 9 2059–2064.

[6] Danhier F, Ansorena E, Silva JM, Coco R, Le Breton A, Préat V (2012), PLGA-based nanoparticles: an overview of biomedical applications, J Control Release 161 505–522.

[7] Neuberg P, Kichler A (2014), Recent developments in nucleic acid delivery with polyethylenimines, Adv Genet 88 263–288.

[8] Almeida PV, Shahbazi M-A, Mäkilä E, Kaasalainen M, Salonen J, Hirvonen J, Santos HA (2014), Amine-modified hyaluronic acid-functionalized porous silicon nanoparticles for targeting breast cancer tumors, Nanoscale 6 10377–10387.

[9] Martens TF, Remaut K, Demeester J, Smedt SC de, Braeckmans K (2014), Intracellular delivery of nanomaterials: How to catch endosomal escape in the act, Nano Today 9 344–364.

[10] Deng ZJ, Morton SW, Ben-Akiva E, Dreaden EC, Shopsowitz KE, Hammond PT (2013), Layer-by-Layer Nanoparticles for Systemic Codelivery of an Anticancer Drug and siRNA for Potential Triple-Negative Breast Cancer Treatment, ACS Nano 7 9571–9584.

[11] Orian-Rousseau V (2010), CD44, a therapeutic target for metastasising tumours, Eur J Canc 46 1271–1277.

[12] Guter M, Dillinger Andrea, Scherl Franziska, Breunig M, Fuchshofer R, Layer-by-layer assembled nanoparticles for glaucoma therapy: Manuscript in process.

[13] Dosio F, Arpicco S, Stella B, Fattal E (2016), Hyaluronic acid for anticancer drug and nucleic acid delivery, Adv Drug Deliver Rev 97 204–236.

[14] Platt VM, Szoka FC (2008), Anticancer Therapeutics: Targeting Macromolecules and Nanocarriers to Hyaluronan or CD44, a Hyaluronan Receptor, Mol Pharm 5 474–486.

[15] Bohrey S, Chourasiya V, Pandey A (2016), Polymeric nanoparticles containing diazepam: preparation, optimization, characterization, in-vitro drug release and release kinetic study, Nano Conv 3 3.

[16] Zweers MLT, Grijpma DW, Engbers GHM, Feijen J (2003), The preparation of monodisperse biodegradable polyester nanoparticles with a controlled size, J Biomed Mater Res B 66 559–566.

[17] Bhattacharjee S (2016), DLS and zeta potential - What they are and what they are not?, J Control Release 235 337–351.

[18] Holzer M, Vogel V, Mäntele W, Schwartz D, Haase W, Langer K (2009), Physico-chemical characterisation of PLGA nanoparticles after freeze-drying and storage, Eur J Pharm Biopharm 72 428–437.

[19] Poon Z, Lee JB, Morton Stephen W., Hamond PT (2011), Controlling in Vivo Stability and Biodistribution in Electrostatically Assembled Nanoparticles for Systemic Delivery, Nano Lett 11 2096–2103.

[20] Elbakry A, Wurster E-C, Zaky A, Liebl R, Schindler E, Bauer-Kreisel P, Blunk T, Rachel R, Goepferich A, Breunig M (2012), Layer-by-layer coated gold nanoparticles: size-dependent delivery of DNA into cells, Small 8 3847–3856.

[21] Morton SW, Poon Z, Hammond PT (2013), The architecture and biological performance of drug-loaded LbL nanoparticles, Biomater 34 5328–5335.

[22] Matsui K, Sasaki Y, Komatsu T, Mukai M, Kikuchi J-i, Aoyama Y (2007), RNAi gene silencing using cerasome as a viral-size siRNA-carrier free from fusion and cross-linking, Bioorgan Med Chem 17 3935–3938.

[23]   Guo P, Coban O, Snead NM, Trebley J, Hoeprich S, Guo S, Shu Y (2010), Engineering RNA for targeted siRNA delivery and medical application, Adv Drug Deliver Rev 62 650–666.

[24]   Pavan GM, Mintzer MA, Simanek EE, Merkel OM, Kissel T, Danani A (2010), Computational insights into the interactions between DNA and siRNA with "rigid" and "flexible" triazine dendrimers, Biomacromolecules 11 721–730.

[25]   Whitehead KA, Langer R, Anderson DG (2009), Knocking down barriers: advances in siRNA delivery, Nat Rev Drug Discov 8 129–138.

[26]   Moore TL, Rodriguez-Lorenzo L, Hirsch V, Balog S, Urban D, Jud C, Rothen-Rutishauser B, Lattuada M, Petri-Fink A (2015), Nanoparticle colloidal stability in cell culture media and impact on cellular interactions, Chem Soc Rev 44 6287–6305.

[27]   Wu L, Zhang J, Watanabe W (2011), Physical and chemical stability of drug nanoparticles, Adv Drug Deliver Rev 63 456–469.

[28]   Lee L, Johnston APR, Caruso F (2012), Probing the dynamic nature of DNA multilayer films using Förster resonance energy transfer, Langmuir 28 12527–12535.

[29]   Piston DW, Kremers G-J (2007), Fluorescent protein FRET: the good, the bad and the ugly, Trends Biochem Sci 32 407–414.

Layer-by-layer assembled nanoparticles for siRNA delivery

1 Quantification of nanoparticles

The concentration RHOD-NP after completed LbL-coating was determined by fluorescence spectroscopy. Resuspended but unpurified NP of the same batch with known concentration were used for a calibration curve. The fluorescence intensity was measured on a microplate reader (FLUOStar Omega, BMG Labtech, Ortenberg, Germany) equipped with 544 nm excitation and 590 nm emission filter sets.
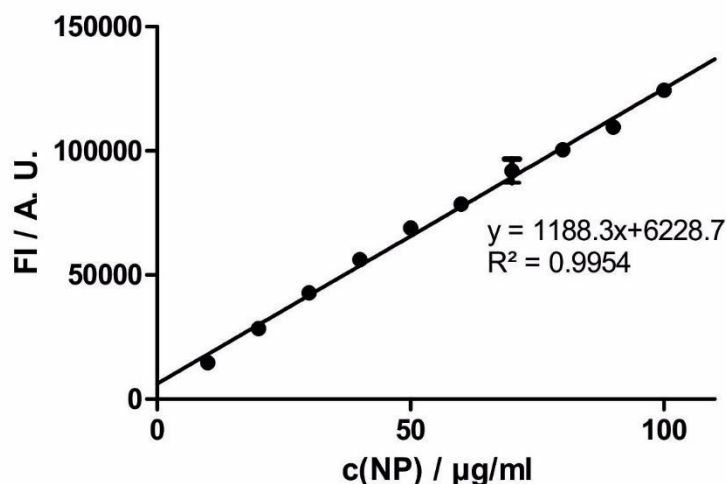
S 1. Calibration curve as used for the quantification of fully assembled LbL-NP. Fluorescence intensities (FI) of diluted samples were covered by the calibration. Shown is the mean $\pm$ SD of a triplicate measurement.

2 siRNA loading efficiency

The number of siRNA molecules attached to a NP was determined by calculating the difference between the siRNA concentration during coating and the siRNA concentration of the supernatant after centrifugation of coated NP in relation to the NP concentration. One part of a 20 μM siRNA solution was mixed with four parts of NP during the coating. After stirring the particles for approximately 30 minutes, NP were purified as described in the material and method section. Absorbance of the supernatant and of the 20 μM siRNA solution was read at 260 nm with a Nanodrop 2000c (Peqlab, Erlangen, Germany). The concentration of uncoated NPs was determined by fluorescence as presented before. The hydrodynamic diameter was measured by dynamic light scattering as described. Each of three different PLGA-PEI NP batches were coated with two siRNA of distinct sequence.

Calculations were performed as follows:

1. siRNA attached to NP

Determination of absorbance at 260 nm: $\qquad OD(siRNA_{20\ \mu M})$

$$OD(siRNA_{supernatant})$$

$$c(siRNA_{supernatant}) = \frac{OD(siRNA_{supernatant})}{OD(siRNA_{20\ \mu M})} \cdot 20\ \mu M$$

$$c(siRNA_{attached}) = \frac{1}{5} \cdot c(siRNA_{20\ \mu M}) - c(siRNA_{supernatant})$$

$$= 4\ \mu M - c(siRNA_{supernatant})$$

2. Molar concentration of NP during coating

Quantification of PLGA-PEI-NP before coating: $\qquad \beta_{before}\ \left[\frac{kg}{L}\right]$

Hydrodynamic diameter: $\qquad d\ [m]$

Density of PLGA[1]: $\qquad \varphi_{PLGA} = 1300\ \frac{kg}{m^3}$

$$m(PLGA - PEI/siRNA) = \varphi_{PLGA} \cdot \frac{4}{3} \cdot \pi \cdot \left(\frac{d}{2}\right)^3$$

$$N(PLGA - PEI/siRNA)_{1L} = \frac{\frac{4}{5}\beta \cdot 1L}{m(PLGA - PEI/siRNA)}$$

$$n(PLGA - PEI/siRNA) = \frac{N(PLGA - PEI/siRNA)}{N_A}$$

$$c(PLGA - PEI/siRNA) = \frac{n(PLGA - PEI/siRNA)}{1L}$$

---

[1]Information in literature varied from 1.2 to 1.5 g/cm³ [1–5]. Hence, a density of 1.3 g/cm³ was used for calculation.

3. siRNA molecules per NP

$$\frac{siRNA}{NP} = \frac{c(siRNA_{attached})}{c(PLGA - PEI/siRNA)}$$

4. Area per siRNA molecule

$$\frac{nm^2}{siRNA} = \frac{\pi d^2}{siRNA/NP}$$

Calculations showed that about 7,500 to 60,000 siRNA molecules adhered to one individual NP or that 2.5 to 20 nm² of the NP surface were occupied by one siRNA molecule. Detailed results are shown in Table 1.

Table 1. siRNA loading of NP assembled via the LbL technique. Shown are the measured (OD, β, d) and calculated (siRNA/NP, nm²/siRNA) values of different batches. The number of siRNA molecules per NP and the space requirement of one siRNA molecule on the NP surface are shown in the last two columns.

siRNA	OD $(siRNA_{20\ \mu M})$	OD $(siRNA_{supernatant})$	β_{before} $\left[\frac{mg}{L}\right]$	d [m]	siRNA /NP	nm² /siRNA
Batch GU179						
siSCRBL	5.544	0.816	227	216.6	24,256	6.1
siEGFP	5.542	0.790	227	216.6	26,324	5.6
Batch GU213						
siSCRBL	4.788	0.835	355	215.1	7,376	19.7
siGFP2	6.281	0.379	355	215.1	17,270	8.4
Batch GU238						
siSCRBL	5.260	0.249	268	216.5	59,261	2.5
siCTGF	5.590	0.291	268	216.5	57,405	2.6

3 Fluorescence emission spectra of RHOD-NP and FITC-siRNA

Rhodamine labeled HA- and PEI-NP were diluted to a final concentration of 10 µg/ml with PBS, FITC-siRNA was measured in a concentration of 0.02 µM. Fluorescence emission spectra from 510 to 700 nm and 570 to 700 nm after excitation at 488 nm or 543 nm respectively were recorded using a Perkin Elmer LS55 fluorescence spectrometer (Waltham, Massachusetts, United States). The slit width was set to 6 nm and the detector voltage to 700 V. Measurements were performed in triplicate, running 3 scans with 200 nm/min each.
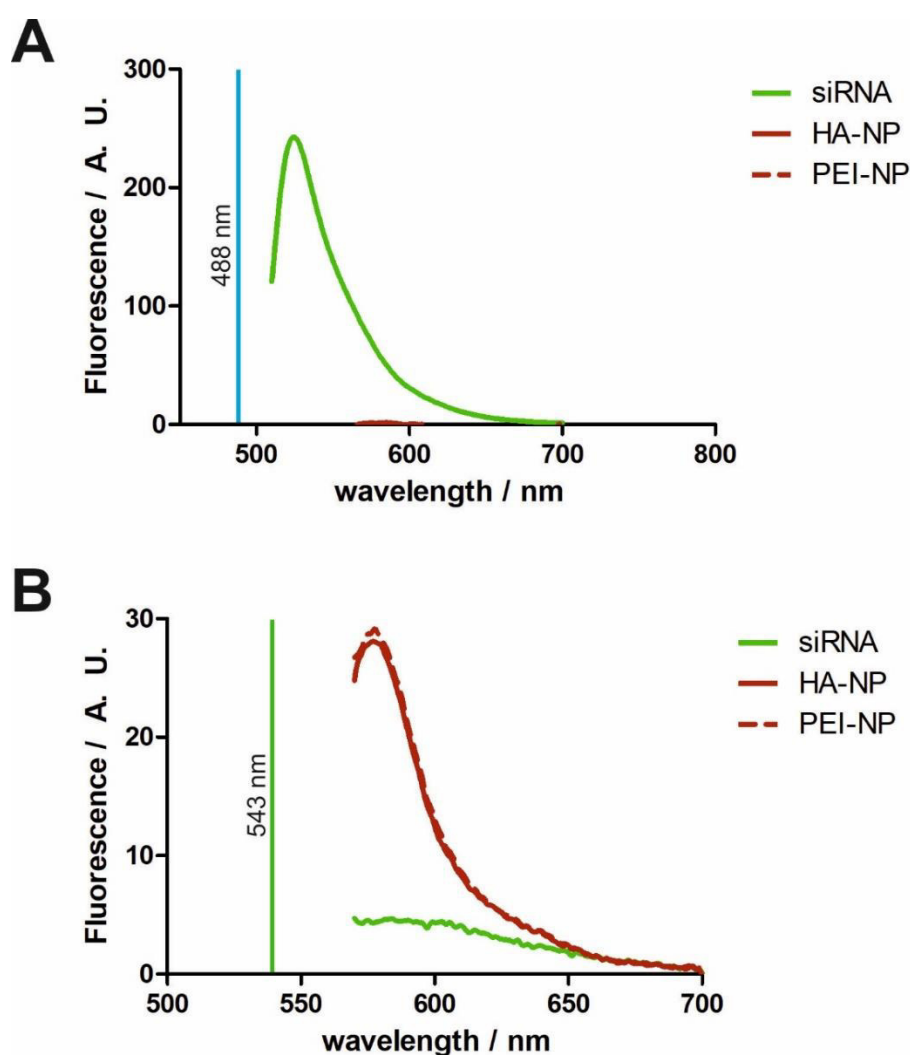
S 2. Fluorescence emission spectra of FITC-siRNA and RHOD-NP. A) A prominent maximum at 525 nm was visible when FITC-siRNA was irradiated with light at 488 nm but no signal was detected for RHOD-NP. B) If the NP were excited with 543 nm light, RHOD-NP showed strong fluorescence emission at a wavelength of 580 nm.

References

[1]   Degradex, Degradex® PLGA Microspheres and PLGA nanoparticles, 2017, http://www.degradex.com/degradexreg-plga-microspheres.html.

[2]   Qi R, Guo R, Shen M, Cao X, Zhang L, Xu J, Yu J, Shi X (2010), Electrospun poly(lactic-co-glycolic acid)/halloysite nanotube composite nanofibers for drug encapsulation and sustained release, J Mater Chem 20 10622.

[3]   I. Polysciences, PLGA (Poly Lactic co-Glycolic Acid) Uniform Dry Microspheres: Technical Data Sheet 858, 2016, accessed 14 November 2017.

[4]   Blasi P, D'Souza SS, Selmin F, DeLuca PP (2005), Plasticizing effect of water on poly(lactide-co-glycolide), J Control Release 108 1–9.

[5]   Cu Y, Saltzman WM (2009), Controlled surface modification with poly(ethylene)glycol enhances diffusion of PLGA nanoparticles in human cervical mucus, Mol Pharm 6 173–181.

Hyaluronic acid decorated nanoparticles for the targeting of trabecular meshwork cells

Abstract
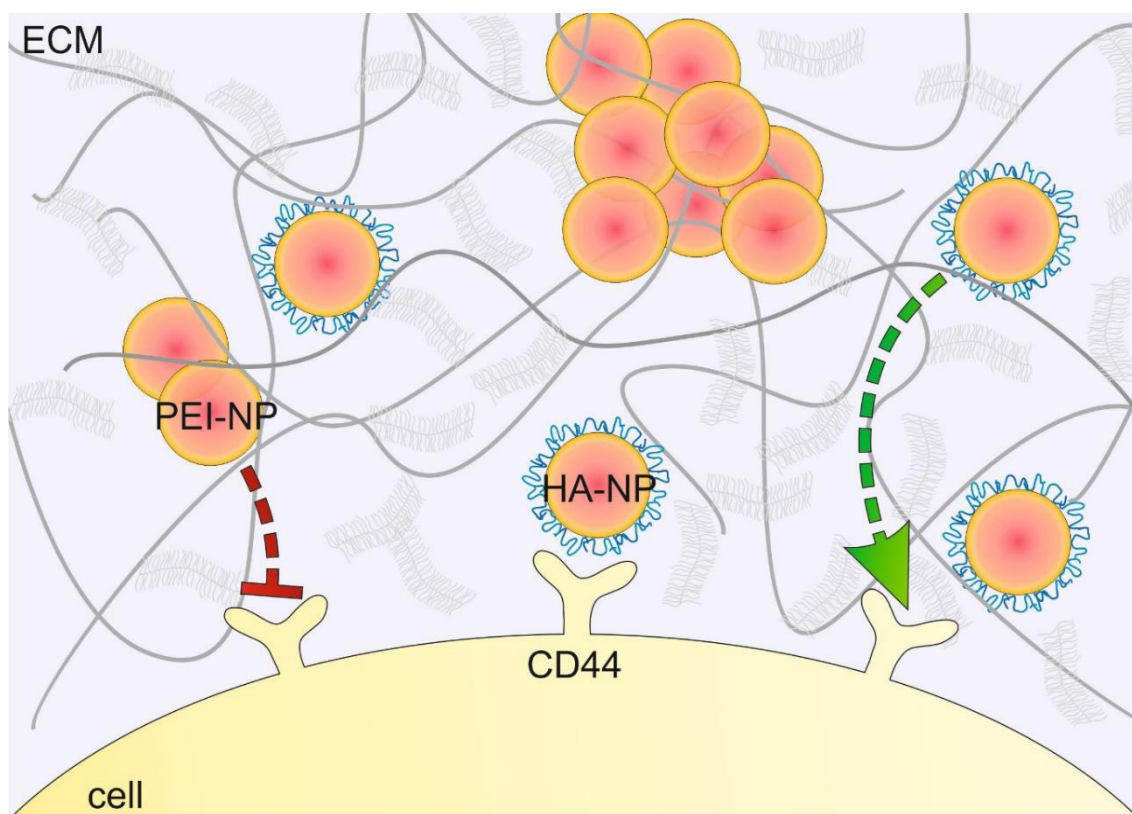
The targeting of cell surface receptors with ligand-decorated nanoparticles (NPs) is widely used to tailor interactions between NPs and cells. Targeting cluster of differentiation (CD) 44 receptors with hyaluronic acid (HA) functionalized NPs (HA-NPs) is a frequently pursued strategy for cancer therapy. We applied the concept of CD44-targeting with HA-NPs to the ocular environment. The dependency of cell/NP interactions on the CD44 receptor were described using cell lines which differ in their CD44 expression. We compared NPs that were either functionalized with HA or the polycation polyethyleneimine (PEI). HA-decorated NPs showed a correlation between cell association and CD44-density and, unexpectedly, PEI-NPs behaved similarly. Receptor blockade studies confirmed the presence of interactions between cell membrane, CD44, and HA or PEI. Further, it was demonstrated that HA modification enhanced the colloidal stability of the NPs *in vitro*. An artificial extracellular matrix model was used to characterize the NP mobility and interaction with cells in a system closer to natural conditions in the eye. Our studies showed that HA-functionalization of NPs is an exceptional method to improve the performance of nanomaterials.

1   Introduction

Nanoparticles (NPs) are powerful tools for drug and gene delivery. Their high tailorability in terms of composition, size and surface functionalization makes it possible to precisely adjust their characteristics according to the individual requirements of specific applications. By the immobilization of receptor ligands on the surface of NPs, interactions with cells can be utilized to target defined organs and tissues [1]. Usually, targeted receptors are not only expressed in diseased but also in healthy organs. However, there is often a difference in receptor quantity or subtype. These principles apply to the cluster of differentiation (CD) 44 protein. The protein is ubiquitously expressed in the human body [2,3] and mediates different effects including not only physiological cell adhesion and migration but also tumor growth, metastasis and angiogenesis depending on the isoform and glycosylation pattern. The subtype CD44v6, for example, is upregulated in various types of cancer but not in normal tissues and has been recognized as a possible target for cancer therapy [4,5]. Functionalization of drugs or NPs with the CD44-ligand hyaluronic acid (HA) provides the substances with a targeting moiety to the CD44 receptor, thus directing them to tumor cells [4]. Although most scientific effort has been put into CD44-targeting for cancer therapy, other fields can also benefit from this approach. In general, the eye is an interesting target for NP therapy [6]. As an immune-privileged organ, the risk of undesired immune responses is reduced. Furthermore, because local application of the NPs is possible, the off-target effects that result from systemic administration are reduced—important since CD44 is ubiquitously expressed throughout the body at a certain level.

We developed HA-decorated layer-by-layer NPs for targeting cells in the trabecular meshwork (TM). NPs will be injected into the anterior chamber of the eye and follow the physiological aqueous humor flow to the outflow pathways of the TM. There, NPs are expected to interact with CD44-receptors on the surface of TM cells and deliver a therapeutic nucleic acid. In addition to CD44-targeting, we assume that the functionalization of NPs with the polysaccharide HA will enhance their mobility in the dense extracellular matrix, which often is a barrier to successful drug delivery. To confirm our hypotheses, we used model NPs described in Figure 1. The core is composed of poly(lactide-*co*-glycolide) (PLGA) and stabilized by polycationic polyethyleneimine (PEI). HA was electrostatically attached right onto the NP core. First, we studied the impact of HA-coating on the colloidal stability of the NPs in a physiologically relevant environment as well as the mobility in an artificial extracellular matrix (ECM) since these factors are crucial for successful drug delivery. Then,

CD44 receptor expression of immortalized TM cells was determined in comparison with two breast cancer cell lines. Finally, the dependency of NP uptake on the CD44 receptor density was investigated and receptor blockade studies were conducted.
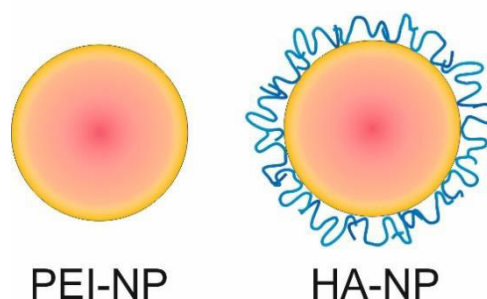

Figure 1. Model NP without siRNA freight. The NP core is made of poly(lactide-co-glycolide) (red) which was stabilized with positively charged polyethyleneimine (yellow). Hyaluronic acid (blue) was electrostatically assembled on the surface.

2   Material and Methods

2.1   Materials

Acid terminated poly(D,L-lactide-*co*-gylcolide) (PLGA) (lactide/glycolide 50/50) with an average molecular weight of 38-54 kDa (PLGA) and branched poly(ethylenimine) 25 kDa (PEI) were bought at Sigma-Aldrich Chemical Company (Taufkirchen, Germany). Sucrose, microbiological grade, was purchased from Merck (Darmstadt, Germany). Rhodamine B endcapped PLGA (50/50, 30 kDa) (RHOD-PLGA) and fluorescein conjugated PLGA (FITC-PLGA) (50/50, 20-40 kDA) were obtained from Polyscitech (West Lafayette, Indiana, United States). Sodium hyaluronate (HA) (13 kDa, 289 kDa) was bought at Lifecore Biomedicals (Chaska, Minnesota, United States). Alexa Fluor® 488 anti-mouse/human CD44 antibody (clone IM7) and the corresponding isotype control were purchased at BioLegend (Fell, Germany). Sodium azide was bought at Merk (Darmstadt, Germany). Bovine serum albumin (lyophilized powder, BioReagent), fetal bovine serum, collagen from bovine skin and propidium iodide were bought at Sigma-Aldrich Chemical Company (Taufkirchen, Germany). Matrigel was bought at Corning (Wiesbaden, Germany). All cell culture reagents were obtained from Gibco (Thermofisher Scientific, Darmstadt, Germany). The substances were used without further purification.

2.2   Methods

Preparation of PEI- and HA-NP

NPs were prepared as described in chapter 3. In brief, 2 mL of a 10 mg/mL solution of PLGA in acetonitrile was slowly injected into 8 mL of a continuously stirred PEI solution (0.5 % w/v). After evaporation of the organic solvent, NPs were purified by stepwise centrifugation and freeze dried using 2 % sucrose as a lyoprotective agent. For the synthesis of fluorescent PLGA-NPs, an equal mixture of PLGA and fluorescent PLGA was used. NPs were resuspended and purified by stepwise centrifugation. Resulting particles were termed PEI-NPs. For HA-functionalized NP, PEI-NPs were dropped into a stirring solution of 1 mg/mL HA in water. Stirring was continued for approximately 30 minutes and excess polysaccharide was removed.

3D cell culture

5 mL of a 3 mg/mL collagen I solution was lyophilized with a Christ LMC-2 freeze dryer (Osterode am Harz, Germany) under sterile conditions. Powdered collagen I was resuspended in 1.6 mL of 0.1 N HCl on ice. After addition of 200 µL 10x EMEM cell culture media, the pH was adjusted to pH 7.4 using 1 N NaOH. The final volume was set to 2 mL with water. 200 µL of this 7.5 mg/mL collagen I solution was mixed with 50 µL PEI- or HA-NPs and 80,000 HeLa cells in 50 µL DMEM containing 10 % serum. The final concentrations were 5 mg/mL of collagen I and 80 µg/mL of NPs. Cells were incubated at 37°C for 48 h. When the gelation was completed after a few hours, 200 µL medium was added on top of the gel to avoid desiccation. If cells were embedded in Matrigel, the procedure was the same. However, Matrigel was used as supplied without freeze-drying and resuspension. Confocal images were taken on a Zeiss confocal laser scanning microscope (Zeiss Axiovert 200 coupled to a LSM 510 META, Oberkochen, Germany).

CD44-expression

MDA-MB-231, hTM, HTM-N and MCF-7 cells were grown in 75 cm² cell culture flasks in normal growth medium (McCoy's, Ham's F12, DMEM + pyruvate or EMEM + pyruvate with 10 % serum). When they reached 70% confluency, cells were washed with PBS and harvested by trypsinization. Cells were stained with an anti-CD44 antibody at a concentration of 0.05 µg / 100,000 cells in FACS-buffer (PBS containing 1 % BSA and 0.1 % sodium

azide) for 30 min in the dark on ice. Cells were washed twice and resuspended in FACS buffer. Live-dead staining with propidium iodide was performed directly before analysis on a FACS Calibur (BD GmbH, Heidelberg, Germany).

Uptake and receptor blockade, colloidal stability

To investigate the interactions of cells with NPs, cells were seeded in their usual medium and grown overnight. NP samples in Leibovitz with respective amounts serum were prepared and left for 1 h at room temperature. Cells were washed with PBS once and NP samples were added for 4 hours. For receptor blocking studies, the cells were treated with 10 mg/mL HA 13 kDa or HA 289 kDa in the respective media for 1 h before adding the particles.

Flow cytometry

Cells analyzed by flow cytometry were handled in 24-well plates. After treatment with NPs, cells were washed with PBS once, harvested by trypsinization, washed again and resuspended in 100 μL PBS. 0.25 μL of a 1 mg/mL propidium iodide solution in PBS was added to the samples directly before measurement on a FACS Calibur (Becton, Dickinson and Company, Heidelberg, Germany). Flowing software was used for analysis.

Confocal microscopy

For imaging, cells were kept in 8-well ibidi chamber slides. When the treatment period with NPs was finished, cells were washed with PBS once and supplemented with Leibovitz containing 10 % serum. Images were taken on a Zeiss confocal laser scanning microscope.

Statistical analysis

Sigma Plot 12.0 software was used for statistical analysis. For the evaluation of CD44-expression and cell associated fluorescence after receptor blockade, a one-way ANOVA was conducted followed by a Holm-Sidak-test (Figure 4 and Figure 6). Figure 5 was analyzed by pairwise comparison of CAF-values obtained for cells treated with HA- or PEI-NP.

.

3 Results and Discussion

3.1 Colloidal stability in cell culture

Figure 2 summarizes the results of a microscopic study of the NP stability in the presence of cells. In a serum free environment (far left), both NP types behaved fairly similarly: NPs were not stable in high osmotic growth media and formed aggregates. 0.5 % serum was sufficient to reduce the aggregation tendency of HA-NPs while 0.75 % was able to completely prevent aggregation (top). PEI-NPs also showed a slight improvement in colloidal stability by the addition of serum, but even 1 % was not enough for complete stabilization. The highly cationic surface of PEI-NPs immobilized a large amount of proteins. Some proteins might even be attracted by two or more NPs and formed a bridge between them. With increasing serum concentration, the protein shells of the NPs become thicker and aggregation is reduced by steric hindrance.
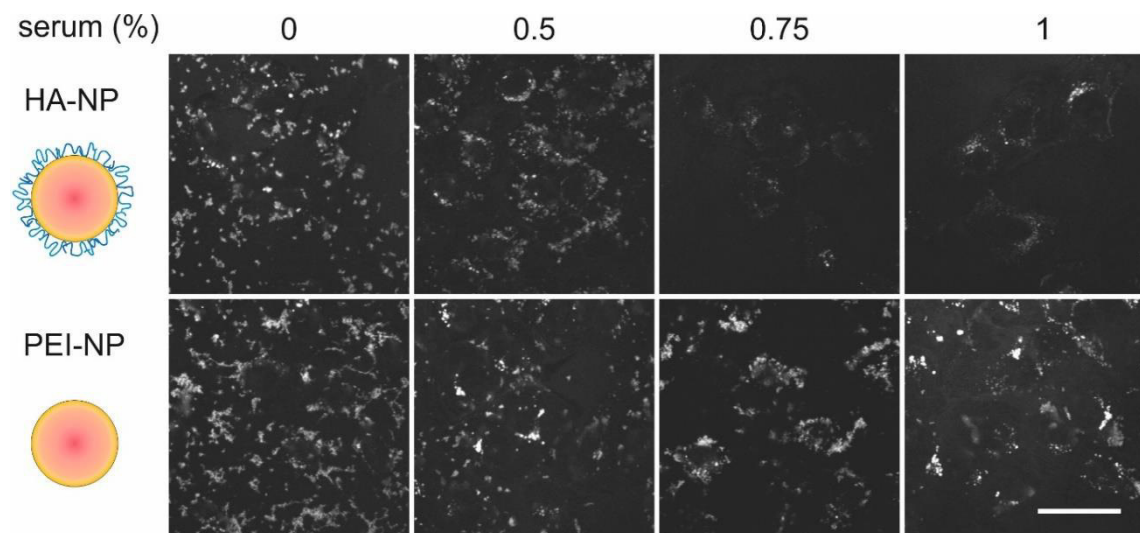
Figure 2: Colloidal stability of NPs in cell culture. HTM-N cells were treated with 10 μg/mL HA- or PEI-NPs and increasing serum concentrations. HA-NPs showed higher colloidal stability beginning at lower serum concentrations. The scale bar represents 50 μm.

We intended to inject the NPs into the anterior chamber of the eye which is filled with aqueous humor, a fluid low in protein concentration (Tripathi et al. determined the total protein content to be 12.4 mg/100 mL [7]). Hence, a high colloidal stability at low protein concentrations is necessary to guarantee a therapeutic effect. This is possible by coating the NPs with HA since few proteins attach to a HA coated surface. This strategy is currently

used in contact lenses, for example, to improve biocompatibility, comfort and to prevent undesirable immune responses [8].

3.2   Nanoparticles in 3D cell culture

As illustrated, the functionalization of NPs with HA reduced the formation of aggregates and the attachment of substances like proteins onto the particles. These characteristics are essential to ensure high NP mobility in macromolecular systems like the ECM. We determined the performance of both NP types (HA- and PEI-coated) in terms of ECM penetration and cellular uptake in 3D cell culture. Two different ECM models were used. The first was a collagen I model in which loose networks of long fibers form a neutrally charged gel with a pore size of approximately 0.47 μm [9]. The second system was Matrigel, which is much denser. This basement membrane matrix forms pores of only 0.14 μm and is highly negatively charged. Both NPs were able to penetrate the gels and distributed into embedded cells to similar extents (Figure 3) despite the fact that the hydrodynamic diameter of the NPs (244 nm for PEI-NPs, 226 nm for HA-NPs) was higher than the pore size of Matrigel. Because pore size represents an average, a distribution of mesh sizes exists. Here, the small proportion of larger pores was sufficient for unrestricted diffusion of the NPs through the EMC models. PEI-NPs formed some aggregates within the models whereas HA-NP showed superior stability (see Figure 3, aggregates marked with an asterisk).
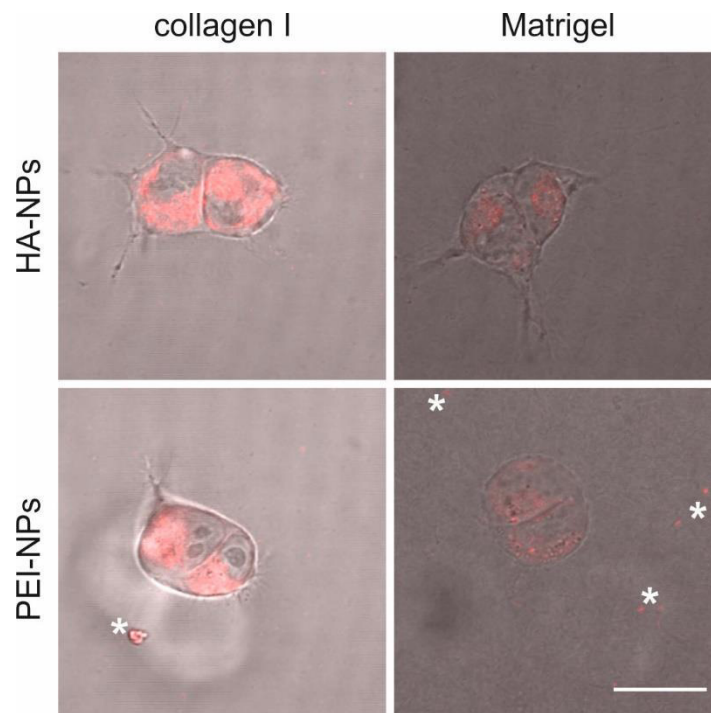
Figure 3. NP mobility in 3D cell culture. HeLa cells were embedded in an artificial extracellular matrix and mixed with rhodamine-labeled HA- or PEI-NPs. Left side: collagen I, right side: Matrigel. Top: HA-NPs, bottom: PEI-NPs. The scale bar represents 20 μm.

A high mobility of HA coated polyplexes in bovine vitreous was previously reported by Martens et al. [10]. Even if the size was slightly increased, NPs maintained their higher mobility in comparison to unfunctionalized complexes. However, one should consider the different pore sizes of the vitreous (0.55 μm) compared to collagen I or Matrigel [11]. Xu and Boylan investigated the mobility of cationic, anionic and neutrally charged NPs in bovine vitreous by multiple particle tracking [11]. Unimpeded diffusion was reported for uncharged, PEGylated NPs up to a size of 500 nm and for negatively charged NPs smaller than 200 nm. Larger NPs, higher concentrations or positively charged, amine modified NPs were completely immobile. Xu attributed the results to electrostatic interactions of cationic NPs with negatively charged fibers in the vitreous. Clearly, gel or matrix composition is important when evaluating the mobility of NPs and one should adjust *in vitro* models as closely as possible to natural conditions.

3.3   CD44 receptor expression

The density of CD44 receptors of primary trabecular meshwork cells and three different cell lines was determined by immunostaining and flow cytometry (Figure 4). The human breast cancer cell line MDA-MB-231 showed a very high CD44 receptor expression whereas the

presence of the membrane protein was negligible for MCF-7 cells. These results supported the findings of various groups with respect to CD44-receptor expression of cancer cells [12–14]. Primary human TM cells (hTM) had a medium CD44 density compared to the cell lines. Therefore, CD44 targeting is a promising approach for the specific delivery of NPs to TM cells. As CD44 expression of hTM and immortalized human trabecular meshwork cells (HTM-N) was similar, immortalized HTM-N were used for further studies.
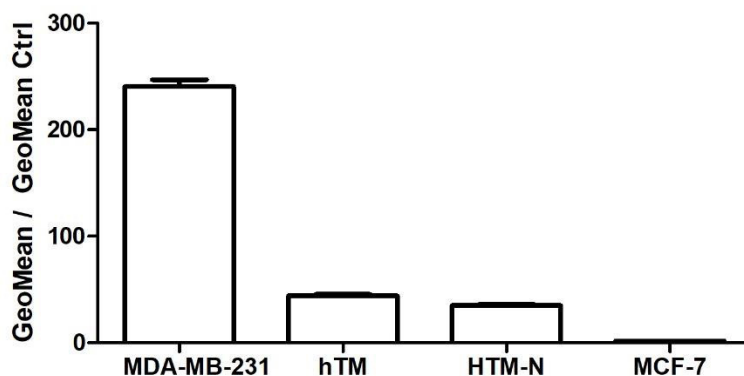
Figure 4. CD44-expression of different cell lines determined by immunostaining and flow cytometry. Shown is the geometric mean fluorescence intensity related to the isotype control averaged over three replicate measurements.

3.4   CD44-exression and nanoparticle uptake

The impact of cellular CD44 expression on the uptake of NPs with and without HA functionalization was investigated by flow cytometry. As it was not possible to distinguish between NPs that were taken up by the cell and NPs only sticking to the surface of the cell, the term "cell associated fluorescence" (CAF) was used to describe both effects. Figure 5A represents the results of the flow cytometry analysis after treating the cells for four hours with NPs without the addition of serum. The CAF was highest for MDA-MB-231 cells and decreased over the HTM-N to MCF-7 cells, which was expected based on the CD44 density as shown in Figure 4. Surprisingly, not only did NPs decorated with the CD44 ligand HA show a correlation between the CAF and receptor density but also PEI-NPs. In literature, no information about PEI-CD44 interactions was found but unspecific interactions with the cell membrane are frequently reported [15–17]. As expected, only the CD44-expressing cell lines MDA-MB-231 and HTM-N showed significantly higher CAF values when treated with HA-NPs compared to the treatment with PEI-NPs. Both NP types accumulated with MCF-7 cells to a similar extent.
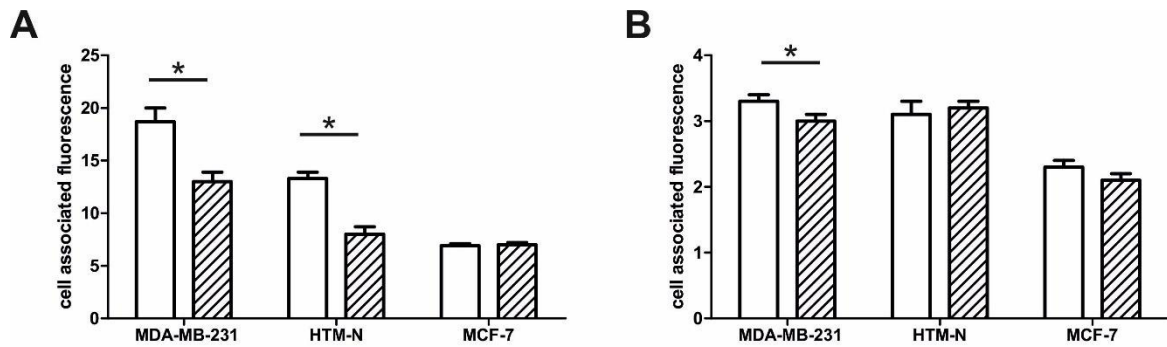
Figure 5. Cell associated fluorescence of cells treated with NPs (c = 120 µg/mL). Shown is the geometric mean fluorescence intensity related to untreated cells averaged over three replicate measurements. p = 0.05. A) without serum. B) with 5 % serum. Blank bars: HA-NPs, striped bars: PEI-NPs.

In general, the CAF values were lower with the supplementation of serum compared to the setup without (Figure 5B). This is due to the adsorption of serum proteins onto the surface of the NPs [18]. This protein corona stabilizes the NPs (as described before) but often also reduces the interaction of the NPs with the cells. Consequently, the uptake rates or therapeutic effects are reduced [19,20]. Despite the low CAF values in general, a slight but statistically significant difference was observable between the treatment with HA- and PEI-NPs for MDA-MB-231 cells. The receptor density of these cells appeared high enough to see this gap as no difference was detectable for HTM-N or MCF-7 cells which exhibit lower or no CD44 expression. Low CAF values of MCF-7 cells were attributable to the absence of CD44 expression and the growth habit of the cells. Because they form tight cell clusters, the surface area accessible for NP interactions is lower compared to more individually growing cells.

As expected, there was a correlation between CD44 density and the extent of interactions between cells and HA-NPs. Unexpectedly, this relation was also visible for PEI-NPs. To demonstrate the participation of CD44 in HA-NP binding and to investigate the influence of CD44 on the interaction with PEI-NPs, receptor blockade studies were conducted. Because an increase in binding strength has been reported when the molecular weight of the ligand increased [21], HA of different molecular weights was used to block the receptor.
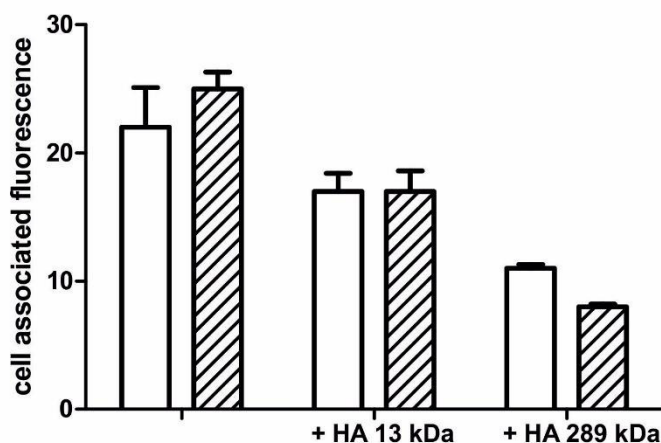
Figure 6. Receptor Blockade. HTM-N cells were treated with HA of different molecular weights prior NP uptake. Serum concentration was 0.35 %; NP were used in a concentration of 40 µg/mL. Shown is the geometric mean fluorescence intensity related to the control averaged over three replicate measurements Blank: HA-NPs, striped: PEI-NPs.

According to expectations, the CAF of HA-NPs was significantly reduced when CD44 receptors were blocked with HA (Figure 6). However, this decrease was also detectable for PEI-NPs. Interestingly, high molecular weight HA (289 kDa) had a stronger effect for both particle species. Long polysaccharide chains show an increased avidity, as various receptors are spanned at the same time [21,22]. Therefore, the replacement of high molecular weight HA by HA-NPs is less likely compared with smaller fragments. However, this does not explain the results gained for the PEI-NPs. There must be an interaction between PEI and the CD44 receptor.

To explain the behavior of the PEI nanoparticles, we first looked at microscopic patterns (Figure 7). In cell culture, PEI-NPs formed large aggregates which were even visible on brightfield images. These aggregates strongly stuck to the cell membrane at least in part due to electrostatic interactions between positively charged NPs and the negatively charged membrane. The addition of 13 kDa HA intensified this effect. The anionic polysaccharide HA adsorbed onto the surface of the positively charged NPs, gluing them together. These aggregates were removed during sample preparation for flow cytometry as CAF values determined by this method were lower with the addition of HA 13 kDa (Figure 6). Interestingly, less NP aggregates were detectable in the presence of high molecular weight HA. One explanation is that the macromolecule was tightly bound to the CD44 receptors and sealed the cellular surface. PEI-NPs – with a neutralized charge due to HA adsorption– were not able to bind to the membrane and could easily be removed during the washing procedure.
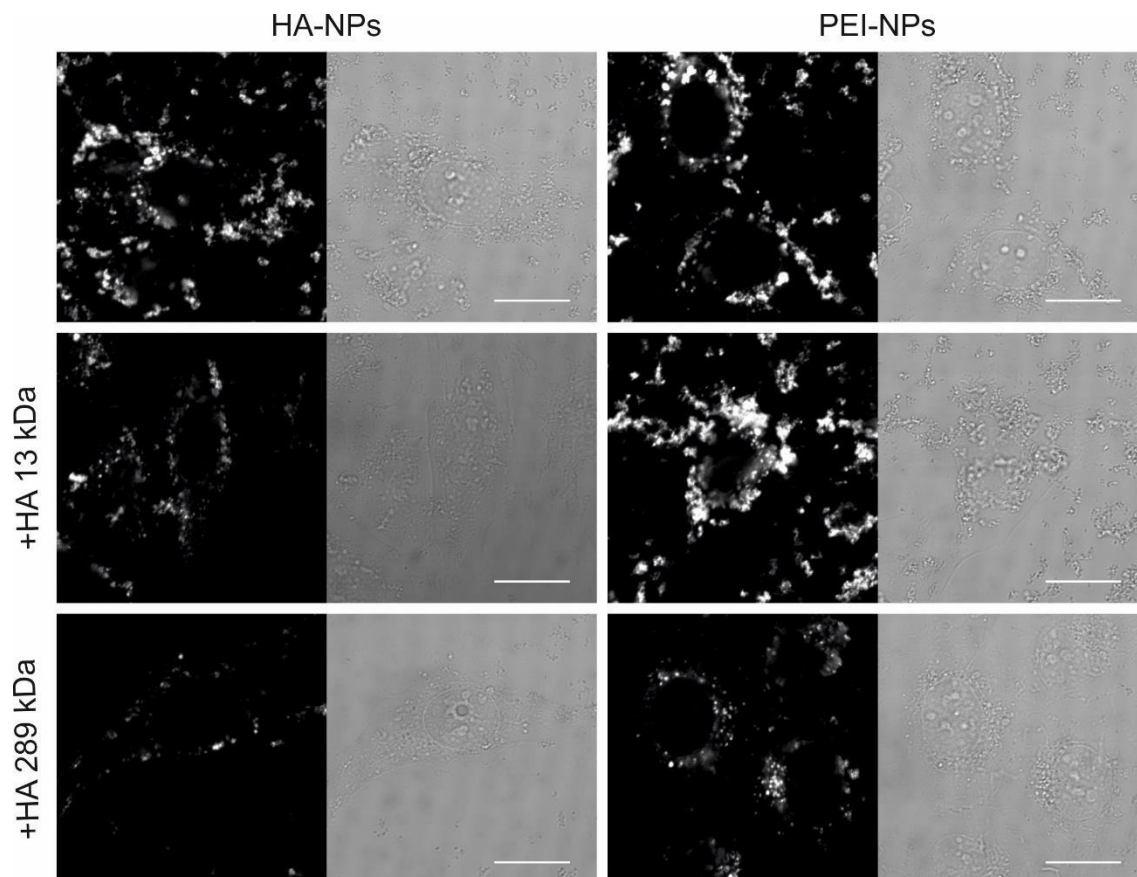
Figure 7. Receptor Blockade. CD44 receptors on HTM-N cells were blocked by HA of different molecular weights prior to treatment with NPs. 0.35 % serum was added to the cell culture medium. NP concentration was 40 µg/mL. Left: HA-NPs, right: PEI-NPs. The scale bar represents 20 µm.

Significant aggregation was detected for HA-NPs as well (Figure 7). The addition of 13 kDa HA, however, reduced the formation of aggregates considerably. As the negatively charged polysaccharide was bound to receptors on the cell membrane, interactions of HA-NPs with cells were reduced by electrostatic repulsion between the cell surface and NPs. Receptor blockage was even more pronounced when high molecular weight HA was used and fewer interactions between cell membrane and NPs were formed.

4 Conclusion

As demonstrated, the functionalization of NPs with HA is a promising approach to specifically direct NPs to cells in the TM. The coating of NPs with HA enhanced their colloidal stability in a low protein environment which is advantageous for therapeutic use in the eye where the NPs will be injected into the anterior chamber and follow the physiological outflow pathways to their target cells in the TM. NPs with a high colloidal stability will follow

this flow easily. Large aggregates, however, might get stuck in the sieve-like structure of the upper TM and, in the worst case, even clog the outflow pathways. Surprisingly, both NP types tested here (HA- and PEI-NPs), showed a correlation between cell association and CD44 expression. Receptor blockade studies confirmed the participation of CD44 in this interaction as fewer NPs were associated with cells when the receptor was occupied. In summary, HA functionalized NPs are expected to be ideally suited as drug delivery system for targeting of the TM.

References

[1] Hennig R, Pollinger K, Veser A, Breunig M, Goepferich A (2014), Nanoparticle multivalency counterbalances the ligand affinity loss upon PEGylation, J Control Release 194 20–27.

[2] Karbownik MS, Nowak, Jerzy, Z. (2013), Hyaluronan: Towards novel anti-cancer therapeutics, Pharmacoll Rep 65 1056–1074.

[3] Ponta H, Sherman L, Herrlich PA (2003), CD44: from adhesion molecules to signalling regulators, Nat Rev Molecul Cell Biol 4 33–45.

[4] Dosio F, Arpicco S, Stella B, Fattal E (2016), Hyaluronic acid for anticancer drug and nucleic acid delivery, Adv Drug Deliver Rev 97 204–236.

[5] Orian-Rousseau V (2010), CD44, a therapeutic target for metastasising tumours, Eur J Cancer 46 1271–1277.

[6] Hennig R, Goepferich A (2015), Nanoparticles for the treatment of ocular neovascularizations, Eur J Pharm Biopharm 95 294–306.

[7] Tripathi RC, Millard CB, Tripathi BJ (1989), Protein composition of human aqueous humor: SDS-PAGE analysis of surgical and post-mortem samples, Exp Eye Res 48 117–130.

[8] Vanbeek, Jones L, Sheardown H (2008), Hyaluronic acid containing hydrogels for the reduction of protein adsorption, Biomaterials 29 780–789.

[9] Tomasetti L, Liebl R, Wastl DS, Breunig M (2016), Influence of PEGylation on nanoparticle mobility in different models of the extracellular matrix, Eur J Pharm Biopharm 108 145-155.

[10] Martens TF, Remaut K, Demeester J, Smedt SC de, Braeckmans K (2014), Intracellular delivery of nanomaterials: How to catch endosomal escape in the act, Nano Today 9 344–364.

[11] Xu Q, Boylan NJ, Suk JS, Wang Y-Y, Nance EA, Yang J-C, McDonnell PJ, Cone RA, Duh EJ, Hanes J (2013), Nanoparticle diffusion in, and microrheology of, the bovine vitreous ex vivo, J Control Release 167 76–84.

[12]   Sironen RK, Tammi M, Tammi R, Auvinen PK, Anttila M, Kosma V-M (2011), Hyaluronan in human malignancies, Exp Cell Res 317 383–391.

[13]   Dreaden EC, Morton SW, Shopsowitz KE, Choi J-H, Deng ZJ, Cho N-J, Hammond PT (2014), Bimodal Tumor-Targeting from Microenvironment Responsive Hyaluronan Layer-by-Layer (LbL) Nanoparticles, ACS Nano 8 8374–8382.

[14]   Steponkiene S, Dapkute D, Riekstina U, Totomskis R (2015), Accumulation and Distribution of Non-targeted and Anti-CD44-conjugated Quantum Dots in Distinct Phenotypes of Breast Cancer, J Nanomed Nanotechnol 06.

[15]   Zhang C, Wu F-G, Hu P, Chen Z (2014), Interaction of Polyethylenimine with Model Cell Membranes Studied by Linear and Nonlinear Spectroscopic Techniques, J Phys Chem C 118 12195–12205.

[16]   Mahmoudi M, Meng J, Xue X, Liang XJ, Rahman M, Pfeiffer C, Hartmann R, Gil PR, Pelaz B, Parak WJ, del Pino P, Carregal-Romero S, Kanaras AG, Tamil Selvan S (2014), Interaction of stable colloidal nanoparticles with cellular membranes, Biotechnol Adv 32 679–692.

[17]   Zhong D, Jiao Y, Zhang Y, Zhang W, Li N, Zuo Q, Wang Q, Xue W, Liu Z (2013), Effects of the gene carrier polyethyleneimines on structure and function of blood components, Biomaterials 34 294–305.

[18]   Pino Pd, Pelaz B, Zhang Q, Maffre P, Nienhaus GU, Parak WJ (2014), Protein corona formation around nanoparticles – from the past to the future, Mater Horiz 1 301–313.

[19]   Zanganeh S, Spitler R, Erfanzadeh M, Alkilany AM, Mahmoudi M (2016), Protein corona: Opportunities and challenges, Int J Biochem Cell B 75 143–147.

[20]   Lesniak A, Salvati A, Santos-Martinez MJ, Radomski MW, Dawson KA, Åberg C (2013), Nanoparticle adhesion to the cell membrane and its effect on nanoparticle uptake efficiency, J Am Chem Soc 135 1438–1444.

[21]   Mizrahy S, Raz SR, Hasgaard M, Liu H, Soffer-Tsur N, Cohen K, Dvash R, Landsman-Milo D, Bremer MG, Moghimi SM, Peer D (2011), Hyaluronan-coated nanoparticles: The influence of the molecular weight on CD44-hyaluronan interactions and on the immune response, J Control Release 156 231–238.

[22]   Lesley J (2000), Hyaluronan Binding by Cell Surface CD44, J Biol Chem 275 26967–26975.

Layer-by-layer nanoparticles for siRNA delivery: Evaluation of gene silencing efficiency, intracellular distribution and exocytosis

Abstract
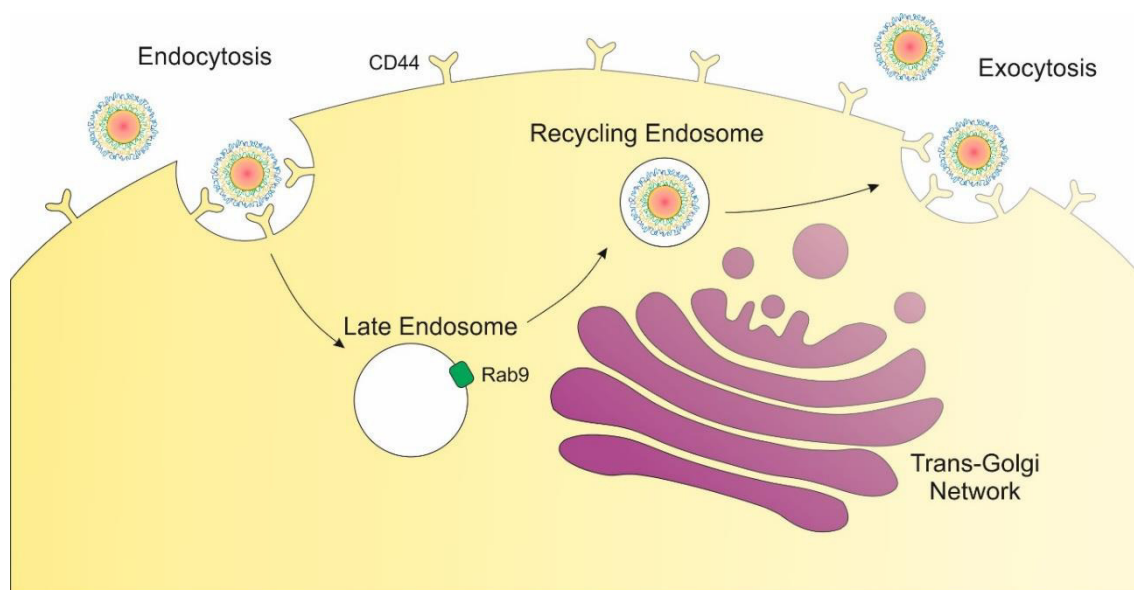
RNA interference is a biological process of specific post-transcriptional gene silencing by short double-stranded RNA. Gene silencing by small interfering RNA (siRNA) offers a great opportunity for the treatment of diseases resulting from protein overexpression. However, successful delivery of the molecule remains an issue as siRNA is highly unstable and cannot cross cell membranes. Nanoparticulate delivery systems are promising solutions for siRNA delivery that overcome these obstacles. We developed layer-by-layer nanoparticles (NPs) functionalized with a moiety to target cluster of differentiation 44 receptors on trabecular meshwork cells and tested them for their ability to serve as delivery systems for siRNA. To investigate the impact of the NP composition, an *in vitro* assay, which involves the silencing of artificially introduced green fluorescent protein in immortalized trabecular meshwork cells, was established. To determine their fate, the intracellular distribution of the NPs and their colocalization with defined intracellular compartments such as endosomes and lysosomes was studied. Finally, the possibility of NP exocytosis from the cells was addressed.

1 Introduction

In 2006, the Nobel Prize in Physiology or Medicine was awarded to Andrew Z. Fire and Craig C. Mello for their discovery of RNA interference (RNAi) gene silencing by double stranded RNA [1]. This fundamental mechanism regulates the expression of proteins and is of utmost importance for the protection against viral infections, genome stabilization and the development of organisms [2–4]. Experimentally, small interfering RNA (siRNA) is used to specifically impede gene expression and tremendous effort has been made to transfer this method into clinics. However, no product is available on the market yet and relatively few are in clinical development [5–7]. Possibly the most promising product is patisiran, an RNAi therapeutic developed for familial amyloidotic polyneuropathy. Only recently, in September 2017, the manufacturer Alnylam published a press release concerning the striking results of a phase III clinical trial (APOLLO) and a report indicating that all of the primary and secondary end points were met. According to their chief executive officer, these were the first ever positive phase III clinical trial results for an RNAi therapeutic [8].

The primary reason for the low number of RNAi therapeutics might be the lack of a suitable delivery system. Nanoparticles (NPs) of different compositions and materials have been heavily investigated as they combine major properties which could be used to create a successful siRNA delivery system. Interestingly, Alnylam – the manufacturer of patisiran - used lipid NPs. NPs can protect siRNA from degradation by omnipresent nucleases which is of utmost importance for successful therapy. Further, a targeted delivery to certain organs or tissues is possible by functionalizing the NPs in an appropriate way [9]. But once the nanoparticulate carriers reach the target cells, other bottlenecks must be overcome until a therapeutic effect is observed [10–12] (Figure 1, left). First, NPs must be taken up by the cell in an adequate amount. Once endocytosed, NPs are commonly trapped within endocytic vesicles where they are destined to undergo digestion and degradation by endolysosomal enzymes. Therefore, an early escape from the endosomes is necessary. In addition, the delivery system must disassemble and release the siRNA into the cytosol to enable its incorporation in the "gene silencing machinery".
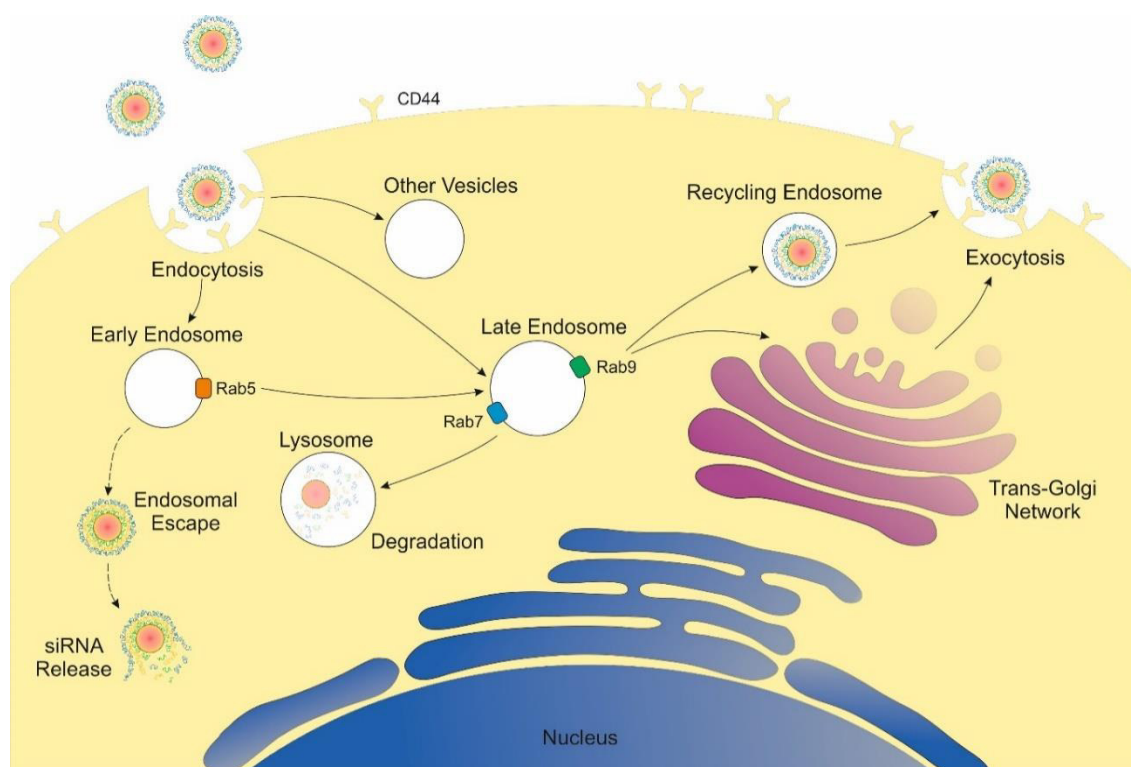
Figure 1. NPs are taken up into the cell via endocytosis and are trapped within early or late endosomes. NPs can either escape into the cytosol where their siRNA freight is released or they are processed to further intracellular compartments like the lysosomes or the trans-Golgi network. There, the vesicular load is degraded or transported to the extracellular space. Vesicular Rab proteins follow a characteristic distribution pattern. Rab 5 is located in the membrane of early endosomes whereas Rab 7 and Rab 9 are anchored to late endosomes.

Our concept is to use layer-by-layer NPs (LbL-NPs) for the delivery of siRNA to cells in the trabecular meshwork (TM) of glaucoma patients. The NPs consist of a poly(lactide-*co*-glycolide) (PLGA) core and electrostatically adsorbed layers of negatively charged siRNA and polycations like polyethyleneimine (PEI) or poly-L-arginine (PLArg) (Figure 2). Both polymers are well established transfection agents, have a high endosomolytic activity and form complexes with siRNA [13–16]. The anionic polysaccharide hyaluronic acid (HA) was chosen as targeting moiety and assembled onto the particles to form the final, outermost layer. As HA is the main ligand of cluster of differentiation (CD) 44, a receptor on the cell surface, improvement of cellular uptake due to interactions of the NPs with CD44 receptors is possible [17–19]. Interestingly, elevated levels of CD44 were found in the TM of patients suffering from glaucoma [chapter 6] and a high NP uptake rate and therapeutic success is expected only in this patient group.
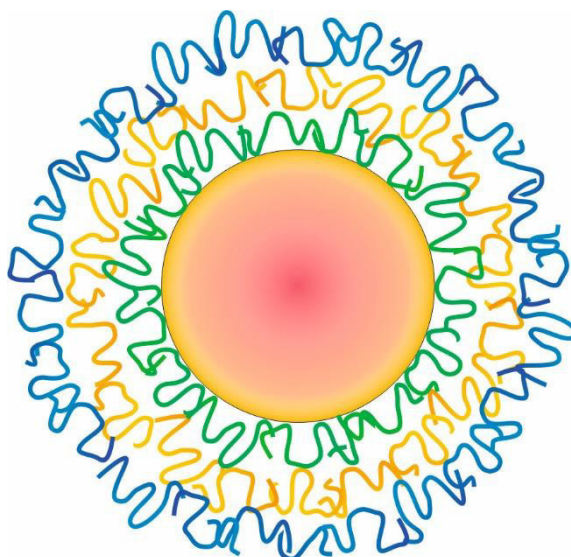
Figure 2. Structure of a LbL-NP. siRNA (green) is electrostatically attached onto a cationic PLGA core (red-yellow) and covered by polycationic PEI or PLArg respectively (yellow). The functionalization with HA (blue) stabilizes the particle and favors targeting and uptake of the NPs.

To investigate the suitability of our NPs for the delivery of siRNA, we generated a TM cell line (HTM-N) for the *in vitro* gene silencing of artificially introduced green fluorescent protein (GFP). After optimizing transfection conditions, a suitable siRNA sequence directed against GFP was chosen and the gene silencing effect of NPs with different layering materials was studied. Although NP uptake was high, no gene silencing was detectable. Therefore, the intracellular distribution of the particles and colocalization with endosomes and lysosomes was visualized by confocal microscopy. Finally, we found that a considerable fraction of NPs was released from the cells after uptake. Based upon these results, consequential challenges and possibilities are discussed.

2 Materials and Methods

2.1 Materials

If not otherwise stated all cell culture materials, reagents and chemicals were purchased from ThermoFisher Scientific (Darmstadt, Germany). Acid terminated poly(D, L-lactide-co-gylcolide) (PLGA) (lactide/glycolide 50/50) with an average molecular weight of 38-54 kDa and branched poly(ethylenimine) 25 kDa (PEI) were purchased from Sigma-Aldrich Chemical Company (Taufkirchen, Germany). Sucrose, microbiological grade, was bought from Merck (Darmstadt, Germany). Rhodamine B endcapped PLGA (lactide/ glycolide 50/50, average molecular weight 30 kDa) (RHOD-PLGA) was obtained from

Polyscitech (West Lafayette, Indiana, United States). siGFP1 (5'- AACUAUAAUUCUCAC AAUdTdT -3'), siGFP2 (5'- GGUGAAGGAGAUGCAACUUAUdTdT -3'), siGFP3 (5'- GAAGGUUAUGUUCAGGAGAGGdTdT -3'), siGFP4 (5'- GAAGGUGAUACA CUGGUUAACdTdT -3') and siSCRBL (5'- UUCUCCGAACGUGUCACGUdTdT -3') were designed with the siRNA wizard v3.1 online application from Invivogen and synthesized by Eurofins Genomics (Ebersberg, Germany). Sodium hyaluronate (HA) (13 kDa) was purchased from Lifecore Biomedicals (Chaska, Minnesota, United States). Hygromycin B was bought at PAN Biotech (Aidenbach, Germany). Thiazolyl blue tetrazolium bromide was obtained by Applichem (Darmstadt, Germany). pMONO-hygro-GFP was bought at Invivogen (Toulouse, France). Plasmides for YFP-tagged fusion proteins of Rab5, 7 and 9 were a kind gift from Massachusetts Institute of Technology (Cambridge, Massachusetts, United States). All chemicals were used without further purification unless otherwise mentioned.

2.2   Methods

Hygromycin B Concentration

HTM-N cells were passaged onto 96-well plates at a density of 3,000 cells per well and grown for 24 h in DMEM$^+$ supplemented with 10 % serum. Fresh medium with varying amounts of Hygromycin B was added for 72 h. Then, bright field pictures were taken and an MTT assay was performed according to the method established in our group. Briefly, cells were incubated with 200 μl of 0.625 mg/mL thiazolyl blue tetrazolium bromide reagent in DMEM$^+$ with 10 % serum for four hours and lysed with a solution of 10 % sodium dodecyl sulfate (SDS) in PBS. Absorbance was read at 570 nm using a microplate reader (FLUOStar Omega, BMG Labtech, Ortenberg, Germany). Measured values were corrected by subtracting background absorbance at 690 nm and related to untreated cells.

Generation of GFP-positive cell line

HTM-N cells at passage 60 were grown in 24-well plates for 24 h. Lipofectamine 3000 transfection reagent was used to transfect HTM-N cells with pMONO-hygro-GFP. Lipoplexes were produced according to manufacturer instructions. Briefly, 1 μg plasmid and 1 μL P3000 of the transfection kit were diluted to 25 μL with OptiMEM. 1.5 μL Lipofectamine 3000 were diluted to 25 μL with OptiMEM separately. Complexes were

formed by mixing the DNA with the Lipofectamine solution. Complexes were added to the cell culture medium for 8 h. Then, the media was changed to DEMEM$^+$ with 10 % serum and 400 µg/mL hygromycin B. Media was replaced daily. Individual cells with bright fluorescence were picked, transferred to a 96-well plate and cultivated to form a population. Successfully transfected cells were termed HTM-N_GFP+.

Optimization of gene silencing conditions

For the optimization of the gene silencing conditions, Lipofectamine RNAiMAX reagent was used. Lipoplexes with siRNA were prepared according to manufacturer's instructions. In brief, siRNA and Lipofectamine were diluted separately to one tenth of the intended final volume. The polymer was mixed with siRNA by pipetting up and down and left 15 min at room temperature to allow complete complex formation. Afterwards, the mixture was further diluted with OptiMEM and used immediately for transfection. 6 h later, lipoplexes were removed, cells were washed with PBS once and fresh media (DMEM$^+$ with 10 % serum and 400 µg/mL hygromycin B) was added for 24 to 72 h. GFP-fluorescence was quantified by flow cytometry. Propidium iodide staining was conducted to exclude dead cells from data analysis.

Flow cytometry

For flow cytometry, HTM-N_GFP+ were handled in 24-well plates. Cells were washed with PBS once, harvested by trypsinization, washed again and resuspended in PBS immediately before measurements on a FACS Calibur (Becton, Dickinson and Company, Germany). Flowing software was used to perform the analysis.

Layer-by-layer NPs (LbL-NPs)

LbL-NPs were prepared as described previously in chapter III. Briefly, PLGA-NP were prepared by slowly dropping a 10 mg/mL solution of PLGA in acetonitrile into an aqueous 0.5 % PEI solution. For the preparation of fluorescently tagged NPs, a mixture of PLGA and RHOD-PLGA (PLGA/RHOD-PLGA 50/50) or FITC-PEI was used. The NPs were stirred for 4 to 5 h to allow complete evaporation of the organic solvent. Purification of NPs was conducted by repeated centrifugation and resuspension steps. NPs were lyophilized with sucrose as a protective agent. Powdered NPs were resuspended in water to 1 mg/mL, purified from sucrose and coated with siRNA, PEI and HA in a LbL-approach. The

concentration of the polymers during coating was 1 mg/mL in water or 4 μM in 10 mM NaCl for the polymers and siRNA respectively. Hydrodynamic size and zeta potential were determined on a Zetasizer Nano ZS (Malvern Instruments, Herrenberg, Germany). For all measurements, 173° backward scatter in the general-purpose mode with automatic measurement position and attenuator selection at 25 °C was applied. Z-Average values and zeta potentials of the NPs lied within following intervals: HA-terminated NP [189;231] nm and [-25;-16] mV; PEI-terminated NP [200;260] nm and [37;52] mV; PLArg-terminated NP [216;217] nm and [38;39] mV. Concentration was determined in relation to the fluorescence intensity of a sample with known concentration on a microplate reader with 544 nm or 480 nm (excitation) and 590 nm or 520 nm (emission) filter sets. NPs were termed according to their final polymer layer.

Gene silencing with LbL-NP

HTM-N_GFP+ cells were seeded in 24-well plates and grown overnight. NPs were mixed with Leibovitz medium and serum in a final concentration of 1 or 0.35 % for 1 h. Then, cells were washed and the samples were added for 6 or 4 h respectively. After the incubation period, NPs were aspirated, cells were washed once with PBS and fresh medium (DMEM$^+$ with 10 % serum and 400 μg/mL hygromycin) was added. Cells were grown at 37 °C and 5 % CO_2 for 72 h. Microscopic images were taken directly after finishing the treatment period with NPs and again after the 72 h incubation interval on a Zeiss confocal laser scanning microscope (Zeiss Axiovert 200 coupled to a LSM 510 META, Zeiss, Oberkochen, Germany). Cells were prepared for flow cytometry as described previously but without propidium iodide staining.

NP-Uptake

For all uptake experiments (endolysosomal pathway, exocytosis), NPs without siRNA freight were mixed with Leibovitz containing 0.35 % serum to a final concentration of 80 μg/mL and incubated at room temperature for one hour. Then, cells where washed with PBS once and the samples where added. After 4 hours, samples where aspirated and cells where washed at least once with PBS and supplemented with medium containing 10 % serum (Leibovitz or DMEM$^+$).

Endolysosomal pathway

For the visualization of Rab-proteins, HTM-N cells were passaged to 8-well ibidi chamber slides at a density of 40,000 cells per well and grown for 24 h. Lipofectamine 2000 was used to transiently transfect the cells with YFP- or GFP-tagged fusion proteins of Rab 5, 7 and 9. Briefly, 0.3 μg pDNA and 1 μL Lipofectamine 2000 were diluted separately with serum free DMEM$^+$ to 50 μL each and then mixed by pipetting. 20 min later, complexes were further diluted with 100 μL DMEM$^+$ and added to the cells after washing them with PBS once. After 4 h, complexes were removed and cells were grown overnight. This treatment was not conducted when staining the lysosomes. Here, HTM-N cells were seeded at a density of 20,000 cells per well in 8-well ibidi glass bottom chamber slides only one day before the experiment. The NP uptake was performed as described above. In the case of lysosomal staining, 60 nM Lysotracker Deep Red in PBS was added to the cells one hour before finishing the uptake. Confocal images and z-stacks were taken on a Zeiss confocal laser scanning microscope.

Exocytosis

HTM-N cells were seeded in a 48-well plate at a density of 25,000 cells per well and grown overnight. The NP uptake was performed as described above. After NP treatment, cells were washed thoroughly with PBS twice and with serum containing medium once. Cells were provided with fresh media (without phenol red) and media samples were taken at defined time points. Fluorescence intensity of the media was determined on a microplate reader with 544 nm (excitation) and 590 nm (emission) filter sets and related to PEI-NPs of known concentration. Cell culture medium of cells without NP-treatment was used for background correction.

Two particle assay

The endo- and subsequent exocytosis was investigated according to El-Dakdouki et al [20] with slight modifications. HTM-N cells were passaged onto 24-well plates at a density of 80,000 cells per well and grown overnight. Cells were treated either with RHOD or FITC-tagged PEI- or HA-NP as described above. 0.35 % serum Leibovitz served as a control. After a period of 4 hours, cells were washed with PBS twice, harvested by trypsinization and washed again with serum containing media. Differently treated cells were mixed in a ratio of 1+1 (RHOD-HA + FITC-HA, RHOD-PEI + FITC-PEI, RHOD-HA + control, FITC-

HA + control, RHOD-PEI + control, FITC-PEI + control) and transferred to an 8-well ibidi chamber slide at a density of 20,000 cells per well. Confocal images were taken on a Zeiss confocal laser scanning microscope after one, two and three days. Media was changed to 10% serum Leibovitz for imaging and back to serum containing DMEM$^+$ for cultivation. The number of cells with FITC- and/or RHOD-fluorescent NPs was counted manually on 10 images per sample and time point.

3 Results and Discussion

3.1 Establishment of a GFP-expressing trabecular meshwork cell line

The appropriate concentration of antibiotic was determined to guarantee satisfactory selection of immortalized human trabecular meshwork cells (HTM-N) that were successfully transfected with the plasmid pMONO-hygro-GFP, encoding the green fluorescent protein (GFP). The viability of HTM-N cells that were treated with increasing amounts of the selection antibiotic hygromycin B was measured by an MTT-assay (Figure 3). A concentration of 400 μg/mL was sufficient to reliably kill untransfected HTM-N cells and guaranteed satisfactory selection of hygromycin resistant clones. Higher concentrations were not beneficial and would possibly even damage cells that were resistant to hygromycin. The results of the MTT-assay were verified by brightfield microscopy (pictures in supporting information).
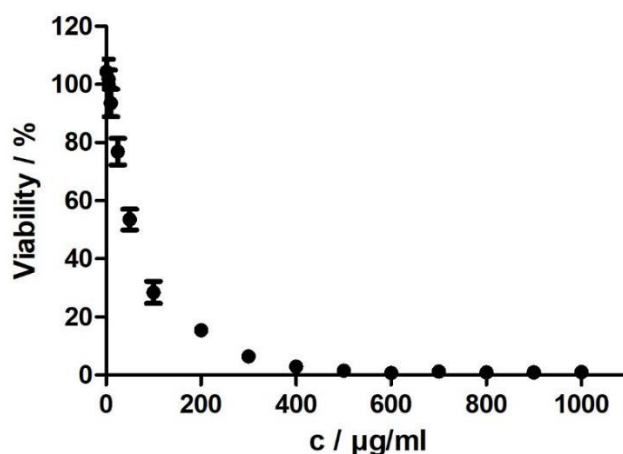
Figure 3. Viability of HTM-N cells treated with increasing amounts of hygromycin for 72 h determined by an MTT assay. A hygromycin concentration of 400 μg/mL was considered sufficiently high enough for the selection of transfected clones.

Four clones of GFP producing trabecular meshwork cells (HTM-N_GFP+) were treated with complexes of siRNA and RNAiMAX to identify the most sensitive one. RNAiMAX was used as it is a common transfection reagent and has guaranteed high transfection rates [21]. GFP-expression could be reduced in all clones but clone 1 showed the greatest response with a decrease in fluorescence intensity (FI) of approximately 70 % (Figure 4A). Further improvement of transfection efficiency was achieved by varying the amounts of siRNA and RNAiMAX (Figure 4B). Complexes with 0.6 µL or 1.32 µL of transfection reagent showed superior performance as the GFP fluorescence was reduced to 25 % of the initial value. However, differences in the effectivity of these complexes were not statistically significant and complexes with lower siRNA and RNAiMAX amounts were regarded as most suitable due to their lower toxicity. Because of the long half-life of GFP [22], it was necessary to find the optimal time point for analysis. A GFP knockdown by nearly 80 % was observed for HTM-N_GFP+ clone 1 when analyzing the cells 72 h after transfection (Figure 4C). Complex composition did not have any influence. With the conditions for optimal transfection identified, the gene silencing potential of four siRNA-candidates with different targeting sequences within the GFP gene was determined. Figure 4D demonstrates the superior results of siGFP 2 and 4 compared to the other candidates. Although there was not a significant difference, siGFP 2 was applied for further gene silencing studies in HTM-N_GFP+.
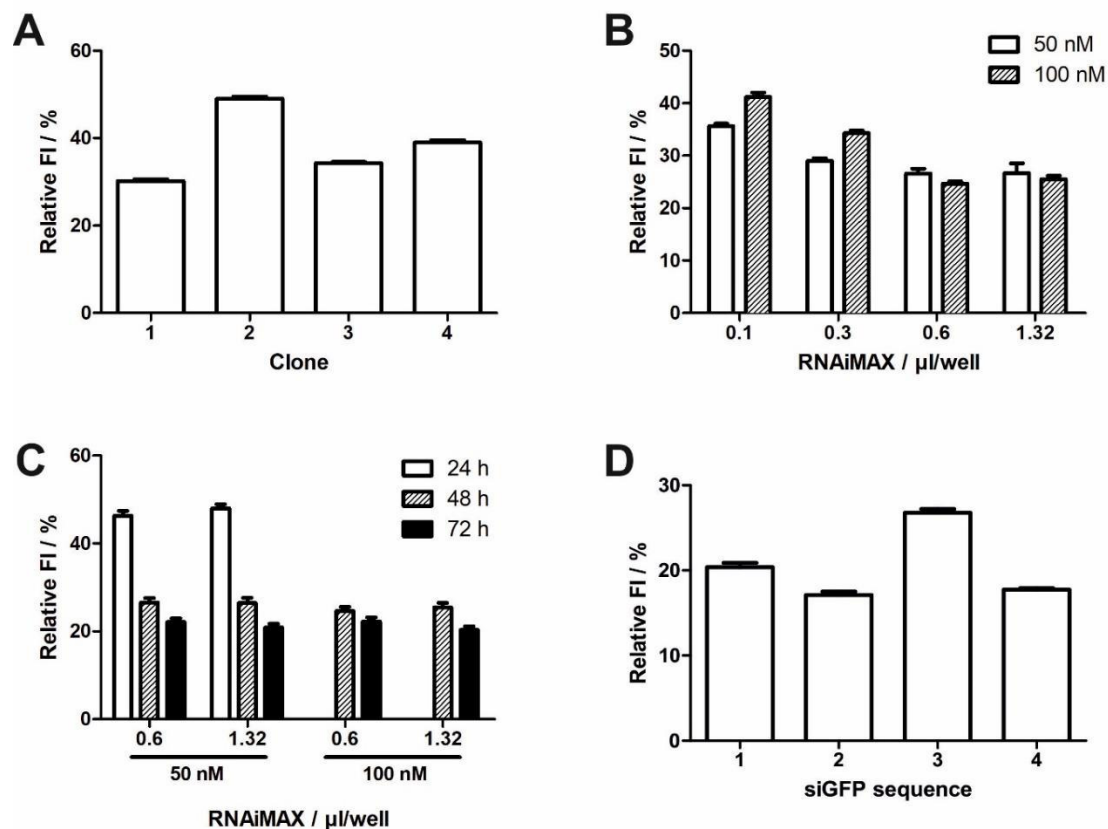
Figure 4. Generation of a suitable cell line for gene silencing. HTM-N cells stably expressing GFP (HTM-N_GFP+) were produced by transfection with pMONO-hygro-GFP plasmid and Lipofectamine 3000. The selection of clones was performed by the addition of 400 μg/mL hygromycin to the cell culture media. A) Four promising cell clones were tested for their sensitivity to lipoplexes containing 100 nM siGFP1 and RNAiMAX. B) The gene silencing efficiency of lipoplexes of different composition was investigated. siGFP 1 was used in concentrations of 50 and 100 nM and a volume of RNAiMAX varying between 0.1 to 1.32 μL. C) The gene silencing performance of lipoplexes (50 or 100 nM siGFP3 and 0.6 or 1.32 μL RNAiMAX) depended on the incubation time after transfection. D) The GFP knock down in HTM-N_GFP+ after optimized treatment (50 nM siRNA, 0.6 μL RNAiMAX, 72 h incubation) with different siRNA sequences is demonstrated. Shown is the mean +/- standard deviation of three replicate measurements.

3.2 LbL-NP for GFP-silencing in a human trabecular meshwork cell line

The suitability of LbL-NPs for siRNA delivery to HTM-N_GFP+ was determined. In a first attempt, NPs with an intermediate layer of PEI were investigated. Figure 5 summarizes the composition of the NPs (bottom) and the results of this study (top).
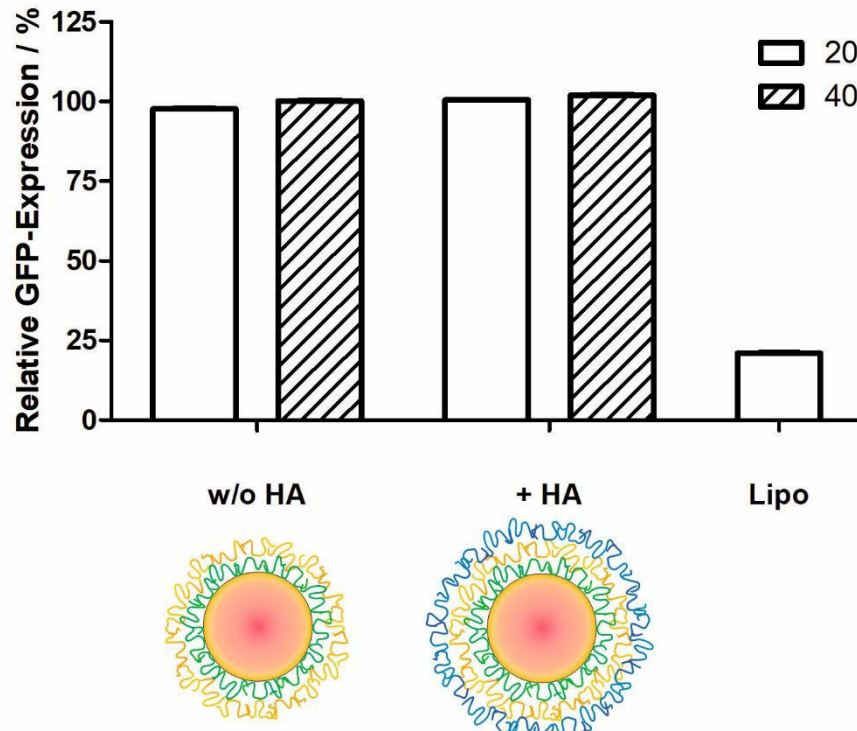
Figure 5. GFP silencing in HTM-N_GFP+ with LbL-NPs. Particles with and without HA functionalization were tested. Fluorescence intensity of cells 72 h after treatment with 20 or 40 μg/mL of NPs for 6 h in the presence of 1 % serum is shown. Lipoplexes containing 50 nM siRNA served as a control. Cellular fluorescence was detected by flow cytometry and related to cells that were treated with an off-target siRNA. Shown is the mean +/- standard deviation of three replicate measurements.

Lipoplexes with RNAiMAX, which were used as a positive control, reduced the FI of GFP to approximately 25 % of the initial value which was in accordance with previous results gained during optimization of the assay. However, the NPs were not able to significantly reduce GFP expression. Although a low molarity of siRNA is sufficient to effectively inhibit the synthesis of a protein [23], NP concentrations of 20 and 40 μg/mL might have been too low to observe any effect. However, toxicity increased considerably when the particle concentration was increased to 80 μg/mL (not shown).

One explanation for the results is that siRNA release from the particle is insufficient as strong electrostatic forces between PEI and siRNA might prevent the disassembly of the polymer layers. The phenomenon of inadequate nucleic acid release from NPs is well documented, reflected by the high number of publications targeting this issue [24–27]. Common strategies to improve the intracellular disassembly of nanoparticles or polyplexes are the incorporation of charge reversal polyelectrolytes, disulfide linkers, ATP-sensitive moieties or substances that serve as an enzymatic substrate [27]. Common to all of them is the exploitation of

differences in the extra- and intracellular milieu in terms of pH, reductive potential, ATP content or enzymatic composition.

To confirm the hypothesis that siRNA was insufficiently released, PLArg was introduced into the NPs as an alternative polycationic compound to weaken electrostatic interactions between the siRNA and protecting layers and to enhance the nucleic acid release from the particles [28,29]. Based upon the protonation state of the polymers under physiological conditions, the calculated distance between the cationic charges of PLArg is approximately 1.65 nm. Compared to the 0.5 nm of PEI, a reduction in electrostatic interactions and an improved siRNA release was expected (see supporting information for calculations). In addition to the lower charge density, PLArg confers further benefits: toxicity is reduced compared to PEI [16,30] and – as it is a peptide – it is biodegradable [31]. This explains its frequent use as transfection reagent for DNA or RNA. However, using PLArg as an intermediate layer in the LbL-NPs in our studies did not improve the GFP gene silencing efficiency (Figure 6). None of the four investigated NP types (PEI or PLArg, with or without HA-functionalization) could overcome all obstacles on their way to successfully deliver siRNA to the cytosol. Besides insufficient siRNA release from the particles, there must be other problems like endosomal entrapment impeding the desired effect.
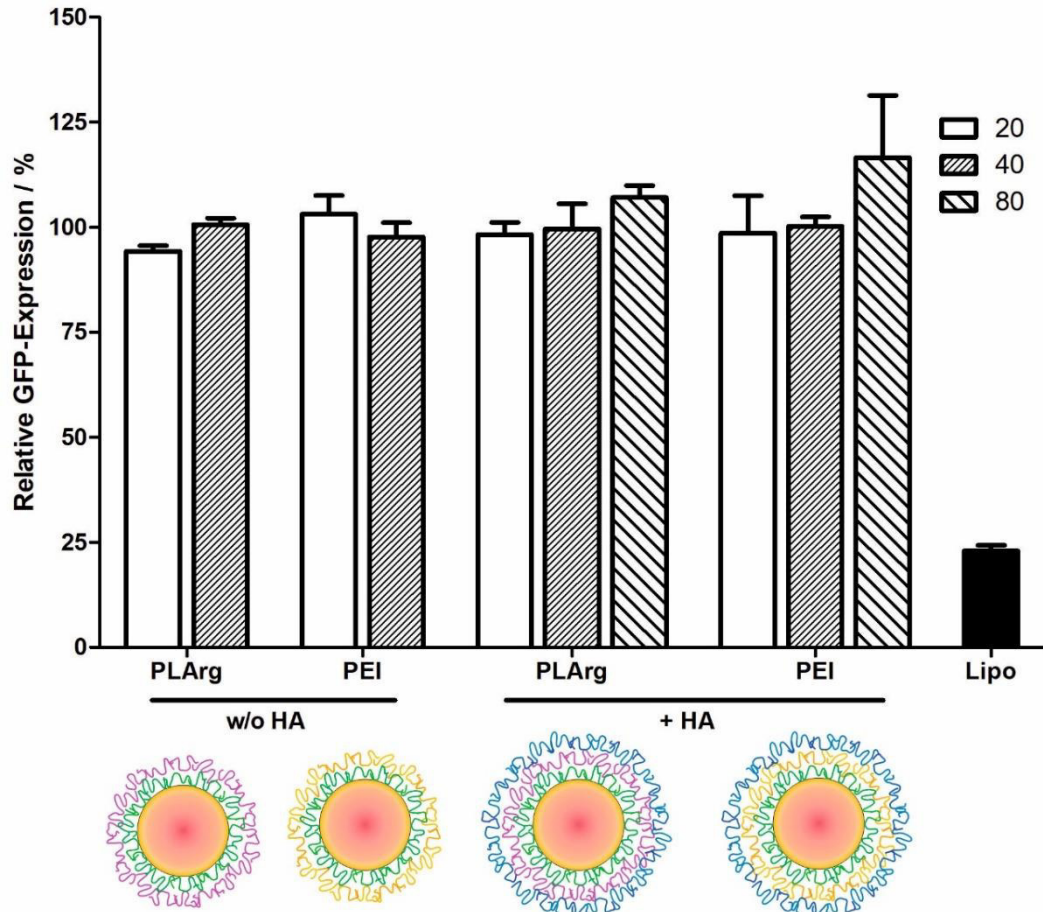
Figure 6. GFP-silencing in HTM-N_GFP+ with LbL-NP. Particles with and without HA functionalization and an intermediate layer of PEI (yellow) or PLArg (violet) were tested. Fluorescence intensity of HTM-N_GFP+ cells 72 h after treatment with 20, 40 or 80 μg/mL NPs for 5 h in the presence of 0.35 % serum is shown. Lipoplexes containing 50 nM siRNA served as a control. Cellular fluorescence was detected by flow cytometry and related to cells that were treated with an off-target siRNA. Shown is the mean +/- standard deviation of three replicate measurements.

3.3   Intracellular distribution of LbL-NPs

To investigate NP uptake and intracellular distribution, HTM-N cells were transfected with a YFP-tagged Rab-protein. Rab-proteins are small vesicular GTPases that are involved in vesicle formation, movement and targeting [32,33]. Different types of Rab-proteins can be found in distinct vesicles of the endolysosomal pathway. The distribution of common Rab-proteins that are involved in relevant steps of endocytosis is summarized in Figure 1. The early endosome associated Rab 5 mediates endocytosis, endosomal fusion and maturation. Rab 7 and Rab 9 are located in the membrane of late endosomes. Rab 7 promotes the maturation of late endosomes and their fusion with lysosomes. Rab 9, however, marks late endosomes destined toward the trans-Golgi-network. Interestingly, Rab 9 is involved in the

143

recycling of mannose-6-phosphate receptors [33] and might also participate in CD44-recycling [34].
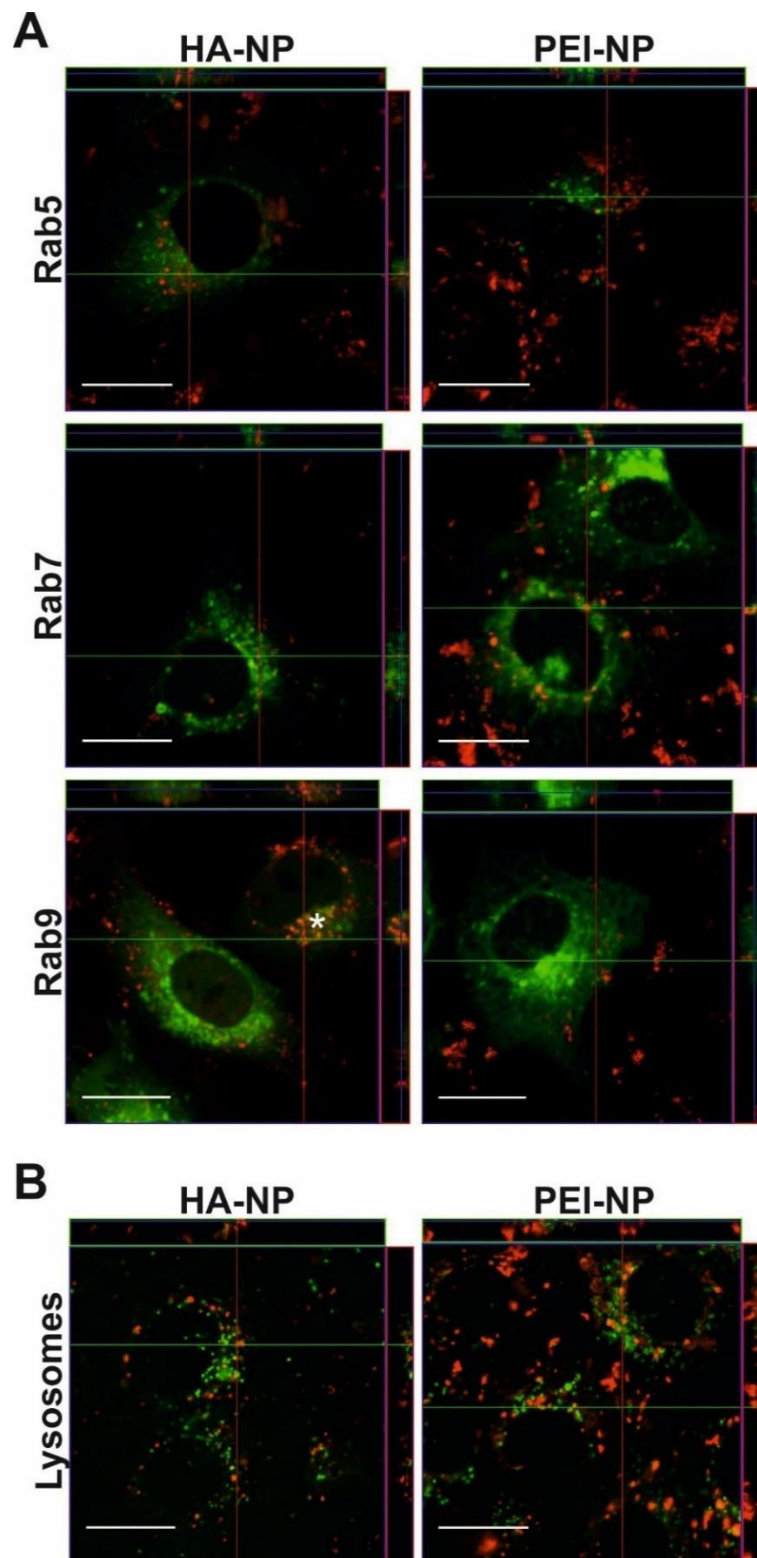

Figure 7. Orthogonal perspective of HTM-N cells stained for different endolysosomal compartments. NPs are shown in red, vesicles in green. Yellow spots (asterisk) indicate colocalization. The scale bar represents 20 µm. A) Rab-proteins. B) Lysosomes.

Figure **7**A shows representative fluorescent images of cells with green fluorescent recombinant Rab-proteins after treatment with NPs (red). As expected (and already discussed in chapter IV), PEI-NPs formed large aggregates that stuck to the cell surface rather than being taken up by the cells. In contrast, HA-coated NPs showed improved colloidal stability. Special attention should be paid to the lateral view of the cells, illustrated as narrow bars to the right of and on top of the square image, which is the top view. The distribution of red HA-NPs among green stained endosomes and lysosomes was homogenous through all layers of the cells. In contrast, PEI-NPs formed large aggregates that stuck to the cell membrane and sometimes pushed against it, deforming the membrane, but were not taken up. Colocalization, indicated by a yellow color, was not visible for either particle type or for any of the investigated Rab-proteins. Only HA-NPs show a low degree of colocalization with Rab 9 (Figure 7A, marked with asterisk), a marker for late endosomes on their way to the Golgi [33]. To exclude the possibility of NP accumulation in lysosomal compartments, cells were stained with a lysotracker dye (Figure 7B). No clear colocalization of NPs (red) with vesicles (green) was detected, raising the question of where the particles were located intracellularly.

To elucidate the fate of particles composed of PLGA, Cartiera et al. investigated the intracellular localization of blank PLGA-NPs of approximately 100 nm in size in opossum kidney cells and human bronchial epithelial cells [35]. They found the particles captured in vesicles associated with the Golgi apparatus or the endoplasmatic reticulum and concluded that the NPs follow an endocytosis-exocytosis route. The group of El-Dakdouki reported about receptor-mediated transcytosis of HA-modified silica-NPs [20]. The NPs were taken up by CD44-mediated endocytosis but were transported out of the cell during receptor recycling. The exported NPs could then be taken up by neighboring cells again. This allowed deep penetration into tissues which was shown in 3D multilayered cell culture and tumor spheroids.

Similar to the approach by El Dakdouki, HTM-N cells were treated with fluorescently tagged HA- or PEI-NPs. The fluorescence intensity of supernatant growth medium after the removal of unbound or uninternalized NPs by thorough washing was monitored over a period of 20 hours (Figure 8A). Although low fluorescence was detectable in the beginning, the fluorescence intensity increased constantly and reached a plateau of about 7 µg/mL after 10 to 15 hours. This makes up approximately 10 % of the maximal value if all available NPs were taken up by the cells and released into the growth medium again. El-Dakdouki related

his observation to the recycling of CD44 receptors and bound NPs. However, the effect also occurred for PEI-NPs and raised the question whether NP exocytosis is really related to receptor recycling. Furthermore, there is the possibility that a considerable fraction of the NPs was only loosely bound to the cell surface despite diligent washing steps. This might particularly count for the results of the experiments with PEI-NPs, as it can be assumed there are strong electrostatic interactions between the cationic NPs and negatively charged cell membranes [36]. NPs might detach from the membrane over time resulting in an increase in fluorescence intensity which is not caused by NP exocytosis.
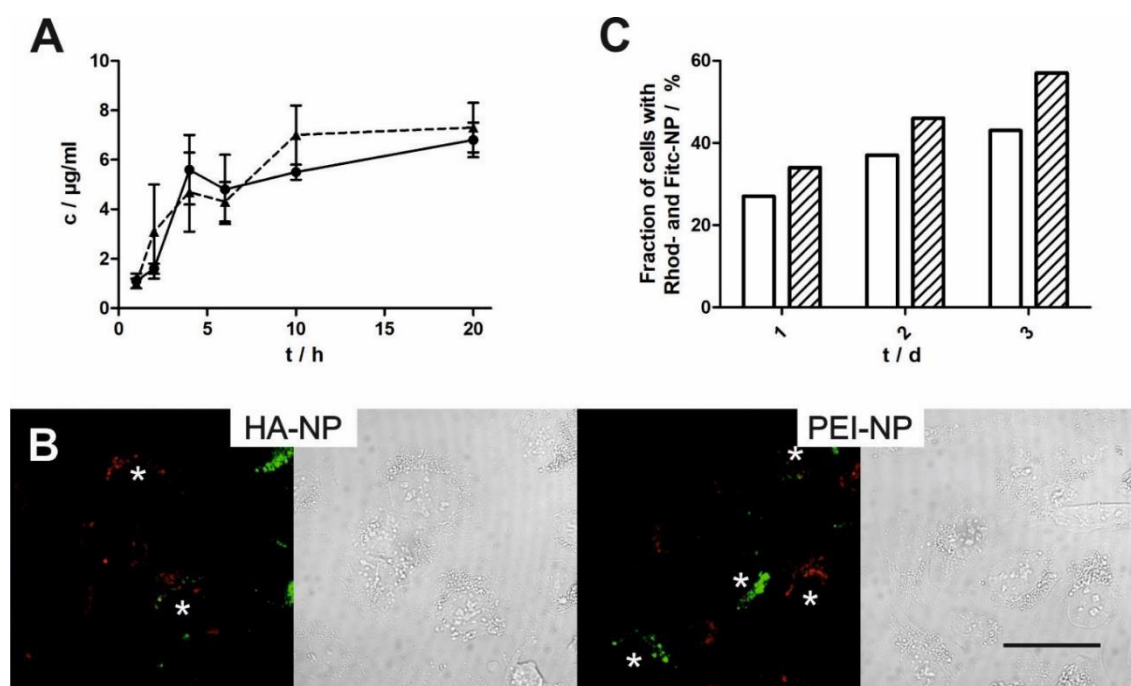
Figure 8. Exocytosis of HA- and PEI-NPs. A) Release of NPs into supernatant growth media from HTM-N cells. Solid line: HA-NPs, dashed line: PEI-NPs. B) Confocal images of HTM-N cells initially loaded with RHOD- or FITC-labeled NPs and cultivated together for 24 h. Some cells (marked with an asterisk) show both types of NPs because of NP-release and subsequent endocytosis from another cell. Scale bar: 50 μm. C) Fraction of cells with RHOD- and FITC-labeled NPs as counted manually in confocal images. Blank: HA-NPs, striped: PEI-NPs.

In order to elucidate the pathway of the NPs, an additional test was performed. Adherent HTM-N cells were separately treated with NPs tagged with either a rhodamine or fluorescein label, washed, harvested by trypsinization and then cultivated together for up to 72 h. The procedure of trypsinizatoin has been used frequently to remove loosely bound NPs [20,37,38]. Although cells were initially treated with only one type of fluorescently labelled NPs, a considerable number of cells with both red and green fluorescent NPs were detected after 24 h (Figure 8B, marked with an asterisk) and increased over time (Figure 8C).

Interestingly, the effect was slightly stronger for PEI-NPs instead of HA-NPs and the hypothesis that CD44 participates in NP exocytosis could not be supported.

The exocytosis of NPs might be – at least in part – an explanation for the poor transfection efficiency of LbL-NPs in GFP-producing HTM-N cells as described previously. NPs entered the cell but were then transported to cellular compartments that secreted them back into the cytosol again. Hence, the NPs were not able to deliver their siRNA freight to the cytosol and RNA interference was not possible. However, this is not the sole cause of poor RNA interference as a high number of NP remained intracellularly (see Figure 8 B). A combination of different factors led to the poor effectivity of the NPs for gene delivery. These factors include insufficient unpacking and siRNA release. Furthermore, the inclusion of PLArg into the LbL-sheath of the NPs did not result in higher transfection rates. Most likely, PLArg was not the ideal alternative to PEI as a polycationic component to enhance the disassembly of the NPs. As the LbL coating procedure is complex with a high number of individual steps, there is also the risk of siRNA degradation. Even if all possible precautions were taken to avoid contamination with RNA digesting enzymes, this possibility cannot be ruled out completely.

4   Conclusion

With the successful preparation of HTM-N_GFP+, an *in vitro* assay for gene silencing was developed which combines the advantages of an easy read-out in cell culture without neglecting specific properties of the trabecular meshwork. The LbL-NPs investigated so far were not successful in reducing GFP expression which would indicate a successful siRNA delivery. PEI-terminated NPs suffered from insufficient colloidal stability and formed large aggregates. These aggregates stuck to the cell membrane rather than being taken up by the cell. HA-NPs, in contrast, showed enhanced colloidal stability and uptake rates are promising. No colocalization was observed with early and late endosomes or lysosomes but NPs were distributed evenly between the vesicles. A small fraction of NPs was found in spatial proximity with vesicles related to the Golgi network. This lead to the presumption that HA-NPs were caught in a cycle of repeated endo- and exocytosis but without releasing their cargo into the cytosol. However, further attempts could not fully support this thesis. Although exocytosis was clearly observed – for both PEI- and HA-terminated particles - a considerable fraction of NPs remained intracellularly. The usage of PLArg as an intermediate layer also did not lead to an appreciable improvement in the gene silencing effect. However, in this case, the advantages offered by the LbL-NPs are most obvious: Varying the particle

size (by using another core particle, possibly made from different material) or the inclusion of functional polymers into the shell (e. g. disulfide-cleavable linkers or pH-responsive polymers) is easily feasible. The diversity of LbL-NPs is enormous and further efforts in research should be made with respect to tailoring this type of NP to meet the requirements of an siRNA delivery system.

References

[1] The Nobel Prize in Physiology or Medicine 2006, http://www.nobelprize.org/nobel_prizes/medicine/laureates/2006/, accessed 19 July 2017.

[2] Sharp PA (2001), RNA interference--2001, Genes & development 15 485–490.

[3] Mello CC, Conte D (2004), Revealing the world of RNA interference, Nature 431 338–342.

[4] Hannon GJ (2002), RNA interference, Nature 418 244–251.

[5] Wittrup A, Lieberman J (2015), Knocking down disease: a progress report on siRNA therapeutics, Nature Rev Genet 16 543–552.

[6] Bobbin ML, Rossi JJ (2016), RNA Interference (RNAi)-Based Therapeutics: Delivering on the Promise?, Ann Rev Pharmacol 56 103–122.

[7] Pecot CV, Calin GA, Coleman RL, Lopez-Berestein G, Sood AK (2011), RNA interference in the clinic: challenges and future directions, Nat Rev Cancer 11 59–67.

[8] Alnylam Pharmaceuticals, Inc. - Alnylam and Sanofi Report Positive Topline Results from APOLLO Phase 3 Study of Patisiran in Hereditary ATTR (hATTR) Amyloidosis Patients with Polyneuropathy, http://investors.alnylam.com/releasedetail.cfm?ReleaseID=1041081, accessed 5 October 2017.

[9] Tatiparti K, Sau S, Kashaw SK, Iyer AK (2017), siRNA Delivery Strategies: A Comprehensive Review of Recent Developments, Nanomaterials-Basel 7.

[10] Yin H, Kanasty RL, Eltoukhy AA, Vegas AJ, Dorkin JR, Anderson DG (2014), Non-viral vectors for gene-based therapy, Nat Rev Genet 15 541–555.

[11] Panyam J, Labhasetwar V (2003), Biodegradable nanoparticles for drug and gene delivery to cells and tissue, Adv Drug Deliver Rev 55 329–347.

[12] Williford J-M, Wu J, Ren Y, Archang MM, Leong KW, Mao H-Q (2014), Recent advances in nanoparticle-mediated siRNA delivery, Annu Rev Biomed Eng 16 347–370.

[13]   Kim E-J, Shim G, Kim K, Kwon IC, Oh Y-K, Shim C-K (2009), Hyaluronic acid complexed to biodegradable poly L-arginine for targeted delivery of siRNAs, J Gene Med 11 791–803.

[14]   Cho H-J, Chong S, Chung S-J, Shim C-K, Kim D-D (2012), Poly-L-arginine and dextran sulfate-based nanocomplex for epidermal growth factor receptor (EGFR) siRNA delivery: its application for head and neck cancer treatment, Pharm Res 29 1007–1019.

[15]   Lungwitz U, Breunig M, Blunk T, Göpferich A (2005), Polyethylenimine-based non-viral gene delivery systems, Eur J Pharm Biopharm 60 247–266.

[16]   Deng ZJ, Morton SW, Ben-Akiva E, Dreaden EC, Shopsowitz KE, Hammond PT (2013), Layer-by-Layer Nanoparticles for Systemic Codelivery of an Anticancer Drug and siRNA for Potential Triple-Negative Breast Cancer Treatment, ACS Nano 7 9571–9584.

[17]   Skandalis SS, Gialeli C, Theocharis AD, Karamanos NK (2014), Advances and advantages of nanomedicine in the pharmacological targeting of hyaluronan-CD44 interactions and signaling in cancer, Adv Cancer Res 123 277–317.

[18]   Dosio F, Arpicco S, Stella B, Fattal E (2016), Hyaluronic acid for anticancer drug and nucleic acid delivery, Adv Drug Delivery Rev 97 204–236.

[19]   Platt VM, Szoka FC (2008), Anticancer Therapeutics: Targeting Macromolecules and Nanocarriers to Hyaluronan or CD44, a Hyaluronan Receptor, Mol Pharm 5 474–486.

[20]   El-Dakdouki MH, Puré E, Huang X (2013), Development of drug loaded nanoparticles for tumor targeting. Part 2: Enhancement of tumor penetration through receptor mediated transcytosis in 3D tumor models, Nanoscale 5 3904–3911.

[21]   Zhao M, Yang H, Jiang X, Zhou W, Zhu B, Zeng Y, Yao K, Ren C (2008), Lipofectamine RNAiMAX: an efficient siRNA transfection reagent in human embryonic stem cells, Mol Biotechnol 40 19–26.

[22]   Corish P, Tyler-Smith Chris (1999), Attenuation of green fluorescent protein half-life in mammalian cells, Protein Eng 1035–1040.

[23] Persengiev SP (2004), Nonspecific, concentration-dependent stimulation and repression of mammalian gene expression by small interfering RNAs (siRNAs), RNA 10 12–18.

[24] Ganta S, Devalapally H, Shahiwala A, Amiji M (2008), A review of stimuli-responsive nanocarriers for drug and gene delivery, J Control Release 126 187–204.

[25] Shim MS, Kwon YJ (2012), Stimuli-responsive polymers and nanomaterials for gene delivery and imaging applications, Adv Drug Deliver Rev 64 1046–1059.

[26] He C, Zhuang X, Tang Z, Tian H, Chen X (2012), Stimuli-sensitive synthetic polypeptide-based materials for drug and gene delivery, Adv Healthc Mater 1 48–78.

[27] Karimi M, Ghasemi A, Sahandi Zangabad P, Rahighi R, Moosavi Basri SM, Mirshekari H, Amiri M, Shafaei Pishabad Z, Aslani A, Bozorgomid M, Ghosh D, Beyzavi A, Vaseghi A, Aref AR, Haghani L, Bahrami S, Hamblin MR (2016), Smart micro/nanoparticles in stimulus-responsive drug/gene delivery systems, Chem Soc Rev 45 1457–1501.

[28] Shim MS, Wang X, Ragan R, Kwon YJ (2010), Dynamics of nucleic acid/cationic polymer complexation and disassembly under biologically simulated conditions using in situ atomic force microscopy, Microsc Res Techniq 73 845–856.

[29] Mann A, Thakur G, Shukla V, Singh AK, Khanduri R, Naik R, Jiang Y, Kalra N, Dwarakanath BS, Langel U, Ganguli M (2011), Differences in DNA condensation and release by lysine and arginine homopeptides govern their DNA delivery efficiencies, Mol Pharm 8 1729–1741.

[30] Alhakamy NA, Berkland CJ (2013), Polyarginine molecular weight determines transfection efficiency of calcium condensed complexes, Mol Pharm 10 1940–1948.

[31] Santos JL, Nouri A, Fernandes T, Rodrigues J, Tomás H (2012), Gene delivery using biodegradable polyelectrolyte microcapsules prepared through the layer-by-layer technique, Biotechnol Prog 28 1088–1094.

[32] Zerial M, McBride H (2001), Rab Proteins as Membrane Organizers, Nat Rev Mol Cell Bio 107–117.

[33] Stenmark H (2009), Rab GTPases as coordinators of vesicle traffic, Nat Rev Mol Cell Bio 10 513–525.

[34]   Grant BD, Donaldson JG (2009), Pathways and mechanisms of endocytic recycling, Nat Rev Mol Cell Bio 10 597–608.

[35]   Cartiera MS, Johnson KM, Rajendran V, Caplan MJ, Saltzman WM (2009), The uptake and intracellular fate of PLGA nanoparticles in epithelial cells, Biomater 30 2790–2798.

[36]   Verma A, Stellacci F (2010), Effect of surface properties on nanoparticle-cell interactions, Small 6 12–21.

[37]   Kakade S, Manickam D, Handa H, Mao G, Oupicky D (2009), Transfection activity of layer-by-layer plasmid DNA/poly(ethylenimine) films deposited on PLGA microparticles, Int J Pharm 365 44–52.

[38]   Ebbesen MF, Olesen MTJ, Gjelstrup MC, Pakula MM, Larsen EKU, Hansen IM, Hansen PL, Mollenhauer J, Malle BM, Howard KA (2015), Tunable CD44-Specific Cellular Retargeting with Hyaluronic Acid Nanoshells, Pharm Res 32 1462–1474.

Layer-by-layer nanoparticles for siRNA delivery: Evaluation of gene silencing efficiency, intracellular distribution and exocytosis
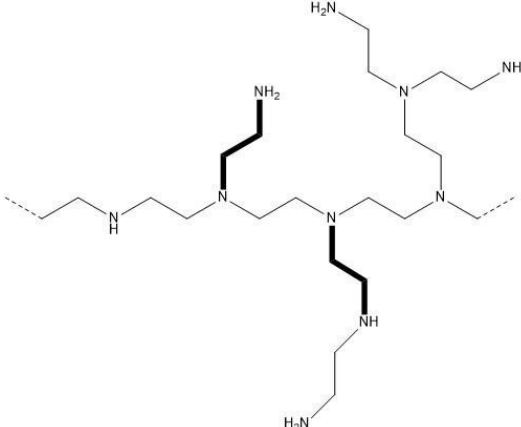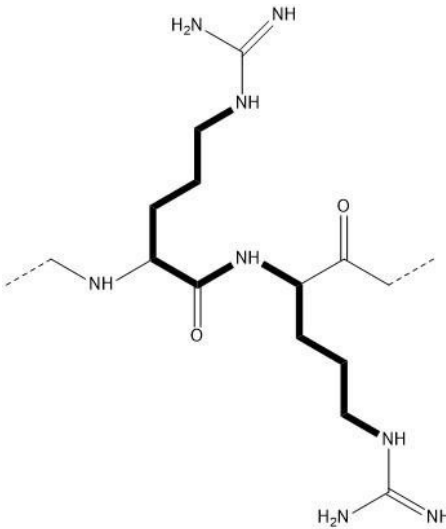
1   Determination of suitable Hygromycin B concentration
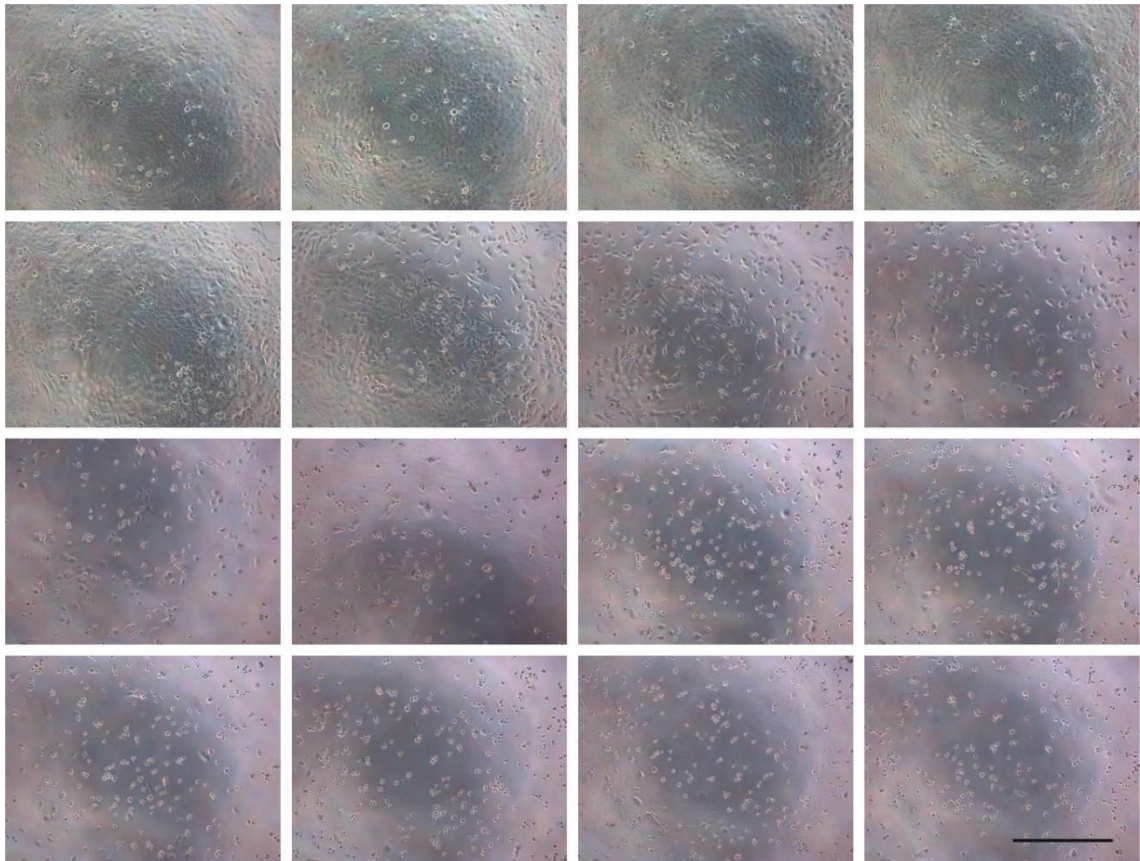
S 1. Representative brightfield images of HTM-N cells treated with increasing amounts of hygromycin B for 72 h. Tested hygromycin concentrations were 0 µg/mL (upper left), 5, 10, 25, 50, 100, 200, 300, 400, 500, 600, 700, 800, 900 and 100 µg/mL (lower right). For concentrations higher than 50 to 100 µg/mL, cell growth is inhibited considerable and stops at 300 µg/mL. Scale bar represent 500 µm.

2 Calculation of distance between cationic charges

S 2. Distance between cationic charges of PEI and PLArg were calculated as follows:

brPEI 25 kDa	pLArg

Bonds between possible charges:
1 x C-C (length: 154 pm)
2 x C-N (length: 147 pm)
→ 1 x 154 pm + 2 x 147 pm = 448 pm

Bonds between possible charges:
6 x C-C (length: 154 pm)
2 x C-N (length: 147 pm)
1 x N-CO (length: 133 pm)
1 x N-alpha C (length: 146 nm)
1 x CO-alpha C(length: 151 nm)
→ 6 x 154 pm + 2 x 147 pm + 1 x 133 pm + 1 x 146 pm + 1 x 151 pm = 1648 pm

Protonation state:
$pK_a = 8.4$
$pH = pK_a + lg (A^-/HA)$
$7.4 = 8.5 + lg (NH_2/NH_3^+)$
$0.1 = (NH_2/NH_3^+)$

Protonation state:
$pK_a = 13.2$
$pH = pK_a + lg (A^-/HA)$
$7.4 = 13.2 + lg (NH_2/NH_3^+)$
$1.6 \times 10^{-6} = (NH_2/NH_3^+)$

Only 90 % of amino groups are protonated, 10 % are not charged

Nearly all amino groups are protonated

Distance between charges increases by 10 %

Distance between charges not changed

Charge density: 492 pm (=0.5 nm)

Charge density: 1648 pm (=1.65 nm)

Hyaluronic acid functionalized nanoparticles for glaucoma therapy

Manuscript under preparation for submission.

The manuscript was prepared by M. Guter, A. Dillinger, F. Scherl, R. Fuchshofer and M. Breunig.

Data that was not obtained or analyzed by M. Guter is highlighted.

Abstract
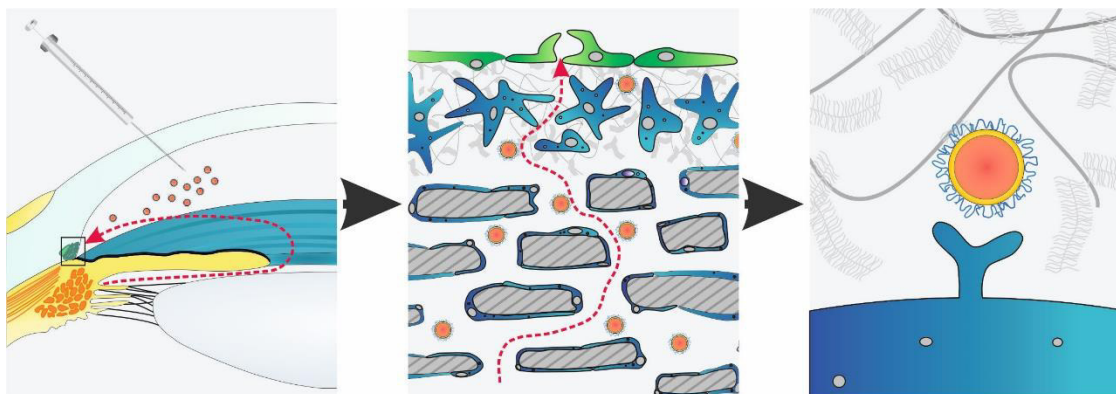
An elevated intraocular pressure (IOP) is regarded as a causative risk factor for the development of glaucoma, a neurodegenerative ocular disease and one of the leading causes of blindness worldwide. IOP is regulated by the production of aqueous humor in the ciliary body and its drainage through the trabecular meshwork (TM). Recently, connective tissue growth factor (CTGF) was identified to increase the resistance to aqueous humor outflow by enhancing the deposition of extracellular matrix and contractility of cells in the TM. Gene silencing using small interfering RNA (siRNA) might be an opportunity to reduce the effects of CTGF and persistently lower IOP. However, with respect to therapeutic use, a suitable delivery system is required. Here we describe the development of hyaluronic acid functionalized layer-by-layer nanoparticles (NPs) for the delivery of siRNA to the TM. The coating with hyaluronic acid prevents the adhesion and nonspecific attachment of the particles to tissue and cells of the outflow system and enables a penetration deep into the TM after intracameral injection. Further, the NPs specifically address cluster of differentiation (CD) 44 receptors on the target cells in the TM and Schlemm's channel guaranteeing high uptake rates. CD44 is particularly suitable as target for the particles, as glaucoma patients show a higher CD44 receptor expression in the relevant regions compared to healthy individuals. *In vitro*, the NPs were able to reduce CTGF mRNA levels depending on the basal expression of the growth factor, opening the door for a new causative glaucoma therapy with minimal risk for undesired side effects.

1   Introduction

Glaucoma, a neurodegenerative disease of the optic nerve, is one of the leading causes of blindness. It is estimated that about 111.8 million people will be affected worldwide by 2040 [1]. Among various sub-types, primary open angle glaucoma (POAG) is the most common form [2]. An elevated intraocular pressure (IOP) was identified as critical risk factor for the pathogenesis of glaucoma. Current medications rely on decreasing the IOP by administering topical eye drops, which have a long list of drawbacks such as poor compliance and inadequate application by patients, poor bioavailability and systemic side effects [3,4]. In addition, eye drops do not tackle the origin of disease thereby failing at sufficiently decreasing the IOP. Consequently, new causative therapeutic concepts are of utmost importance.

The IOP is generated in the anterior chamber of the eye due to a resistance to the outflow of aqueous humor (AH) through the trabecular meshwork (TM) and Schlemm's canal (SC) (Scheme 1A) [5]. A significant change in the quality and amount of extracellular matrix (ECM) in the TM [6–9] together with an enhanced contractility of TM and SC cells contribute to an abnormal increase in outflow resistance [10–12]. We recently identified connective tissue growth factor (CTGF) as a major mediator of these pathological effects, based on an increased expression rate of CTGF in glaucomatous SC cells [13] and its potential to cause increased ECM synthesis and contractility of TM cells [6,11]. Moreover, a direct implication of CTGF in the dysregulation of the AH outflow facility was demonstrated in transgenic animals, which had a significant elevated IOP leading to a progressive loss of axons in the optic nerve [11]. Hence, we speculate that a reduction of CTGF would achieve a more permanent and causative effect in regulating the IOP compared to available standard treatment regimes.

A favorable tool to reduce the production of specific proteins is small interfering RNA (siRNA) [14,15]. The eye is particularly attractive for siRNA application because of a possible local administration and the immune privilege of the eye [14,15]. The principle feasibility of ocular siRNA therapy is being demonstrated in a limited number of ongoing clinical trials and pre-clinical studies [14–17]. For example, one recent study focused on glaucoma therapy, and naked siRNA was applied to the anterior chamber with the intention to reduce tight junction proteins of endothelial cells lining the SC [16,16]. Unfortunately, the approach was quite unspecific and may therefore have severe adverse effects on the integrity of the blood-aqueous-barrier of the ciliary body. Moreover, all studies have a major shortcoming: siRNA drug candidates are delivered in their naked form, but naked siRNA is subjected to

degradation and not able to efficiently cross cellular membranes [14,18,19]. Thus, a huge amount of siRNA molecules would be required for eliciting a therapeutic effect. Consequently, our approach will decisively depend on the development of nanoparticles (NPs). The NPs will have to be injected into the anterior chamber of the eye (Scheme 1A). From there, we envision NPs to follow the natural trabecular outflow to reach the target cells in the outflow pathway. The TM consists of various morphologically and functionally different parts (Scheme 1B) [5]. The corneoscleral TM is due to its high porosity comparable to a filter with large pores. In the juxtacanalicular TM (JCT), pore size significantly decreases and the ECM, in which the JCT cells are embedded, becomes much denser [20]. The JCT is followed by the endothelial lining of the SC. The transport of particles through the interstitial space of the TM is poorly understood and scarcely investigated. A very early study of the 1990s revealed that up to 45 % of polystyrene particles (0.176 and 0.46 μm) were captured in the TM of perfused enucleated human eyes [21]. Because particles were smaller than the morphologically determined pore dimensions and a significant fraction of all particle sizes were retained, particle retention was most likely due to adhesion interaction. A portion of intracamerally injected cationic gold NPs of 5 or 10 nm seemed to penetrate the JCT, but particles were then associated with the ECM beneath the inner wall endothelium [22]. These examples illustrate that preventing adhesive hindrance and overcoming the TM barrier poses a huge challenge.
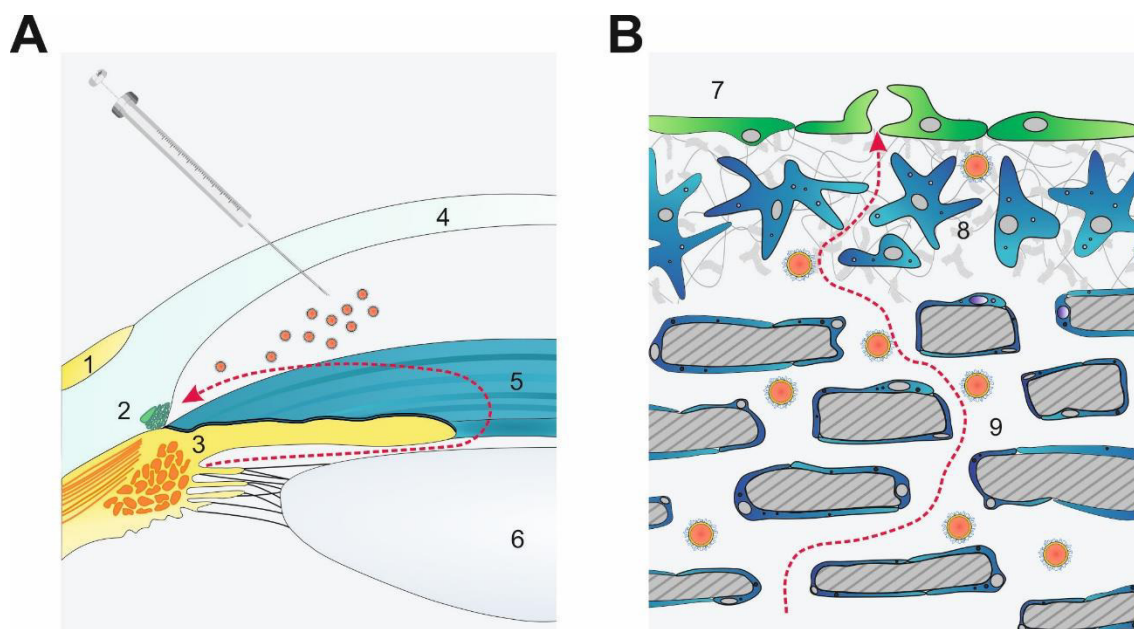
Scheme 1. Strategy for delivering NPs to cells of the trabecular meshwork (TM) and Schlemm´s canal (SC). A) Aqueous humor (dashed red line) is secreted by the ciliary body and flows from the posterior chamber to the anterior chamber and is finally drained via the TM and SC into the veins. Nano-carriers will be injected into the anterior chamber of the eye and are envisioned to follow the natural trabecular outflow pathway. B) Magnified schematic drawing of the trabecular outflow pathway illustrating corneoscleral, juxtacanalicular (JCT) TM and inner endothelial wall of SC. NPs are envisioned to target TM cells of the JCT and endothelial cells of SC via the CD44 receptor followed by knockdown of CTGF, which is known as glaucoma-inducing growth factor. 1 = sclera, 2 = TM, 3 = ciliary body, 4 = cornea, 5 = iris, 6 = lens, 7 = SC, 8 = JCT, 9 = corneoscleral meshwork.

After penetrating the ECM, delivering the therapeutic freight to TM and SC cells is an equally important challenge. Both cell types express the cluster of differentiation (CD) 44 receptor under normal, healthy conditions [20]. In addition, CD44 expression is highly elevated on TM cells of glaucomatous patients [23], which could be exploited for a potential therapy. Accordingly, patients with glaucoma would respond to a treatment in a different way compared to healthy individuals. If such a difference of the CD44 expression level also exists for SC cells has not been investigated. Nano-carriers have been surface coated with the naturally occurring polysaccharide hyaluronan (HA) to achieve CD44 targeting [24]. Although this principle has been successfully demonstrated for CD44-overexpressing cancer cells, a proof of concept remains to be demonstrated for other diseases such as glaucoma.

In this study, we will address the key question: How have NPs to be designed to prevent adhesive hindrance in the TM and target TM and SC cells of glaucoma patients at the same time? To follow up our goal we will focus on NPs that are assembled in a layer-by-layer (LbL) approach [25] (Scheme 2). The siRNA will be sandwiched between two polycationic polyethylenimine (PEI) layers and most important, NPs will be coated with a final HA layer.

163

We ascribe this natural polymer a dual function. First, we speculate that HA-decorated NPs are not maintained in the ECM of the TM by interaction forces because HA is per se a highly abundant molecule in the ECM [20]. Second, HA-decorated NPs are expected to bind to the CD44 receptor of the TM and SC cells of glaucomatous patients which would potentially allow for precisely delivering therapeutic molecules for future therapies, in a way as it is envisioned in personalized medicine.
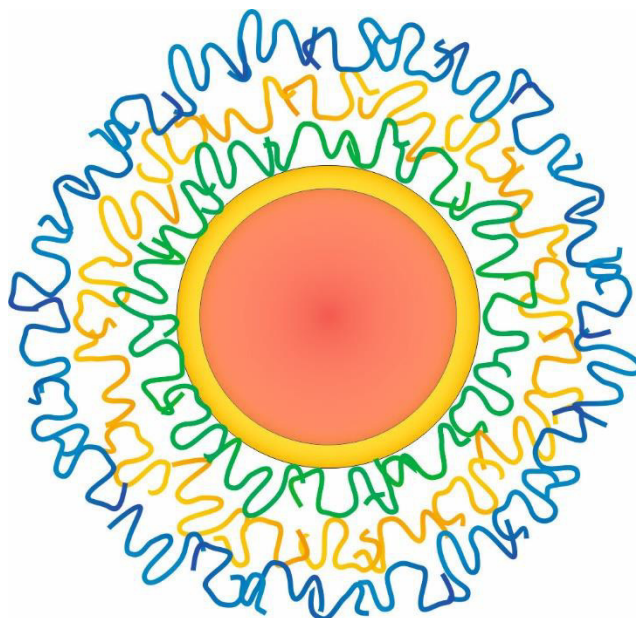
Scheme 2. Schematic drawing of LbL assembled NPs applied in this study: PLGA NPs are stabilized with PEI (25 kDa) (red core, orange shell), followed by a layer of siRNA (green) and again PEI (orange). Finally, the particles are coated with HA (blue) with a MW of 13 kDa.

2 Materials and Methods

2.1 Materials

Acid terminated poly(D,L-lactide-*co*-gylcolide) (PLGA) (lactide/glycolide 50/50) with an average molecular weight of 38-54 kDa and branched polyethylenimine (PEI) 25 kDa were purchased from Sigma-Aldrich Chemical Company (Taufkirchen, Germany). Rhodamine B (RHOD) endcapped PLGA (lactide/glycolide 50/50, 30 kDa) (RHOD-PLGA) was obtained from Polyscitech (West Lafayette, Indiana, United States). Sodium hyaluronate (13 kDa) was bought from Lifecore Biomedicals (Chaska, Minnesota, United States). Non-targeting siRNA (5'-UUC UCC GAA CGU GUC ACG UdTdT-3') and siRNA directed against CTGF (5'-AGA UUC CCA CCC AAU UCA ATT dTdT-3') were purchased from Qiagen (Hilden, Germany) and Eurofins (Ebersberg, Germany). Lipofectamine 2000 and RNAiMAX were

from ThermoFisher Scientific (Darmstadt, Germany). Cav1-GFP (plasmid #14433) was obtained from Addgen (Cambridge, Massachusetts, United States). Sucrose, microbiological grade, was from Merck (Darmstadt, Germany).

2.2   Methods

Cell culture

Primary human trabecular meshwork (hTM) cells were cultivated in Ham's F12 medium with the addition of 5 % serum and used until passage number 8. Immortalized human trabecular meshwork (HTM-N) cells were cultivated in EMEM+ containing 10 % serum. If indicated, cells were stimulated for 24 hours in serum-free medium, followed by another 24 hours in serum-free medium supplemented with 1 ng/mL human TGF-β2 (R&D systems, Wiesbaden, Germany) or 50 ng/mL CTGF (EMP Genetech, Ingolstadt, Germany), respectively. All cell culture reagents were obtained from Gibco (ThermoFisher Scientific, Waltham, Massachusetts, United States).

mRNA analysis

mRNA was isolated from hTM cells after CTGF silencing, anterior eye segments of transgenic and WT mice and primary SC cells as follows: Total RNA was extracted using TriFast™ (Peqlab, Erlangen, Germany) reagent according to the manufacturer's recommendations. cDNA was prepared using the qScript™cDNA Synthesis Kit (Quanta Biosciencies, Gaithersburg, USA) according to the manufacturer's instructions. All primers were from Invitrogen and extended over exon-intron boundaries. The sequence of the primers was as follows: 5'-gacacattccaccccagtg-3' (huCD44 forward), 5'-tggaatttggggtgtcctta-3' (huCD44 reverse), 5'-gaagttcctggtccacaacg -3' (huRPL32 forward), 5'-gcgatctcggcacagtaag -3' (huRPL32 reverse), 5'-actcaagtgcgaaccaggac-3' (msCD44 forward), 5'-gccaagatgatgagccattc-3' (msCD44 reverse), 5'-gctgccatctgttttacgg -3' (msRPL32 forward), 5'-tgactggtgcctgatgaact -3' (msRPL32 reverse), 5'-ctcctgcaggctagagaagg-3' (CTGF forward), 5'-gatgcacttttgccgttctt-3' (CTGF reverse), 5'- cctaaccgctactggctgtg-3' (Gnb2L forward), 5-ctacaatgatctttccctctaaatcc-3' (Gnb2L reverse). RT-PCR was performed on a BioRad iCycler (BioRad, München, Germany) in 50 cycles with the temperature profile of 20 s melting at 94°C, 10 s annealing at 60°C and 20 s extension at 60°C. RNA that was not reverse transcribed served as negative control. For relative quantification of the experiments, Gnb2L

or RPL32, respectively, were used as a housekeeping gene. Bio-Rad iQ5 Optical System Software (version 2.0) was used for analysis and ΔΔct-method was applied for normalization.

Western Blot analysis

Proteins of primary hTM cells for investigation of CD44 and CTFG expression were isolated after RNA separation according to the manufacturer's instructions (TriFast™, Peqlab, Erlangen, Germany). Proteins were dissolved in 1 % SDS containing protease and phosphatase inhibitors. Protein concentration was determined by the bicinchoninic acid assay (Interchim, Montluçon Cedex, France). Thereafter, proteins were separated by SDS-PAGE and transferred to polyvinylidene difluoride membranes (Roche, Mannheim, Germany). Western blot analysis was performed with specific antibodies as described previously [26]. Antibodies were used as follows: mouse anti-CD44 (1:1000, R&D systems, Minneapolis, USA), goat anti-CTGF (1:500; Santa Cruz, Dallas, USA; and horse anti-mouse (1:2000, Cell Signaling Technology, Danvers, USA). rabbit anti-α-tubulin (1:2500, Rockland Immunochemicals Inc., Gilbertsville, USA) was used as loading control. Chemiluminescence was detected on an LAS 3000 imaging workstation (Fujifilm, Düsseldorf, Germany) and signal intensity was estimated by the AIDA Image analyzer software (Raytest, Straubenhardt, Germany).

Immunocytochemistry of in vitro samples

hTM cells were seeded on coverslips and stimulated with 1 ng/mL TGF-β2, 50 ng/mL CTGF (24 h serum-free, followed by another 24 h in serum-free medium supplemented with TGF-β2 or CTGF) or left untreated as control. Cells were washed twice with PBS, fixed with 4 % (w/v) paraformaldehyde (PFA) for 5 minutes and washed again three times with PBS. Specific antibodies were used as follows: mouse anti-CD44 (1:100) and Alexa Fluor 488-conjugated anti-mouse IgG (1:1000, Invitrogen, Darmstadt, Germany). As a control for unspecific binding of the secondary antibody, negative controls were performed. Finally, 4,6-diamidino-2-phenylindole (DAPI) (Vector Laboratories, Burlingame, USA) was added to counterstain nuclear DNA and the immunofluorescence was visualized using a Zeiss Axio Imager fluorescence microscope (Carl Zeiss AG, Göttingen, Germany).

Nanoparticle preparation and characterization

Particle preparation. RHOD-labeled PLGA NPs were prepared by nanoprecipitation. In brief, 2 mL of a 10 mg/mL solution of PLGA (PLGA/RHOD-PLGA=50/50) in acetonitrile was slowly injected into 8 mL of a solution of 0.5 % PEI in ultrapure water and stirred for 4 hours until the organic solvent totally evaporated. Excess PEI was removed by stepwise centrifugation at a speed of 5,000, 7,000 and 9,000 g for 7 minutes each, the complete centrifugation cycle was once repeated. Resulting PEI-coated NPs were subsequently resuspended in ultrapure water, then lyophilized with the addition of 2 % sucrose as a protective agent. NP yield was gravimetrically determined and particles were stored at -20°C until further use. For subsequent coating steps, lyophilized NPs were resuspended in ultrapure water at a concentration of 1 mg/mL and purified from sucrose according to the procedure described above. Then, NPs were dropwisely added to a stirring solution of the respective polyelectrolyte (final concentration: HA 1 mg/mL in water, siRNA 4 μM in 10 mM NaCl, PEI 1 mg/mL in water), according to the process described by Elbakry et al [25]. Dispersions were kept on a stirring plate for 30 to 60 minutes. Unbound polyelectrolyte was removed by stepwise centrifugation, followed by resuspension in ultrapure water. If siRNA or HA was the outermost layer, centrifugation speed was reduced to 1,000, 2,000 and 3,000 g for 7 minutes each, without repetition of the complete centrifugation cycle. Concentration of assembled NPs was determined in relation to the florescence of resuspended, but unpurified NPs of known concentration on a microplate reader (FLUOStar Omega, BMG Labtech, Ortenberg, Germany) equipped with a 544 nm excitation and a 590 nm emission filter set.

Physicochemical Characterization. Hydrodynamic diameter and zeta potential of diluted (in water) samples was determined by dynamic and electrophoretic light scattering using a Zetasizer Nano ZS (Malvern Instruments, UK). For all size measurements, 173° backward scatter in the general-purpose mode with automatic measurement position and attenuator selection at 25°C was applied. Z-Average values were determined from three independent samples, each measured three times with 11 runs per measurement. Zeta potential was determined in the monomodal mode using the Smoluchoswki approximation, measuring three independent samples three times each.

Scanning electron microscopy. A drop of purified NPs was added to conductive pads (Plano GmbH, Wetzlar, Germany) attached to aluminum specimen stubs (Agar Scientific, Stansted, Essex, UK) and air dried. The samples were sputtered with Au/Pd using a Polaron SC 515 SEM Sputter Coating System. Images were taken on a Zeiss DSM 950 scanning

electron microscope (Jena, Germany). An acceleration voltage of 10 kV was used. The working distance was set to 15 mm and a magnification of 30,000 x was chosen.

Colloidal stability. NPs were incubated at a concentration of 40 μg/mL in Leibovitz medium supplemented with 0 to 1 % serum for one hour at room temperature to allow for the formation of a protein corona. hTM cells that were seeded into μ-Slide 8 Well ibidi slides (ibidi, Planegg, Germany) at a density of 20,000 cells per well 24 hours before use, were rinsed with PBS and incubated with NPs for four hours. Thereafter, cells were washed two times with PBS, supplied with fresh Leibovitz medium containing 10 % serum and analyzed by confocal laser scanning microscopy (CLSM) (LSM 510 META, Carl Zeiss, Jena, Germany). RHOD-labeled NPs were excited at 543 nm and fluorescence emission was detected at 560 – 615 nm. The optical slice thickness was < 16.3 nm.

Cellular uptake of nanoparticles

HTM-N cells were seeded at a density of 40,000 into μ-Slide 8 Well ibidi slides. After 24 hours, cells were transfected with a cav1-GFP plasmid. Lipoplexes were prepared according to manufacturer's instruction, using 0.3 μg DNA and 1 μl Lipofectamine 2000 per well and added to the cells for 4 hours. The next day, cells were treated with 40 μg/mL NPs in Leibovitz medium supplemented with 0.35 % serum as described above. Cells were observed by confocal laser scanning microscopy (CLSM) in the multitracking mode using 488 and 543 nm lasers for excitation, and a 505-530 nm bandpass or a 560 nm longpass filter for fluorescence emission detection. Optical z-sections were taken with an optical slice thickness of 0.7 μm.

CTGF gene silencing in vitro

hTM cells in passage 5 to 7 were grown in 6-well cell culture dishes. After reaching 80 % confluency, cells were cultivated for 24 hours without serum and another 24 hours with the addition of 1 ng/mL TGF-β2 or left as untreated control. NPs were prepared at a concentration of 80 μg/mL in Leibovitz medium containing 0.35 % serum and 1 ng/mL TGF-β2 and left one hour at room temperature for the formation of a protein corona. Cells were incubated for additional four hours with NPs, washed with PBS once and left for 24 h in serum-supplemented medium. Thereafter, cells were cultured for additional 24 hours without serum before RNA and protein extraction followed by mRNA analysis and Western Blotting.

In vivo experiments with transgenic animals

Transgenic βB1-CTGF mice were generated as described previously [11] and compared to wild type (WT) mice. Animals were housed under standardized conditions of 62 % air humidity and 21°C room temperature. Feeding was ad libitum. Animals were kept at a 12-hour light/dark cycle (6:00 – 18:00). To evaluate differences of CD44 expression on the mRNA level, 8 week old βB1-CTGF and WT mice were killed by exarticulation of the atlanto-occipital joint. Corneal-scleral rings were dissected, the anterior eye segment was separated from the posterior part of the eye along the ora serata and the lens was taken out. The anterior eye segment was cut in half and most of the cornea was removed. Total RNA was extracted, analyzed by RT-PCR and quantified as described above. Alternatively, for immunohistochemistry, eyes of 8 week old βB1-CTGF transgenic and wild-type (WT) mice were enucleated and fixed in 4 % (w/v) paraformaldehyde for 4 hours. The eyes were equilibrated in 10 %, 20 % and 30 % sucrose, embedded in Tissue-Tek optimal cooling temperature compound (Sakura Finetek Europe B.V., Zoeterwounde, Netherlands), and stored at -20°C. Frozen 12 μm sections were cut on the cryostat. Cross sections of the ON were obtained. After blocking with 2 % bovine serum albumin (BSA), 0.2 % cold water fish skin gelatin (Sigma-Aldrich), 0.1 % Triton X-100 in 0.1 M phosphate buffer, frozen sections were incubated with rabbit anti-CD44 (1:100) at 4°C overnight. Afterwards, tissue sections were washed three times with 0.1 M phosphate buffer, followed by an incubation with the secondary antibody Cy3™ goat anti rabbit (1:2000, Jackson Immuno Research Europe Ltd., Suffolk, UK) for 1 h at room temperature. As a control for unspecific binding of secondary antibodies, negative controls were performed. After washing three times with PBS, the slides were mounted using the DakoCytomation fluorescent mounting medium with DAPI 1:10 (Dako). Slides were dried overnight at 4°C before microscopy.

Ex vivo perfusion of porcine and human eyes

Fresh enucleated porcine eyes were obtained from a local abattoir. Eyes with a visible damage were excluded. Human eyes were obtained from body donors of the university of Regensburg. After the extraocular tissue was removed, the porcine and human eyes were submerged to the limbus in 0.89 % NaCl at 35°C. The perfusion system contained a perfusion chamber and a collection chamber. The infusion needle was intracamerally inserted through the transparent cornea into each eye and connected to the perfusion chamber. The needle was then carefully pushed through the pupil and the tip of the needle was placed in the posterior chamber. Then, a second needle was placed into the anterior chamber and

connected to the collection reservoir. The needle was closed during the perfusion excepted during the exchange periods. First, a volume of 3 mL glucose solution (5 %) was exchanged over a time period of about 10 to 15 minutes. In the next step, the collection reservoir was closed and the eyes were perfused with 3 mL NPs at a constant pressure of 10 mmHg for 3 hours. Then, a second exchange with 3 mL glucose solution was performed, which took again 10 to 15 minutes, followed by a second perfusion for 2 hours with glucose. The anterior chamber of the porcine and human eyes was dissected and most of the sclera and the cornea were removed. The tissue was separated into small pieces and fixed with 4 % (w/v) PFA for 4 hours and washed three times with 0.1 M phosphate buffer. Samples were prepared as described above for sectioning and staining with a mouse anti-human CD44 antibody (1:1000, R&D Systems, Minneapolis, Minnesota, United States) or an anti-CD31 antibody. As a control for unspecific binding of secondary antibodies, negative controls were performed. Confocal images and z-stacks were taken on a confocal laser scanning microscopy (CLSM) in the multitracking mode using 488 and 543 nm lasers for excitation, and a 505-530 nm bandpass or a 560 nm longpass filter.

Statistical analysis.

Sigma Plot 12.0 software was used for statistical analysis. For the evaluation of the gene silencing results, a one-way ANOVA of the ΔΔct-values was conducted followed by a Holm-Sidak-test.

3 Results

3.1 CD44 prevalence in primary cells in vitro, in transgenic mice in vivo and in human eyes ex vivo

To demonstrate the principle feasibility of our approach, the CD44 prevalence in glaucomatous versus healthy cells of the outflow pathway in the anterior eye chamber was investigated. In a first step, the expression level of CD44 was evaluated in primary human TM (hTM) cells *in vitro*. Tumor growth factor β2 (TGF-β2) is causatively involved in the pathogenesis of POAG and well known as glaucoma-inducing growth factor [7,27]. Hence, hTM cells were treated with TGF-β2 (1 ng/mL) and its down-stream mediator CTGF (50 ng/mL) in order to compare glaucomatous to untreated, healthy control cells [6,11]. Protein expression was detected by Western Blot analysis after 24 hours (Figure 1A). Both

TGF-β2 and CTGF treatment led to a significant increase of the CD44 protein level compared to untreated control cells. Immunocytochemical staining of CD44 in confluent hTM monolayers confirmed the results (Figure 1B). A characteristic fiber-like pattern of CD44 was revealed on the surface of hTM cells. Again, cells treated with the glaucoma factors TGF-β2 or CTGF, respectively, showed a brighter fluorescence compared to untreated controls. Presence of CD44 was also studied in primary SC cells that were isolated from healthy as well as glaucomatous human donors (Figure 1C). Consistently, real time RT-PCR analysis showed a significant increase of the CD44 mRNA level in glaucomatous SC compared to healthy control cells.

In a second step, transgenic mice with lens-specific CTGF overexpression (βB1-CTGF) were compared to healthy, wild-type (WT) mice. The transgenic animals develop POAG characterized by higher IOP and progressive loss of axons in the optical nerve head and show significant pathologic changes within the outflow pathway [11]. Anterior eye segments of 2-month old βB1-CTGF and WT mice were investigated to evaluate if morphological changes are connected to alterations in the amount and distribution of CD44. The relative mRNA level of CD44 was significantly increased in corneal-scleral rims of βB1-CTGF animals compared to their WT littermates (Figure 1D). Because the corneoscleral-rim contains not only the TM and SC, but also parts of the sclera, immunohistochemical staining was performed to precisely localize CD44 in the anterior eye segment. CD44 signal was detected in the iris, ciliary body, TM and the SC of 2-month old WT mice, and no signal was observed in the sclera (Figure 1E). In βB1-CTGF mice, a similar distribution of CD44 in the anterior chamber angle was observed, however, the signal was markedly increased in the tissues of the outflow pathway, namely the TM and SC, and no changes were observed in the sclera (Figure 1E). Consequently, changes of CD44 expression in the outflow tissues can be related to the CTGF-induced increase of CD44 mRNA.

Finally and most important, the CD44 expression was investigated in the iridocorneal angle of glaucomatous and healthy human donors eyes. Immunohistochemical staining of cryosections clearly visualized a remarkably enhanced CD44 signal in the TM, SC and the iris of glaucomatous eyes (Figure 1F).
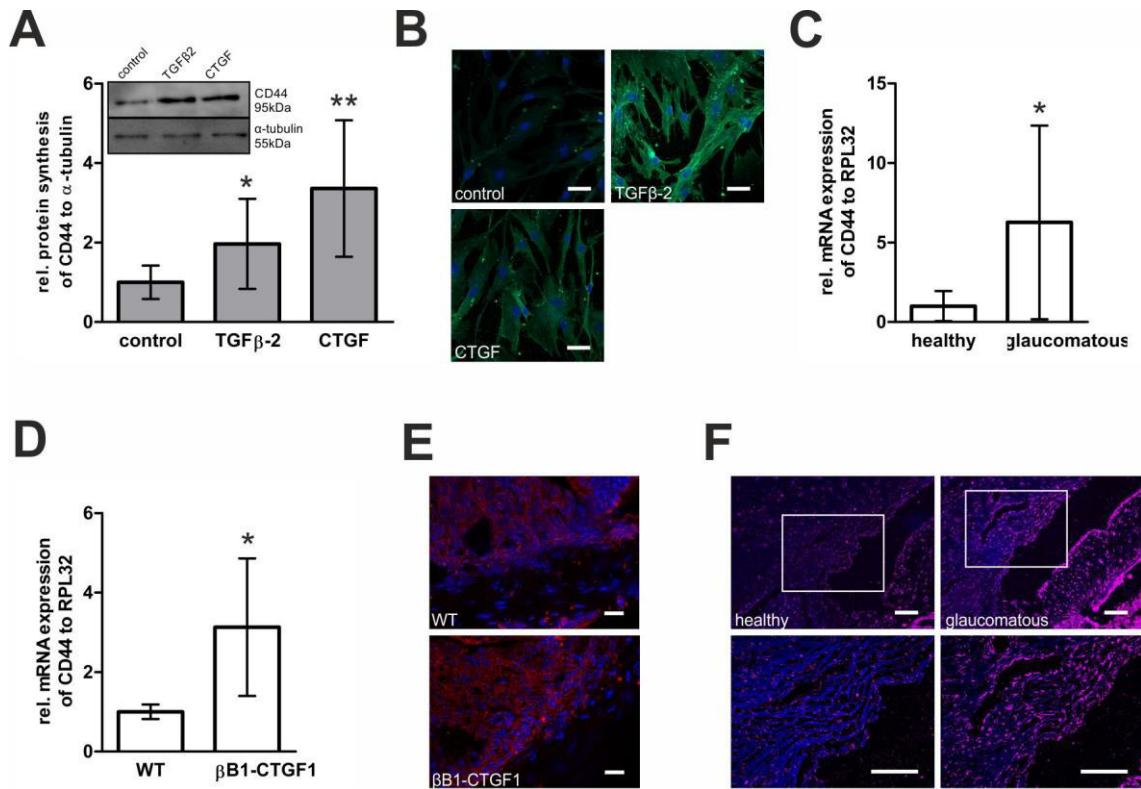
Figure 1. The CD44 prevalence was analyzed in healthy and glaucomatous cells *in vitro* (A-C), in transgenic mice *in vivo* (D, E) and in eyes of human donors *ex vivo* (F). A) Primary human TM (hTM) cells were treated with TGF-β2 (1 ng/mL) or its down-stream mediator CTGF (50 ng/mL), respectively, and compared to untreated control cells *in vitro*. Western blot analysis (inlet Figure 1A) with anti-CD44 antibody revealed a significantly enhanced CD44 expression of treated versus untreated cells. CD44 signal was related to the α-tubulin signal as a reference. Histograms represent densitometry-based average values (mean ± SD) of 5 independent experiments. B) Likewise, immunocytochemical staining of confluent hTM cells with an anti-CD44 antibody and fluorescently-labeled secondary antibody revealed a brighter signal of TGF-β2 and CTGF treated versus control cells. Blue: DAPI staining of cell nuclei; green: Alexa Fluor 488 conjugated anti-CD44 antibody. Bar represents 50 μm. C) Primary SC cells of human glaucomatous versus healthy donor eyes were analyzed regarding their CD44 mRNA level. Relative amount of CD44 mRNA of glaucomatous SC cells was significantly enhanced compared to heathy cells. Values were normalized to the housekeeping gene RPL32. Values represent mean ± SD (healthy: n = 4, glaucomatous: n = 5). D) Corneal scleral rims of transgenic animals with lens-specific CTGF overexpression (βB1-CTGF) were compared to their wild type (WT) littermates regarding the CD44 prevalence. Relative mRNA level was significantly enhanced in corneal-scleral rims of βB1-CTGF compared to WT animals. Values represent mean ± SD of four independent experiments. E) Immunohistochemical staining illustrated that the CD44 signal was primarily enhanced in TM and SC, but not in the sclera. Blue: DAPI staining of cell nuclei; red: Cy3-conjugated anti-CD44 antibody. Scale bar represents 100 μm. F) Analysis of the chamber angle of three human donor eyes also revealed a remarkably brighter CD44 signal in the TM, SC and iris of glaucomatous versus healthy donor cells. Blue: DAPI staining of cell nuclei; red: Cy3-conjugated anti-CD44 antibody. The scale bar represents 100 μm.

3.2   Synthesis and characterization of nanoparticles

To address the question how NPs have to be designed to prevent adhesive, nonspecific attachment to tissue and cells in the outflow pathway and target TM and SC cells of glaucoma patients at the same time, nanocarriers were fabricated in a first step without therapeutic siRNA and had either a final layer of PEI (PEI-NPs) or HA (HA-NPs) on the surface (Figure 2). PEI-NPs served as control because they are known to nonspecifically interact with cells and tissue [28], while HA-NPs are envisioned – as already outlined - to bind to CD44 and prevent nonspecific, adhesive interactions. According to Figure 2A the core of the NPs consisted of biodegradable, FDA approved poly(D,L-lactide-*co*-glycolide) (PLGA) with a MW of 38-54 kDa. PLGA-NPs were prepared by nanoprecipitation and then stabilized with the polycationic polymer PEI with a MW of 25 kDa. PEI-NPs were then coated with negatively charged HA of 13 kDa resulting in HA-NPs (Figure 2A and B). To remove free, unbound polyelectrolyte, PEI- and HA-NPs were purified by stepwise centrifugation. Otherwise, ill-defined inter-polyelectrolyte complexes would have formed which are hard to separate from coated NPs. The hydrodynamic diameter of both NP species was in a similar range, the z-average value was about 255 nm and 240 nm for PEI- and HA-NPs, respectively, as determined by dynamic light scattering. The absence of additional peaks in the intensity distribution and a polydispersity index (PDI) lower than 0.05 confirmed a narrow size distribution (Figure 2C and D, respectively). As expected, PEI-NPs had a positive zeta potential of about 48 mV, HA-NPs were negatively charged with a zeta potential of about –18 mV. Scanning electron microscopy of dried NPs confirmed their spherical shape (Figure 2C and D, respectively).

The colloidal stability of NPs was investigated after 1 hour of incubation in culture medium supplemented with serum in a concentration range from 0 to 1 %. Based on previous findings, a time frame of 1 hour was expected to be adequate for the formation of a potential protein corona [29–31]. Rhodamine B (RHOD)-labeled particles were then added to primary hTM cells and observed by confocal laser scanning microscopy (CLSM) after 4 hours of incubation (Figure 2E). Without serum, both types of NPs formed large aggregates on the surface of hTM cells as the high electrolyte ionic strength of cell culture medium with physiological osmolarity resulted in screening of electrostatic interactions [32]. Already 0.35 % serum favorably enhanced the colloidal stability of HA-NPs, they were nicely distributed onto or most likely into hTM cells. In contrast, NPs decorated with PEI needed significantly higher serum concentration of about 1 % for a sufficient colloidal stability. Interestingly, 0.35 % serum is equal to the total protein content of the AH (12.4 mg/100 mL)

[33]. Hence, the functionalization of NPs with HA will guarantee for the colloidal stability of NPs in the therapeutic relevant milieu. We hypothesize that colloidally stable NPs most likely will follow the natural AH flow, while aggregates might stick to upper segments of the sieve-like TM or even clog the outflow pathway.
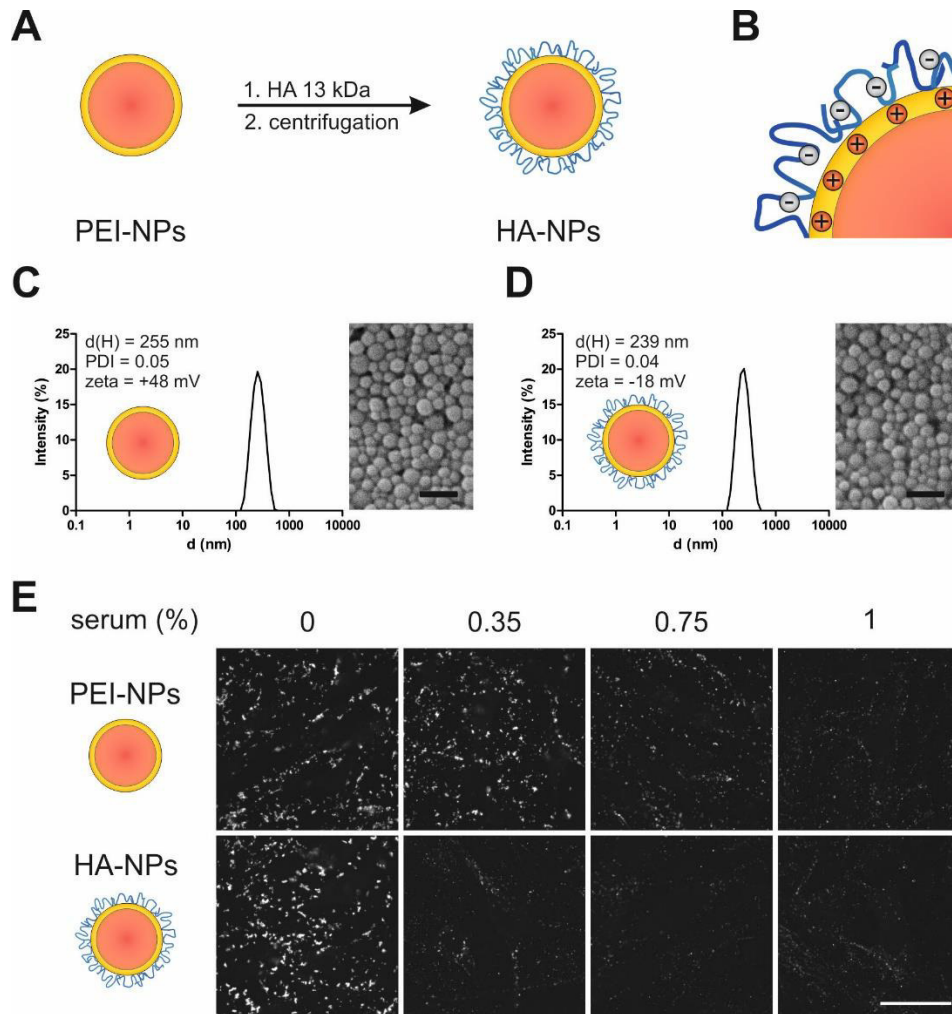

Figure 2. Fabrication and characterization of NPs without therapeutic siRNA. A) PLGA (MW 38-54 kDa) NPs were prepared by nanoprecipitation and stabilized with PEI (25 kDa). Resulting PEI-NPs (red-orange) were the coated with HA (blue) with a MW of 13 kDa (HA-NPs). The NPs were purified by centrifugation after each coating step. B) Cross-section through a schematic NP illustrating the type of charge of each layer. C and D) Physico-chemical characterization of PEI- and HA-NPs, respectively: Intensity distribution of hydrodynamic diameter averaged over three independent measurements as determined by dynamic light scattering. Particle size distribution was narrow and no aggregates were present in dispersion (PDI: PEI-NPs 0.05, HA-NPs 0.04). PEI-NPs had a zeta potential of +48 mV, while HA-NPs were negatively charged with a zeta potential of about -18 mV. Scanning electron micrographs display homogenous, spherical particles. The scale bar represents 500 nm. E) RHOD-labeled PEI- and HA-NPs (40 μg/mL) were incubated in culture medium with different serum concentrations ranging from 0 to 1 %. After 1 hour, NPs were added to primary hTM cells and imaged after for 4 hours of incubation by CLSM. A low serum concentration was sufficient to enhance the colloidal stability of HA-NPs, in contrast, PEI-NPs formed large aggregates. White: RHOD-labeled NPs. The scale bar represents 50 μm.

3.3 Cellular uptake of nanoparticles

To reliably discriminate between extra- versus intracellular localization of NPs, caveolin-1 (Cav1) -a structural protein of caveolin-dependent endocytosis- of immortalized human TM (HTM-N) cells was fluorescently labeled before incubation with NPs. To this end, HTM-N cells were transfected with plasmid DNA encoding a fusion protein of Cav1 and green fluorescent protein (Cav1-GFP) using the commercially available transfection reagent Lipofectamine 2000. After 24 hours, HTM-N cells were incubated with RHOD-labeled PEI- and HA-NPs at a serum concentration of 0.35 %. Z-sections of HTM-N cells were recorded after 4 hours by CLSM. Optical image sections were either illustrated as 3D rendering (which gives besides the XY image, the XZ and YZ images on a certain spot) or as composite image of the z-sections (Figure 3). As expected, PEI-terminated NPs formed large aggregates and were not taken up by HTM-N cells, but rather stuck to the outer membrane or were attached on the bottom of the culture ware. In contrast, HA-NPs were detected inside HTM-N cells. They were evenly distributed between Cav1 vesicles and located throughout all planes of the cell. This emphasizes the high potential of HA-coated NPs as vector for intracellular delivery.
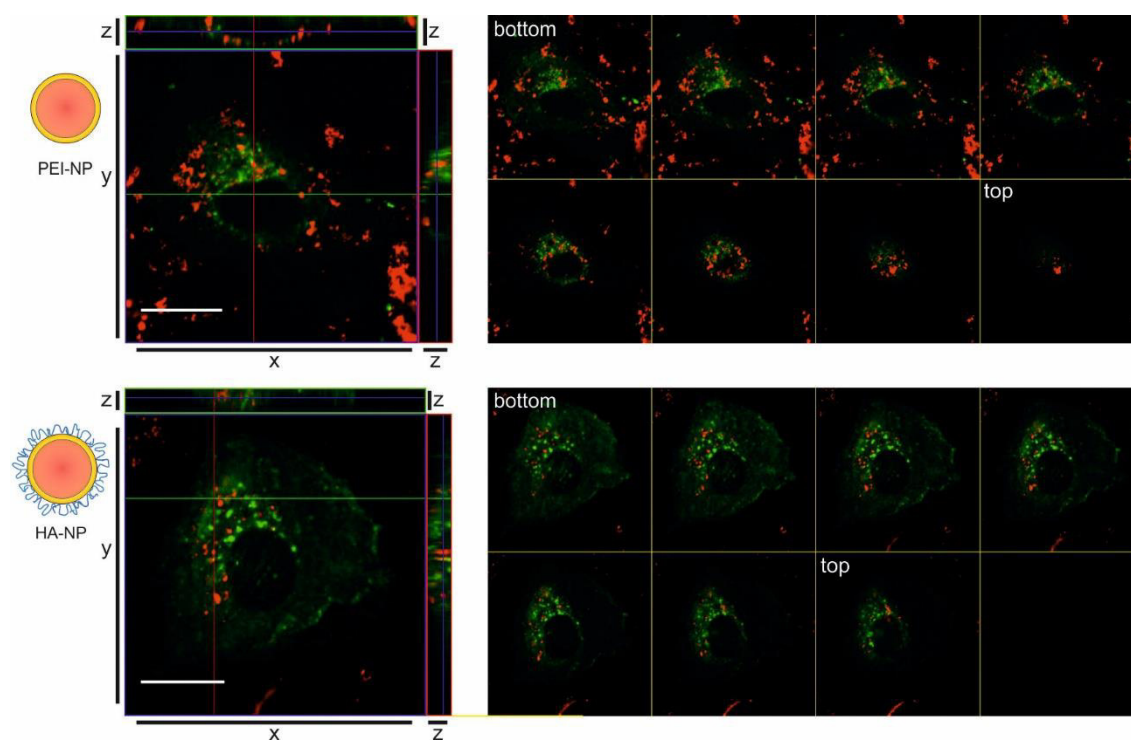
Figure 3. Extra- versus intracellular distribution of PEI- and HA-NPs. Immortalized human TM (HTM-N) cells were transiently transfected with Caveolin-1 (Cav1) -GFP fusion protein and incubated with 40 μg/mL RHOD-labeled HA- or PEI-NPs, respectively for 4 hours in culture medium containing 0.35 % serum. Cells were observed by CLSM in the multitracking mode. Red: RHOD-labeled NPs; green: Cav1-GFP fusion protein. Left panel: 3D rendering of 8 z-sections through a HTM-cell with top (XY) and lateral (XZ and YZ) view. Right panel: composite image of same 8 z sections from bottom to top view of a HTM-N cell. PEI-NPs formed large aggregates that stuck to the cell surface and were not detected inside cells as illustrated by the top and lateral view on a cell (left panel) and the image sequence from bottom to top (right panel). HA-NPs homogeneously spread between green stained intracellular vesicles and were evenly distributed through all image planes. The scale bar represents 20 μm.

3.4 Perfusion of porcine eyes with nanoparticles ex vivo

To proof the hypothesis that HA-coated NPs would follow the natural outflow pathway and reach the TM and SC, both RHOD-labeled PEI- and HA-NPs were perfused into the anterior chamber of porcine eyes. After perfusion, the anterior chamber was dissected and fluorescent imaging of the whole outflow ring was performed as illustrated in Figure 4A. PEI-NPs were detected only in few areas of the outflow ring and fluorescence of NPs was irregularly distributed (Figure 4B). In contrast, HA-NPs were homogeneously localized in the whole outflow ring of perfused porcine eyes (Figure 4B). Quantitative measurement of integrated fluorescence density corroborated the significantly higher amount of HA-NPs compared to PEI-NPs in the outflow system after perfusion (Figure 4 C).

To determine the exact localization of the NPs in the outflow system, sagittal tissue sections were stained with specific antibodies against CD44 after the perfusion procedure

176

(Figure 4D). As expected, the CD44 receptor was homogeneously distributed in all parts of the TM and the aqueous plexus (AP), which is an anatomic peculiarity of pigs and correlates to SC in human and mice. In more detail, the endothelial cells of the corneoscleral TM which is the first part of the TM, and TM cells of the JCT which is a deeper region of the TM, where the target cells for CTGF silencing are located, showed a bright fluorescence signal of the anti-CD44 antibody. In addition, endothelial cells of the venous plexus (VP), which are the second important target cells, showed also a pronounced signal (for better overview of different regions of the TM and SC also refer to Scheme 1). PEI-NPs accumulated at the entrance region of the TM which is the corneoscleral TM, and did not reach deeper regions such as the JCT or the AP at all (Figure 4D, left panel). PEI-NPs tended to build aggregates and were unable to pass TM's pores due to their size or surface charge. In contrast, HA-NPs were distributed throughout the entire TM including the corneoscleral TM and JCT, and also seemed to have reached the lumen of the AP (Figure 4D, right panel). Optical z-sections that were reconstructed to a 3D image with top and lateral view on the section, also illustrated the homogeneous distribution and deeper penetration of HA- compared to PEI-NPs (Figure 4D).

To demonstrate the localization of HA-NPs in the porcine lumen of the AP, endothelial cells of tissue sections were stained with a fluorescently labeled anti-CD31 antibody (Figure 4E). Thus, venous vessels of the porcine AP were nicely highlighted. In none of the examined sections, PEI-NPs were detected in the lumen of the AP. In contrast, HA-NPs were distributed all over the outflow pathway, namely in the corneoscleral TM, the JCT - as already evaluated by CD44 staining- and also in the lumen of the AP, which is again underlined by z-stacks of optical sections with a higher magnification (Figure 4E).
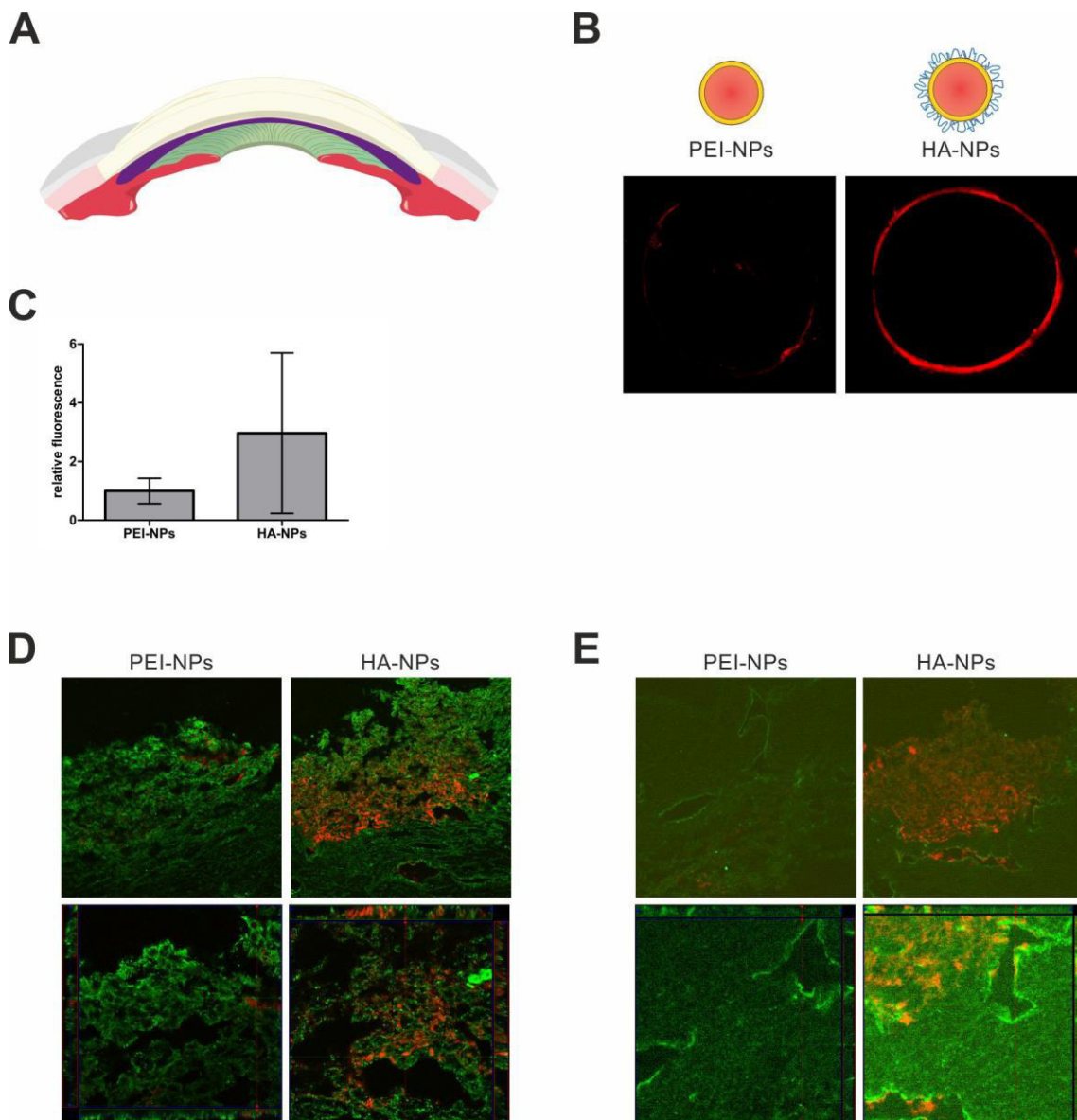
Figure 4. Porcine eyes were perfused *ex vivo* with RHOD-labeled PEI- and HA-NPs. A) As illustrated in Scheme A, a needle was placed into the posterior chamber and the eye was perfused with RHOD-labeled NP with a pressure of 10 mmHg. After the perfusion, the anterior chamber was dissected and flat mounted or prepared for immunohistochemistry. B) Fluorescence imaging of whole outflow rings was performed using a Zeiss Observer Z1 microscope. RHOD was excited at 563 nm and fluorescence was detected at 581 nm. PEI-NPs were sparsely detected in limited areas of the outflow ring. In contrast, red fluorescence intensity of RHOD-labeled HA-NPs was much higher and was detected over the whole outflow ring. Representative images of nine independent porcine eyes are shown. C) Fluorescence of 8 images for PEI-NPs and 9 images for HA-NPs were quantified by ImageJ. D and E) To precisely localize NPs in the outflow tissue, sagittal sections were prepared and additionally stained with anti-CD44 (D) or anti-CD31 (E) antibody, respectively. Sections were analyzed by CLSM in the multitracking mode with excitation at 488 and 543 nm, respectively, and detection of emission with a bandpass filter 505 – 530 nm and a 630 longpass filter. Top row: 20x magnification, bottom row: 63x magnification. Green: anti-CD44 antibody in D and anti-CD31 antibody in E, red: RHOD-labeled PEI- and HA-NPs. HA-NPs were distributed in the whole outflow pathway and lumen of the AP, but PEI-NPs were only detected in the entrance region of the TM.

3.5 Perfusion of human eyes with nanoparticles ex vivo

In analogy to experiments with porcine eyes, two human donor eyes were perfused with NPs. Again, cryo-sections of the outflow pathway were counterstained with fluorescently labeled anti-CD44 antibody. According to perfusion experiments of porcine eyes, PEI-NPs were detected in a limited amount and only in the entrance region of the TM (Figure 5A). In contrast, a much higher amount of RHOD-labeled HA-NPs was detected in the outflow region. In addition, HA-coated NPs spread over a wider region and penetrated into much deeper areas of the TM (Figure 5B).
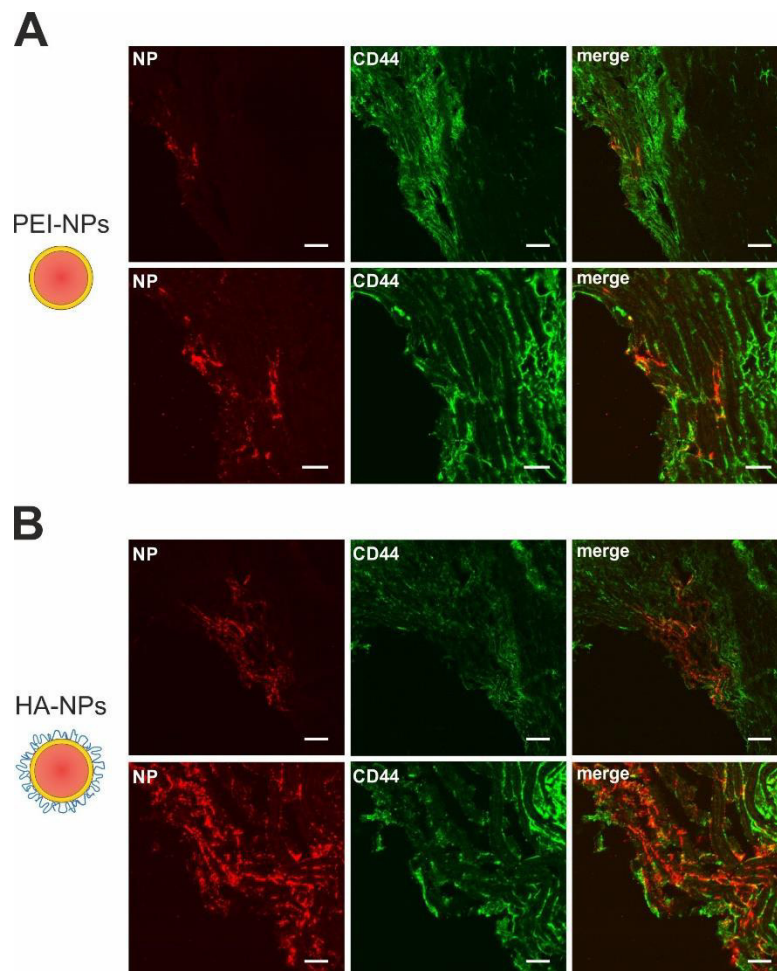
Figure 5. Human eyes were perfused *ex vivo* with RHOD-labeled (A) PEI- and (B) HA-NPs. To precisely localize NPs in the outflow tissue, sagittal sections were prepared and additionally stained with anti-CD44 antibody. Sections were analyzed by CLSM in the multitracking mode with excitation at 488 and 543 nm, respectively, and detection of emission with a bandpass filter 505 – 530 nm and a 630 longpass filter. Representative images of two independent experiments are shown. Green: anti-CD44 antibody, red: RHOD-labeled PEI- and HA-NPs. Bar represents 50 μm (top row) and 20 μm (bottom row).

3.6   CTGF gene silencing in vitro

After demonstrating that NPs are capable of being drained to the TM and SC after injection into the anterior chamber of the eye, the gene silencing capability of siRNA-loaded NPs was tested in hTM cells *in vitro*. To this end, NPs were assembled in a LbL process according to Figure 6A. The NP core again consisted of PLGA and was stabilized with the polycationic polymer PEI. PEI was chosen, as it is a well-established transfection agent [34], in addition, PEI also provided for a permanent positive surface charge, which was necessary for the electrostatic attachment of negatively charged siRNA in the next layer. NPs were fabricated either with functionally verified siRNA against human CTGF or non-targeted control siRNA. To protect the fragile siRNA from degradation by nucleases, an additional layer of PEI was applied (PEI(siRNA)-NPs). Finally, the particles were coated with the negatively charged polysaccharide HA (HA(siRNA)-NPs). Complete removal of unbound polyelectrolytes before addition of the next polyelectrolyte layer was of utmost importance and was again realized by stepwise centrifugation. With this coating procedure, it was again possible to compare NPs with a final PEI- or HA- layer, respectively. The size of PEI(siRNA)-NPs was about 260 nm, HA(siRNA)-NPs were with a hydrodynamic diameter of about 214 nm slightly smaller as determined by dynamic laser light scattering (Figure 6B). Both particle species had a narrow size distribution, which is reflected by a PDI below 0.1; the PDI of HA(siRNA)-NPs was even as small as 0.03 (Figure 6B). A reversal of the zeta potential after addition of each polycation layer indicated a successful coating (Figure 6C). PEI(siRNA)-NPs had a strong positive surface charge of about 56 mV, while HA(siRNA)-NPs had a negative zeta potential of about −14 mV. Interestingly, polyanion coated NPs had a slightly lower size and absolute value of zeta potential than polycation coated ones most likely due to differences in thickness of the hydration shell. Altogether, the physicochemical characteristics of siRNA-loaded NPs were comparable to those applied for the perfusion studies without siRNA.

CTGF gene silencing studies were performed in primary hTM cells taken from different body donors. hTM cells were stimulated with 1 ng/mL TGF-β2 and then incubated with 80 µg/mL of PEI- or HA(siRNA)-NPs. The CTGF mRNA level was analyzed by real time polymerase chain reaction (RT-PCR) and related to Guanine Nucleotide-Binding Protein Subunit Beta-Like Protein (Gnb2L) as housekeeping gene (Figure 6D). Gene silencing with the commercially available Lipofectamine™ RNAiMAX led to a reduction of relative CTGF mRNA to about 17 % and served as positive control. Both, HA- and PEI-terminated NPs reduced the CTGF mRNA level. HA(siRNA)-NPs caused a slightly stronger effect than

PEI(siRNA)-NPs (silencing by approximately 30 % or 20 %, respectively), but without statistical significance. It is an important point that relative CTGF mRNA values were an average of four different donor cells types. Having a closer look at the results of single donor cells, huge differences became evident (Figure 6E and F). CTGF silencing in primary cells with a high basal CTGF level was more efficient compared to donors with a lower basal CTGF expression (refer to donors no. 739 and 211). However, due to the lack of a source for further primary cells of human donors, this trend could not be further corroborated. However, if true, this relation might be a great therapeutic opportunity: As the silencing with HA-functionalized NPs was only effective in cells with high CTGF levels, healthy cells remain unaffected by therapy and undesired effects caused by "over-silencing" can be avoided. Finally, we performed Western Blot analysis of same samples. Here, the differences between PEI- and HA-coated NPs were more impressive. HA(siRNA)-NPs lead to a reduction of CTGF of about 50 %, in contrast PEI-NPs showed no effect. As expected, positive control with Lipofectamine RNAiMAX reduced CTGF levels to about 20 %.
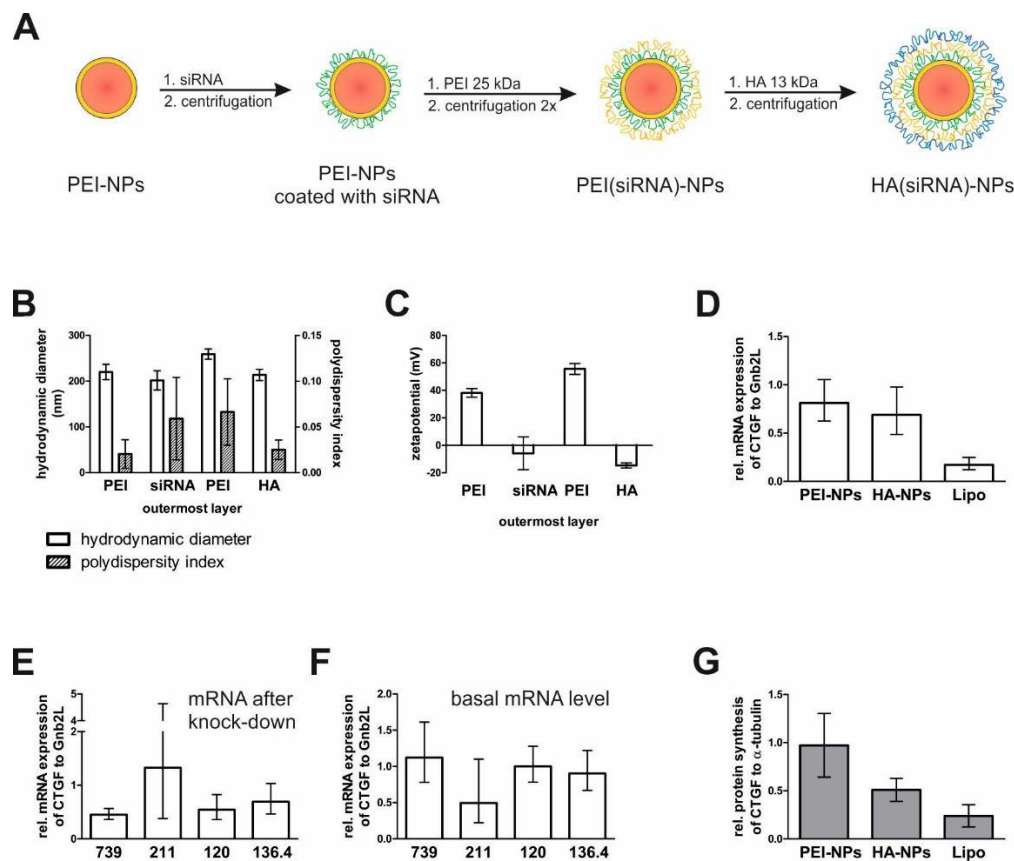
Figure 6. Fabrication, characterization and CTGF gene silencing of siRNA-loaded NPs in hTM cells. A) LbL assembly of NPs for gene silencing studies in hTM cells. PLGA NPs were stabilized with PEI (25 kDa) (red core, orange shell) and then coated with siRNA (green). The next PEI layer (orange) protected siRNA from degradation. Finally, the particles were coated with HA (blue) with a MW of 13 kDa. The NPs were purified by stepwise centrifugation between the individual coating steps. B) Hydrodynamic diameter and polydispersity index of NPs during the coating process. The x-axis indicates the outermost layer of the NPs. A PDI lower than 0.1 confirmed the absence of aggregates. The values represent the mean ± SD of three independent measurements. C) Surface charge reversal after each layering step demonstrated successful adsorption of the respective polyelectrolyte. The values represent the mean ± SD of three independent measurements. (D-G) *In vitro* CTGF-silencing efficacy of PEI- and HA(siRNA)-NPs in hTM cells on the mRNA and protein level. hTM cells were treated with 1 ng/mL TGF-β2 and incubated with PEI- or HA(siRNA)-NPs. Lipoplexes were built with Lipofectamine RNAiMAX served as control. (D-F) CTGF mRNA level was analyzed by RT-PCR and values were expressed as relative mRNA CTGF/Gnb2L and were related to non-targeted control particles. D) Both treatment with PEI- and HA(siRNA)NPs slightly reduced the CTGF mRNA level of hTM cells, but difference between both groups was not statistically significant. E) However, at the single donor levels differences were measured. F) hTM cells of donor no. 739 had a higher basal CTGF mRNA level compared to other donor cell types. At the same time, relative mRNA CTGF reduction of donor no. 739 was also more pronounced compared to other donor cells. G) CTGF protein expression was detected by Western Blot analysis. Values were expressed as relative CTGF/α-tubulin and related to non-targeted control particles. HA(siRNA)NPs reduced the CTGF protein expression of hTM cells to about 50 %, while PEI(siRNA)NPs did not elicit any effect. Shown is the mean ± SD of three (PEI(siRNA)-NPs and lipoplexes) or four (HA(siRNA)-NPs) individual experiments each performed in triplicate.

Western blot for CTGF and Gnb2L was conducted and analyzed at the Department for Human Anatomy and Embryology (University of Regensburg) by Andrea Dillinger and Rudolf Fuchshofer.

4   Discussion

The progression of glaucoma is characterized by an irreversible damage of optic nerve fibers in the back of the eye. An elevated IOP is regarded to be causatively involved in this process. Pathological alterations in the TM, namely an enhanced deposition and stiffening of the ECM and an increased contractility of actin stress fibers, raise the resistance to AH flow and IOP consequently. Junglas et al. identified CTGF, a down-stream mediator of TGF-β2, to cause these effects, and demonstrated a suppression of TGF-β2 induced effects on the ECM [6] and an attenuation of the cellular actin cytoskeleton [11] by siRNA gene knock-down of CTGF *in vitro*. However, for a therapeutic use of siRNA directed against CTGF, a suitable delivery system was needed.

In this study, LbL-NP were developed for the delivery of siRNA to cells in the TM. Our approach was to functionalize the NPs with HA, a polysaccharide with naturally high concentration in the TM. HA was intended to reduce the interactions of the particles with the dense ECM-network, which might hinder their distribution into the deeper TM, where outflow resistance is generated. Further, HA served as targeting structure to CD44 receptors on TM cells, specifically increasing uptake rates in relevant cells and reducing side effects.

We were able to support previous findings of Knepper et al. regarding elevated CD44 levels in the TM of glaucoma patients [23] and could show, that changes of CD44 expression in the outflow pathways are related to the CTGF induced increase in CD44 mRNA. Interestingly, CD44 levels were only elevated in the TM and SC where outflow resistance is generated [35,36] but not in the sclera. Hence, by using CD44 receptors as targets for a nanoparticulate siRNA delivery system, diseased cells with high receptor expression in TM regions will be addressed whereas healthy cells with low receptor density will not be affected. The risk of undesired off-target effects is reduced and deposition of NPs in regions, where no therapeutic effect is expected, is avoided.

NP for this investigation were assembled in a LbL approach by alternating deposition of oppositely charged polyelectrolytes on a NP core. Although this technique is leveraged for applications in material science, physical chemistry, electrochemistry and biomedical engineering [37], the coating of templates on the nano-scale is challenging due to their tendency towards aggregation [25]. With the protocol developed by us it was possible to produce monodisperse NPs with up to three polyelectrolyte layers without the formation of aggregates. Interestingly, although HA-functionalized particles consisted of one additional layer compared to PEI-NPs, their hydrodynamic diameter was smaller (214 nm compared to

260 nm). Most likely, this effect was caused by differences in surface charge values. As PEI-NPs were highly positively charged, a thick hydration shell formed around the particles. Lower absolute zeta potential values of negatively charged HA-NPs resulted in a thinner hydration shell. As only minor size differences were determined by scanning electron microscopy on dried samples, this seems to be a rational explanation.

The size of the particles was chosen carefully. On the one hand, NPs had to be small enough to circumvent sterically hindrance in the TM. Johnson et al. calculated that most pores in the TM have a size of 0.15 μm but yet a high number of larger pores allowed particles of 200 to 500 nm to pass [21]. On the other hand, as TM cells share properties with endothelial cells and are capable of phagocytosis [38], a particle size larger than 250 nm was desired for high uptake rates [39]. Consequently, the HA-decorated NPs developed by us with a size of 214 nm were expected to be large enough to be barely taken up via phagocytosis but small enough to freely move through the larger pores of the TM. One might assume, that this particle size will initiate a strong immune response and that particles are not only taken up by TM cells but also by macrophages. However, due to the immune privilege of the eye, only few immune cells are located in the ocular environment [40,41] and problems due to undesired activation of the immune system can be avoided by local application, which is intended for the LbL-NPs.

Even if individual particles are not maintained in the sieve-like structure of the TM due to their size, NP aggregates might still be too large to pass unhindered. Because of the unique structure of LbL-NPs with charged polyelectrolytes on the surface, electrostatic repulsion was expected to guarantee a high colloidal stability. However, in an environment with an electrolyte concentration of physiological osmolarity (e. g. cell culture media, AH), the charges on the NP surface are screened and aggregation becomes a severe problem [32]. Proteins, which are commonly present under these physiological conditions, contribute to the stability of the particles as they form an additional layer around them (which is called protein corona) and sterically stabilize the particles. Unfortunately, the protein concentration in the AH is very low (only 12.4 mg/ 100 mL [33]) and we could demonstrate, that this amount of protein is not sufficient to prevent the aggregation of positively charged PEI-NP. Due to its physicochemical properties, less proteins are adsorbed onto HA-decorated surfaces and low amounts of protein are adequate to maintain colloidal stability in fluids of high osmolarity like cell culture media or physiologic liquids. Hence, the formation of aggregates was prevented by the sheath of HA and particles were assumed to freely follow the AH flow to their target cells in deeper regions of the TM.

Steric hindrance is not the only limitation to unrestricted transport. Interaction forces between NPs and components of the ECM network also might retain the particles [21]. We assumed that possible sites of interaction are already occupied by HA, which is naturally present in the TM. In perfusion studies of porcine and human eyes we were able to demonstrate the feasibility of this concept. Whereas NPs without HA-functionalization were detected only in the upper regions, HA-NPs distributed into the whole outflow system including the deep TM and the SC. In further *in vitro* assays we could show that HA-NPs are sufficiently taken up by hTM cells, an absolute necessity for particles serving as siRNA delivery system. Nevertheless, additional bottlenecks have to be overcome for successful gene silencing.

Hence and finally, the gene silencing potential of siRNA loaded HA-decorated LbL-NP was investigated *in vitro*. HA-NPs were able to reduce CTGF protein expression by approximately 50 %. It implicates, that the particles protected the fragile siRNA from degradation, were taken up to a sufficient extent, escaped the endolysosomal pathway and released the nucleic acid into the cytosol of the cell, where it is incorporated into the gene silencing machinery.

To our surprise, CTGF-silencing was more pronounced when the initial CTGF mRNA levels were high. This finding bears an enormous potential as it may be understood as protection against "over-silencing" and significantly improves the safety profile of the NPs. CTGF is a physiologically active substance involved in a plethora of different processes like wound healing, endochondral ossification or angiogenesis [42,43] and a concentration below a certain limit may have unforeseen consequences. This CTGF-silencing therapy, however, limits itself. As untreated patients show a high CD44 receptor density in the TM and SC, a remarkable accumulation of the NP can be expected in glaucomatous but not in healthy eyes. Additionally, CTGF silencing will only work when the levels are elevated and comes to an end when concentrations decline. Because of lower CTGF levels, also CD44 expression will decrease and less NP will be taken up into the cells, resulting in a smaller gene silencing effect.

5. Conclusion

In conclusion, we have identified CD44 as a promising target receptor to deliver NPs to the outflow pathway tissue. The assumption is based on the induction of CD44 by CTGF *in vitro*, the increased presence of CD44 in the anterior chamber angle in a glaucoma mouse model and the marked increase of CD44 in TM and SC cells of glaucomatous patients. The

development of HA-decorated NPs addresses directly the CD44 receptor. The uptake of HA-decorated NPs into the outflow pathway cells was much more efficient than the conventionally used PEI-NPs as shown by cell culture and perfusion experiments of porcine and human organ culture. The *in vitro* experiments revealed that an efficient knock-down by the delivery of a specific siRNA was dependent on the expression profile of CTGF in TM cells, which in turn demonstrates the high specificity of the HA-decorated NPs to pathologic expression changes in the outflow tissues. We suggest that the HA-decorated NPs are an excellent therapeutic approach to deliver specific agents like CTGF-siRNA to the outflow tissues and thereby to prevent the progression of the glaucomatous disease.

References

[1]   Tham Y-C, Li X, Wong TY, Quigley HA, Aung T, Cheng C-Y (2014), Global prevalence of glaucoma and projections of glaucoma burden through 2040: a systematic review and meta-analysis, Ophthalmology 121 2081–2090.

[2]   Weinreb RN, Khaw PT (2004), Primary open-angle glaucoma, The Lancet 363 1711–1720.

[3]   Weinreb RN, Aung T, Medeiros FA (2014), The Pathophysiology and Treatment of Glaucoma, JAMA 311 1901.

[4]   Pita-Thomas DW, Goldberg JL (2013), Nanotechnology and glaucoma: little particles for a big disease, Cur Opin Ophthalmol 24 130–135.

[5]   Tamm ER (2009), The trabecular meshwork outflow pathways: Structural and functional aspects, Exp Eye Res 88 648–655.

[6]   Junglas B, Yu AHL, Welge-Lussen U, Tamm ER, Fuchshofer R (2009), Connective tissue growth factor induces extracellular matrix deposition in human trabecular meshwork cells, Exp Eye Res 88 1065–1075.

[7]   Fuchshofer R, Tamm ER (2012), The role of TGF-β in the pathogenesis of primary open-angle glaucoma, Cell Tissue Res 347 279–290.

[8]   Fuchshofer R, Tamm ER (2009), Modulation of extracellular matrix turnover in the trabecular meshwork, Exp Eye Res 88 683–688.

[9]   Tektas O-Y, Lütjen-Drecoll E (2009), Structural changes of the trabecular meshwork in different kinds of glaucoma, Exp Eye Res 88 769–775.

[10]   Stamer WD, Acott TS (2012), Current understanding of conventional outflow dysfunction in glaucoma, Cur Opin Ophthalmol 23 135–143.

[11]   Junglas B, Kuespert S, Seleem AA, Struller T, Ullmann S, Bösl M, Bosserhoff A, Köstler J, Wagner R, Tamm ER, Fuchshofer R (2012), Connective Tissue Growth Factor Causes Glaucoma by Modifying the Actin Cytoskeleton of the Trabecular Meshwork, Am J Pathol 180 2386–2403.

[12]   Wiederholt M, Thieme H, Stump Friederike (200), The Regulation of Trabecular Meshwork and Ciliary Muscle Contractility, Prog Retin Eye Res 19 271–295.

[13]   Overby DR, Zhou EH, Vargas-Pinto R, Pedrigi RM, Fuchshofer R, Braakman ST, Gupta R, Perkumas KM, Sherwood JM, Vahabikashi A, Dang Q, Kim JH, Ethier CR, Stamer WD, Fredberg JJ, Johnson M (2014), Altered mechanobiology of Schlemm's canal endothelial cells in glaucoma, P Natl Acad Sci USA 111 13876–13881.

[14]   Thakur A, Fitzpatrick S, Zaman A, Kugathasan K, Muirhead B, Hortelano G, Sheardown H (2012), Strategies for ocular siRNA delivery: Potential and limitations of non-viral nanocarriers, J Biol Eng 6 7.

[15]   Guzman-Aranguez A, Loma P, Pintor J (2013), Small-interfering RNAs (siRNAs) as a promising tool for ocular therapy, Brit J Pharmacol 170 730–747.

[16]   Tam LCS, Reina-Torres E, Sherwood JM, Cassidy PS, Crosbie DE, Lütjen-Drecoll E, Flügel-Koch C, Perkumas K, Humphries MM, Kiang A-S, O'Callaghan J, Callanan JJ, Read AT, Ethier CR, O'Brien C, Lawrence M, Campbell M, Stamer WD, Overby DR, Humphries P (2017), Enhancement of Outflow Facility in the Murine Eye by Targeting Selected Tight-Junctions of Schlemm's Canal Endothelia, Sci Rep- 7 40717.

[17]   Bobbin ML, Rossi JJ (2016), RNA Interference (RNAi)-Based Therapeutics: Delivering on the Promise?, Annu Rev Pharmacol 56 103–122.

[18]   Tatiparti K, Sau S, Kashaw SK, Iyer AK (2017), siRNA Delivery Strategies: A Comprehensive Review of Recent Developments, Nanomaterials-Basel 7.

[19]   Kanasty R, Dorkin JR, Vegas A, Anderson D (2013), Delivery materials for siRNA therapeutics, Nat Mater 12 967–977.

[20]   Acott TS, Kelley MJ (2008), Extracellular matrix in the trabecular meshwork, Exp Eye Res 86 543–561.

[21]   Johnson M, Johnson DH, Kamm RD, Kater AW de, Epstein DL (1990), The Filtration Characteristics of the Aqueous Outflow System, Exp Eye Res 50 407–418.

[22]   Overby DR, Gong H, Qiu, Guanting, Freddo, Thomas F., Johnson M (2002), The Mechanism of Increasing Outflow Facility during Washout in the Bovine Eye, Invest Ophth Vis Sci 43 3455–3464.

[23]   Knepper PA, Goossens W, Mayanil, Chandra S. K. (1998), CD44H Localization in Primary Open-Angle Glaucoma, Invest Ophth Vis Sci 39 673–680.

[24]   Dosio F, Arpicco S, Stella B, Fattal E (2016), Hyaluronic acid for anticancer drug and nucleic acid delivery, Adv Drug Deliver Rev 97 204–236.

[25]   Elbakry A, Zaky A, Liebl R, Rachel R, Goepferich A, Breunig M (2009), Layer-by-Layer Assembled Gold Nanoparticles for siRNA Delivery, Nano Lett 9 2059–2064.

[26]   Fuchshofer R, Yu AHL, Weige-Lüssen U, Tamm ER (2007), Bone Morphogenetic Protein-7 Is an Antagonist of Transforming Growth Factor-β2 in Human Trabecular Meshwork Cells, Invest Ophth Vis Sci 48 715–726.

[27]   Fuchshofer R (2011), The pathogenic role of transforming growth factor-beta2 in glaucomatous damage to the optic nerve head, Exp Eye Res 93 165–169.

[28]   Zhang C, Wu F-G, Hu P, Chen Z (2014), Interaction of Polyethylenimine with Model Cell Membranes Studied by Linear and Nonlinear Spectroscopic Techniques, J Phys Chem C 118 12195–12205.

[29]   Tenzer S, Docter D, Kuharev J, Musyanovych A, Fetz V, Hecht R, Schlenk F, Fischer D, Kiouptsi K, Reinhardt C, Landfester K, Schild H, Maskos M, Knauer SK, Stauber RH (2013), Rapid formation of plasma protein corona critically affects nanoparticle pathophysiology, Nat Nanotechnol 8 772–781.

[30]   Monopoli MP, Walczyk D, Campbell A, Elia G, Lynch I, Bombelli FB, Dawson KA (2011), Physical-chemical aspects of protein corona: relevance to *in vitro* and *in vivo* biological impacts of nanoparticles, J Am Chem Soc 133 2525–2534.

[31]   Lundqvist M (2013), Nanoparticles: Tracking protein corona over time, Nat Nanotechnol 8 701–702.

[32]   Moore TL, Rodriguez-Lorenzo L, Hirsch V, Balog S, Urban D, Jud C, Rothen-Rutishauser B, Lattuada M, Petri-Fink A (2015), Nanoparticle colloidal stability in cell culture media and impact on cellular interactions, Chem Soc Rev 44 6287–6305.

[33]   Tripathi RC, Millard CB, Tripathi BJ (1989), Protein composition of human aqueous humor: SDS-PAGE analysis of surgical and post-mortem samples, Exp Eye Res 48 117–130.

[34]   Lungwitz U, Breunig M, Blunk T, Göpferich A (2005), Polyethylenimine-based non-viral gene delivery systems, Eur J Pharm Biopharm 60 247–266.

[35]   Tamm ER, Fuchshofer R (2007), What increases outflow resistance in primary open-angle glaucoma?, Surv Ophthalmol 52 Suppl 2 S101-4.

[36]   Tamm ER, Braunger BM, Fuchshofer R (2015), Intraocular Pressure and the Mechanisms Involved in Resistance of the Aqueous Humor Flow in the Trabecular Meshwork Outflow Pathways, Prog Mol Biol Transl 134 301–314.

[37]   Ariga K, Yamauchi Y, Rydzek G, Ji Q, Yonamine Y, Wu KC-W, Hill JP (2014), Layer-by-layer Nanoarchitectonics: Invention, Innovation, and Evolution: Invention, Innovation, and Evolution, Chem Lett 43 36–68.

[38]   Stamer WD, Clark AF (2017), The many faces of the trabecular meshwork cell, Exp Eye Res 158 112–123.

[39]   Yan Y, Such GK, Johnston APR, Best JP, Caruso F (2012), Engineering particles for therapeutic delivery: prospects and challenges, ACS Nano 6 3663–3669.

[40]   Streilein JW (2003), Ocular immune privilege: therapeutic opportunities from an experiment of nature, Nat Rev Immunol 3 879–889.

[41]   Niederkorn JY (2006), See no evil, hear no evil, do no evil: the lessons of immune privilege, Nat Immunol 7 354–359.

[42]   Barrientos S, Stojadinovic O, Golinko MS, Brem H, Tomic-Canic M (2008), Growth factors and cytokines in wound healing, Wound Repair Regen 16 585–601.

[43]   Moussad EE, Brigstock DR (2000), Connective tissue growth factor: what's in a name?, Mol Gen Metabol 71 276–292.

Chapter 7

Summary and Conclusion

Summary

The incidence of glaucoma is on the rise. By the end of this decade almost 80 million people will be affected by this vision threatening disease [1]. Current therapeutic concepts rely on a reduction of intraocular pressure by pharmacological substances or surgery [2]. Thus far, however, no treatment is available which address the underlying mechanisms of the disease. As knowledge about pathological processes on the molecular level increases, other therapeutic strategies also come into focus. One such promising approach is interference with connective tissue growth factor (CTGF), a matricellular protein mediating intraocular pressure (IOP) elevation. Post transcriptional gene silencing using small interfering RNA (siRNA) is an elegant strategy to reduce elevated levels of CTGF and consequently IOP. Nevertheless, delivering nucleic acids of this type remains a challenge. Nanoparticles (NPs) of different composition are a frequently applied system as they protect the fragile siRNA from degradation and facilitate cellular uptake.

An extremely versatile and valuable excipient for ocular drug delivery systems is hyaluronic acid (HA). Several dosage forms benefit from its excellent biocompatibility and properties like transparency, high water binding capacity and mucoadhesivity. For example, HA has been used in eye drops as pharmaceutical ingredient itself or to enhance the bioavailability of other substances. Ocular inserts, implants or lenses benefit from an HA coating which improves wettability and biocompatibility and prevents fouling. As shown in this work, properties of more innovative technologies like nanoparticles (NPs) are also improved by HA functionalization (chapter 2). It was hypothesized that NPs designed for the delivery of siRNA to the trabecular meshwork (TM) in the anterior segment of the eye might also benefit from this approach. HA was expected to improve the mobility of the particles in the extracellular space and simultaneously generate high uptake rates due to interactions with cluster of differentiation (CD) 44 receptors on the surface of TM cells.

The negative charge of HA can be used to electrostatically attach the polysaccharide to a suitable, positively charged NP. As siRNA is also negatively charged, assembly of the NP in a layer-by-layer (LbL) process is reasonable. However, the coating of nanomaterials with polyelectrolytes is challenging. Thus, it was first necessary to develop a robust protocol. Using the method described here, the manufacturing of monodispersed siRNA-loaded and HA-functionalized NPs with a size of approximately 220 nm was possible. Dynamic light scattering (DLS) and fluorescence based techniques were used to monitor NP aggregation and disassembly in different dispersants, mimicking conditions before and after ocular

application. The coating with HA seemed to improve the colloidal stability of the particles as an increase in size was delayed by one hour and the individual layers of the particles did not detach (chapter 3).

HA-functionalization of NPs is a widely investigated approach in cancer therapy to enhance penetration into tumors and cellular uptake via interactions with CD44 cell surface receptors. This concept might also work for targeting the trabecular meshwork (TM) as a considerable receptor density was found on immortalized and primary TM cells. *In vitro* studies demonstrated a dependence of cell-associated NPs on the density of CD44 receptors, which was more pronounced when NPs were coated with HA. Additionally, HA decoration improved the colloidal stability of the NPs in 2D or 3D cell culture, which is in accordance with DLS measurements as reported above. This is beneficial regarding the therapeutic use of the NPs, as larger aggregates might clog pores in the TM outflow pathways (chapter 4).

Frequently, the real difficulty is not the delivery of siRNA to the cell but the intracellular release of the nucleic acid from the NP into the cytosol. By determining the gene silencing effect of the drug delivery system, both, the delivery and release could be studied. LbL-NPs of different composition were not able to reduce the artificially induced production of green fluorescent protein in immortalized TM cells. Detailed investigations of the intracellular fate of the particles by analyzing their colocalization with various intracellular compartments did not result in any information about the missing gene silencing effect. However, further experiments indicated that NP exocytosis might contribute at least in part to the observed results (chapter 5).

Finally, basic investigations and model systems were left behind. As demonstrated in perfusion studies of pig and human eyes, the targeting of CD44 receptors proved to be an effective strategy to increase NP accumulation in the TM as three times more NPs were found in this region when functionalized with HA compared to positively charged control particles. Glaucoma patients might especially benefit from this approach as CD44 upregulation by CTGF and tumor growth factor β2 was demonstrated *in vitro* and a higher receptor density was found in the TM of transgenic mice and glaucoma patients. LbL-NPs proved to be effective in significantly reducing CTGF expression at the mRNA and protein level in primary TM cells. Interestingly, mRNA analysis indicated a dependence of the silencing effect on basal CTGF values which might be of interest with respect to individualized therapeutic use of the particles. Furthermore, HA decorated NPs reduced CTGF protein synthesis by 50 % whereas positively charged PEI-NPs did not show any effect (chapter 6).

Conclusion

In the present work, initial assumptions were confirmed: HA functionalization improved the colloidal stability and consequently the mobility of the particles. Additionally, targeting CD44 cell surface receptors proved to be a successful strategy to increase accumulation of the particles in the TM as well as the cellular uptake. Initial *in vitro* data convincingly demonstrated the potential of the NPs in reducing CTGF expression. As these results indicate a promising development, the project should be pursued further. Additional research is needed to answer all remaining and emerging questions. A critical next step towards therapeutic application is the scale-up of manufacturing processes as larger quantities of particles will be needed. Then, *in vivo* studies and *ex vivo* organ cultures might give a first indication as to whether glaucoma patients will benefit from this new therapeutic concept in future.

References

[1]   Tham Y-C, Li X, Wong TY, Quigley HA, Aung T, Cheng C-Y (2014), Global prevalence of glaucoma and projections of glaucoma burden through 2040: a systematic review and meta-analysis, Ophthalmology 121 2081–2090.

[2]   Schmidl D, Schmetterer L, Garhofer G, Popa-Cherecheanu A (2015), Pharmacotherapy of glaucoma, J Ocul Pharmacol 31 63–77.

Appendix

Abbreviations

3D	three-dimensional
AH	aqueous humor
AP	aqueous plexus
ATP	adenosine triphosphate
Cav1	caveolin-1
CD44	cluster of differentiation 44
CLSM	confocal laser scanning microscope/microscopy
CTGF	connective tissue growth factor
DAPI	4',6-diamidino-2-phenylindole
D(E)MEM	Dulbecco's modified eagle medium
DLS	dynamic light scattering
ECM	extracellular matrix
EMEM	Eagle's minimum essential medium
FDA	Food and Drug Administration
FI	fluorescence intensity
FITC	fluorescein
GFP	green fluorescent protein
Gnb2L	guanine nucleotide-binding protein subunit beta-like protein
HA	hyaluronic acid
HA-NPs	hyaluronic acid functionalized nanoparticles
hTM	primary human trabecular meshwork cells
HTM-N	immortalized human trabecular meshwork cells
IOP	intraocular pressure
JCT	juxtacanalicular connective tissue

Appendix

LbL	layer-by-layer
LbL-NPs	layer-by-layer nanoparticles
mRNA	messenger ribonucleic acid
NPs	nanoparticles
PBS	phosphate buffered saline
PDI	polydispersity index
PEI	polyethyleneimine
PEI-NPs	polyethyleneimine functionalized nanoparticles
pH	potential of hydrogen
PLArg	poly-L-arginine
PLGA	poly(lactic-*co*-glycolic acid)
POAG	primary open angle glaucoma
RHOD	rhodamine
RISC	RNA-induced silencing complex
RNA	ribonucleic acid
RNAi	RNA interference
RT-PCR	real time polymerase chain reaction
SC	Schlemm's canal
SD	standard deviation
SEM	scanning electron microscopy, standard error of the mean
siRNA	short interfering RNA
TGF-β2	tumor growth factor β2
TM	trabecular meshwork
VP	venous plexus
WT	wild type

Acknowledgements

Statement in Lieu of an Oath

I hereby confirm that I have written this thesis on my own and that I have not used any other media or materials than the ones referred to in this thesis.

Regensburg, ……………..   …………………………….